NASA CR-114474
Available to U.S. Government
Agencies and Their Contractors

DESIGN INTEGRATION AND NOISE STUDIES FOR JET STOL AIRCRAFT

FINAL REPORT

Volume IV—Wind Tunnel Test Program

By T. Wang, F. Wright, and A. Mahal

D6-40552-4
May 1972

Distribution of this report is provided in the interest of information exchange. Responsibility for the contents resides in the author or organization that prepared it.

Prepared under contract NAS2-6344 by

THE BOEING COMPANY
Commercial Airplane Group
P.O. Box 3707
Seattle, Washington 98124

for
Ames Research Center

NATIONAL AERONAUTICS AND SPACE ADMINISTRATION

CR# 114474

DESIGN INTEGRATION AND NOISE STUDIES FOR JET STOL AIRCRAFT

FINAL REPORT

Volume IV—Wind Tunnel Test Program

By T. Wang, F. Wright, and A. Mahal

D6-40552-4
May 1972

Prepared under contract NAS2-6344 by

THE BOEING COMPANY
Commercial Airplane Group
P.O. Box 3707
Seattle, Washington 98124

for
Ames Research Center

NATIONAL AERONAUTICS AND SPACE ADMINISTRATION

5

PRECEDING PAGE BLANK NOT FILMED

A

DESIGN INTEGRATION AND NOISE STUDIES FOR JET STOL AIRCRAFT

FINAL REPORT

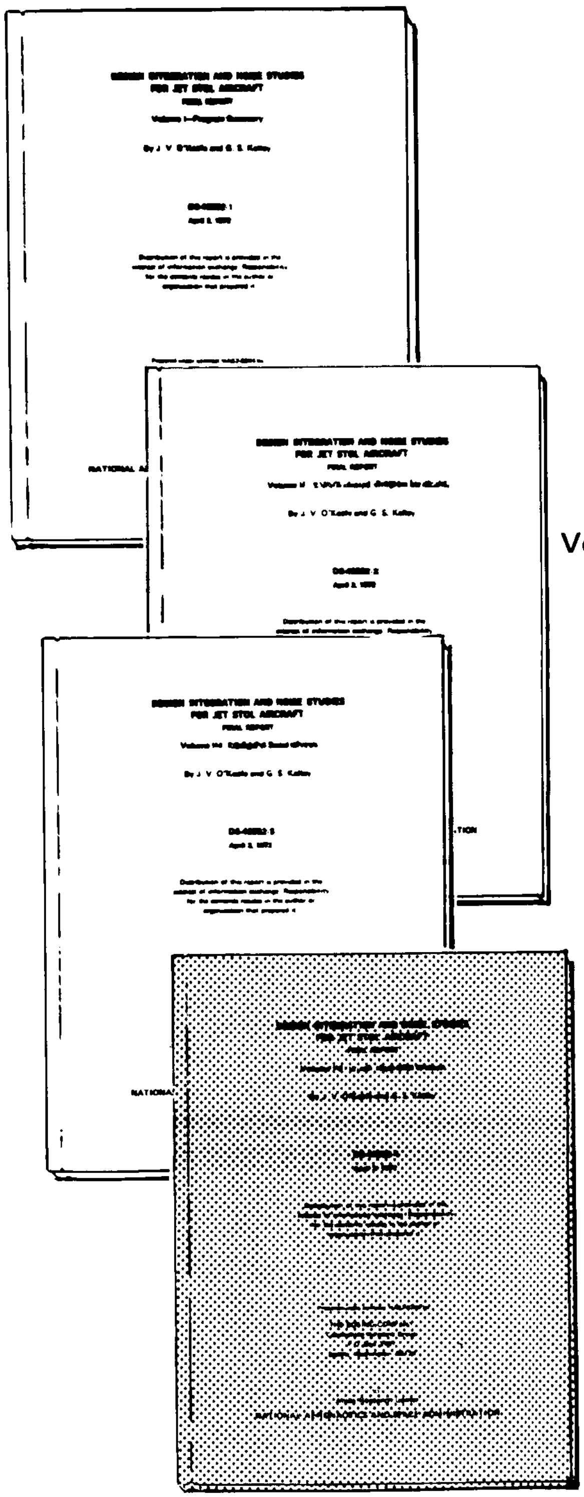

Volume I—Program Summary
CR# 114471
D6-40552-1

Volume II—System Design and Evaluation Studies
CR# 114472
D6-40552-2

Volume III—Static Test Program
CR# 114473
D6-40552-3

Volume IV—Wind Tunnel Test Program
CR# 114474
D6-40552-4

CONTENTS

DESIGN INTEGRATION AND NOISE STUDIES

FOR JET STOL AIRCRAFT

Volume IV—Wind Tunnel Test Program

By T. Wang, F. Wright, and A. Mahal

1.0 SUMMARY

The aerodynamic characteristics of four augmentor wing configurations were evaluated by two-dimensional wind tunnel tests in the 3- by 8-ft Boeing low-speed research tunnel. The purpose is to develop an augmentor wing configuration having a low noise level and good aerodynamic performance during takeoff and landing. Configurations with multielement nozzles, having lower noise and better propulsive characteristics than slot nozzle augmentors, have been developed on the static test rig (see vol. III). These configurations were further developed in the wind tunnel and their performance compared with that of the slot nozzle augmentor flap derived from NASA/DHC design.

The wind tunnel study showed that the multilobe nozzle augmentor flap configuration possesses aerodynamic characteristics comparable to those of the slot nozzle augmentor. Tests at various airspeeds showed that the thrust augmentation properties of an augmentor wing are partially offset by ram drag. In contrast to a plain jet flap, the force coefficients of an augmentor flap cannot be correlated by the nozzle thrust coefficient alone.

The models, having a 16-in. chord and 3-ft span, were tested over ranges of airspeed varying from 0 to 115 kn, primary nozzle to ambient pressure ratio varying from 1.0 to 3.8, and flap deflection varying from 30° to 70°. The results presented are based on the three-component balance measurements, model surface pressures and augmentor exit total pressure data, and measurements related to blowing and air stream parameters.

1.1 CONFIGURATIONS

The principal features of the four augmentor wing configurations are listed below.

Configuration	Type of Primary Nozzle	Flap Chord/ Wing Chord	Flap Area/ Nozzle Exit Area
NASA wing section	Continuous slot	0.35	100
Scaled NASA section	Continuous slot	0.27	50
Lobe nozzle augmentor	Multilobe	0.27	57
Tube nozzle augmentor	Multitube	0.27	50

The two augmentors with slot nozzles are shown in figure 1. The NASA wing section represents a streamwise section of the NASA Ames swept-wing STOL model (ref. 1). As a result of sizing studies presented in volume II, the NASA augmentor flap segments were scaled down to give a 0.27 flap chord and the slot height increased to provide the desired thrust per wing area.

The two augmentors with different multielement nozzles used the same flap segments. The geometry of the lobe and tube nozzles is shown in figure 2 and that of the flap segments in figure 3. The internal contours of the augmentor flap assembly were developed from static rig tests described in volume III. The external contours were designed using a semiempirical method developed in task I and reported in reference 2.

Leading edge geometry is illustrated in figure 1. The 0.15 c leading edge slat was used only on the NASA wing section. The other three configurations incorporated the 0.11 c leading edge flap designed at Boeing for use with leading edge blowing boundary layer control.

For each augmentor configuration, geometry variations to improve the aerodynamic performance were carried out by repositioning model parts at every flap angle. The extent of this process varied from one configuration to another. The effects of the following changes were studied to evaluate configuration sensitivity:

- Flap chord and augmentor mixing length
- Shroud position
- Intake door angle
- Flap coanda position
- Diffuser angle
- Throat area
- Lobe nozzle sealing to reduce ventilation (see fig. 3)
- Wing leading edge geometry
- Wing leading edge boundary layer control (BLC)

1.2 TEST PROGRAM

The wind tunnel tests were accomplished in three separate periods:

Test Period	Test Objective
June 1 to July 20, 1971	To evaluate the aerodynamic characteristics of the two slot nozzle augmentors
January 18 to January 28, 1972	To evaluate the effects of airspeed on the aerodynamic performance of the slot nozzle augmentor at 30° flap angle
February 5 to March 3, 1972	To evaluate the aerodynamic characteristics of the two multielement nozzle augmentors

The test procedure was to carry out geometry optimization and then select the best configuration on the basis of static and $q = 20$ psf force data at a nominal design thrust level (nozzle pressure ratio (NPR) of 2.5 to 2.8). For this configuration, a complete series of constant nozzle pressure ratio and varying angle-of-attack runs was then made. This procedure was repeated for all flap angles tested, except in the case of the NASA wing section.

1.3 TEST RESULTS

1.3.1 Aerodynamic Characteristics

The aerodynamic performance of an augmentor wing depends strongly upon avoiding flow separation from the shroud upper surface. Shroud flow separation tends to increase with flap deflection, angle of attack, and reduction of nozzle thrust coefficient. It has also been found to depend upon intake door angle and shroud and flap position. In general, at $\delta_f = 30°$ and $50°$ complete flow attachment was achieved at the C_j's of interest, but this was not the case at $\delta_f = 70°$. The best data obtained for $\delta_f = 70°$ were with a low shroud position, as shown in figure 3. Representative force and pitching moment data at a thrust coefficient, C_j, of 1.16 are shown in figure 4 for the scaled NASA section and optimum geometry at each flap deflection. The variation of force data with C_j is summarized in figure 5. The shapes of the C_l vs C_j curves indicate that the C_j required for flow attachment is considerably higher than in the case of a plain jet flap (sometimes known as a blown flap or jet augmented flap). The thrust effectiveness* represented by the variation of C_X with C_j at a constant C_l are about 1.1 for $\delta_f = 30°$ and $50°$. The data points at $C_j = 1.8$ in figure 5 correspond to an NPR = 3.5. At that condition, performance was degraded noticeably by the change in flaps-off jet path, which would require a change in flap (coanda) position.

The sensitivity of performance to the flap position relative to the jet path was extensively demonstrated by the results presented in this report. The failure to achieve a reasonable performance level with the NASA wing section, particularly at high flap angles, is attributed to the nonoptimum flap position. The results for the two slot nozzles augmentors are compared in figure 6, which clearly illustrates the performance degradation of the NASA wing section at $\delta_f > 40°$. This configuration was repositioned at $\delta_f = 50°$, and substantial improvements are shown.

For every configuration tested at forward speed, the static reaction was also measured to determine the static thrust augmentation ratio. The significance of this quantity is illustrated by its relationship to aerodynamic performance. In general, increases in static thrust augmentation are manifested in streamwise force data at low flap angles. This is evident in figure 7, where variations of C_X at constant C_l with ϕ are shown for $\delta_f = 30°$ and $50°$. The variation of ϕ for the configurations having the same δ_f is generally due to small differences in throat area, diffuser angle, or flap position. The drag polars, not shown in the figure, are well behaved and do not cross except near stall. The change in streamwise force coefficient at a constant C_l represents a shift in the drag polar. Similar relationships between C_X and ϕ cannot be established at $\delta_f = 70°$.

---

*Thrust effectiveness is defined as the rate of change in streamwise force coefficient with primary nozzle thrust coefficient $\partial C_X/\partial C_j$. It includes both thrust recovery and thrust augmentation.

The above findings from slot nozzle augmentor tests are equally valid for multielement nozzle augmentors. The aerodynamic performance of the lobe nozzle augmentor was compared with that of the tube nozzle augmentor at $\delta_f = 50°$ only. The differences are generally small. Since the lobe nozzle augmentor had significantly lower noise level than the tube nozzle augmentor (see vol. III), the former was extensively developed in the wind tunnel test.

The variation of force coefficients with C_j is shown in figure 8 for the lobe nozzle augmentor. The trends are similar to those shown in figure 5 for the slot nozzle augmentor. A significant improvement was found at $\delta_f = 70°$ when the nozzle ventilation from the lower side was reduced by sealing tape (see fig. 3). Tufts observation indicated that taping improved the flow over the nozzle boattail and the intake door at $\delta_f = 70°$. Taping was not tried at $\delta_f = 50°$, but at $\delta_f = 30°$ it resulted in a small lift increment accompanied by a thrust decrement. The effects of taping on the force coefficients are also illustrated in figure 8.

The aerodynamic performance of the lobe nozzle augmentor compared quite favorably with that of the slot nozzle augmentor at $\delta_f = 30°$ and 70° but was inferior at $\delta_f = 50°$. However, the difference at $\delta_f = 50°$ is expected to become insignificant if nozzle ventilation is restricted. Since nozzle ventilation effects have only been briefly explored, further study is highly recommended in view of their demonstrated effect on aerodynamic performance and potential effect on noise properties.

The effect of leading edge blowing BLC on the aerodynamic performance of an augmentor wing was investigated. The primary effect was to delay stalling and increase maximum lift, as expected. The rate of recovery of the blowing momentum as thrust was generally less than 0.6%. Compared to a thrust effectiveness, $|\partial C_X / \partial C_j|$, of 1.2 for the augmentor primary thrust, leading edge blowing is not an efficient means for thrust augmentation.

1.3.2 Effect of Airspeed Variation

The approach taken to evaluate the thrust augmentation characteristics of an augmentor wing as a function of forward speed is to use the forward speed characteristics of a plain jet flap as the base. The plain jet flap is chosen because its characteristics are well understood, and considerable experience has accumulated in applying wind tunnel data to predict airplane performance. The difference in the forward speed effects for the two configurations forms the basis for modifying the established method used for jet flap airplanes so that it applies to augmentor wing airplanes.

The data addressed to the airspeed effects were taken primarily on typical takeoff configurations, $\delta_f = 30°$, for two reasons: (1) the effect of airspeed on the streamwise force is particularly important during takeoff and (2) the shroud upper surface is relatively free of flow separation.

The configurations included two scaled NASA slot nozzle augmentors with different throat areas, one lobe nozzle augmentor, and one jet flap with slot nozzle. All three configurations have a 0.27 c flap chord.

The results showed that the drag polars at a given C_j are essentially independent of airspeed for the jet flap but not for the augmentor flaps. Typically, the variations of C_X with airspeed at $C_j = 0.8$ and $C_l = 4$ are illustrated in figure 9 for the jet flap and the three augmentor flap configurations. While C_X is essentially constant for the jet flap, it varied substantially with airspeed for the augmentors. However, note that the C_X for the augmentors is more negative (more thrust) than that of the plain jet flap. For each augmentor, a minimum drag occurred at some airspeed between 60 and 80 kn. The variation of C_X, though not the level, is reasonably well approximated by the sum of ram drag and augmented thrust, $2C_q - \phi C_j$, shown in the same figure. The differences between C_X and $2C_q - \phi C_j$ are reasonably (within ±0.01) independent of airspeed, which allows one to predict the performance at various airspeeds based on data taken at static and one forward speed condition.

The fact that static thrust augmentation and entrainment can be used to correlate forward speed data suggests that the ejector internal flow is little affected by airspeed. Both static pressure distribution and augmentor exit total pressure data support this hypothesis.

At a given primary nozzle thrust, the drag increase with forward speed at either constant α or constant C_l was more rapid with the augmentor than with the jet flap. The source of the additional drag experienced by the augmentor has been identified through an analysis of static pressure distribution. Pressure drag of the intake and the shroud was the major contributor.

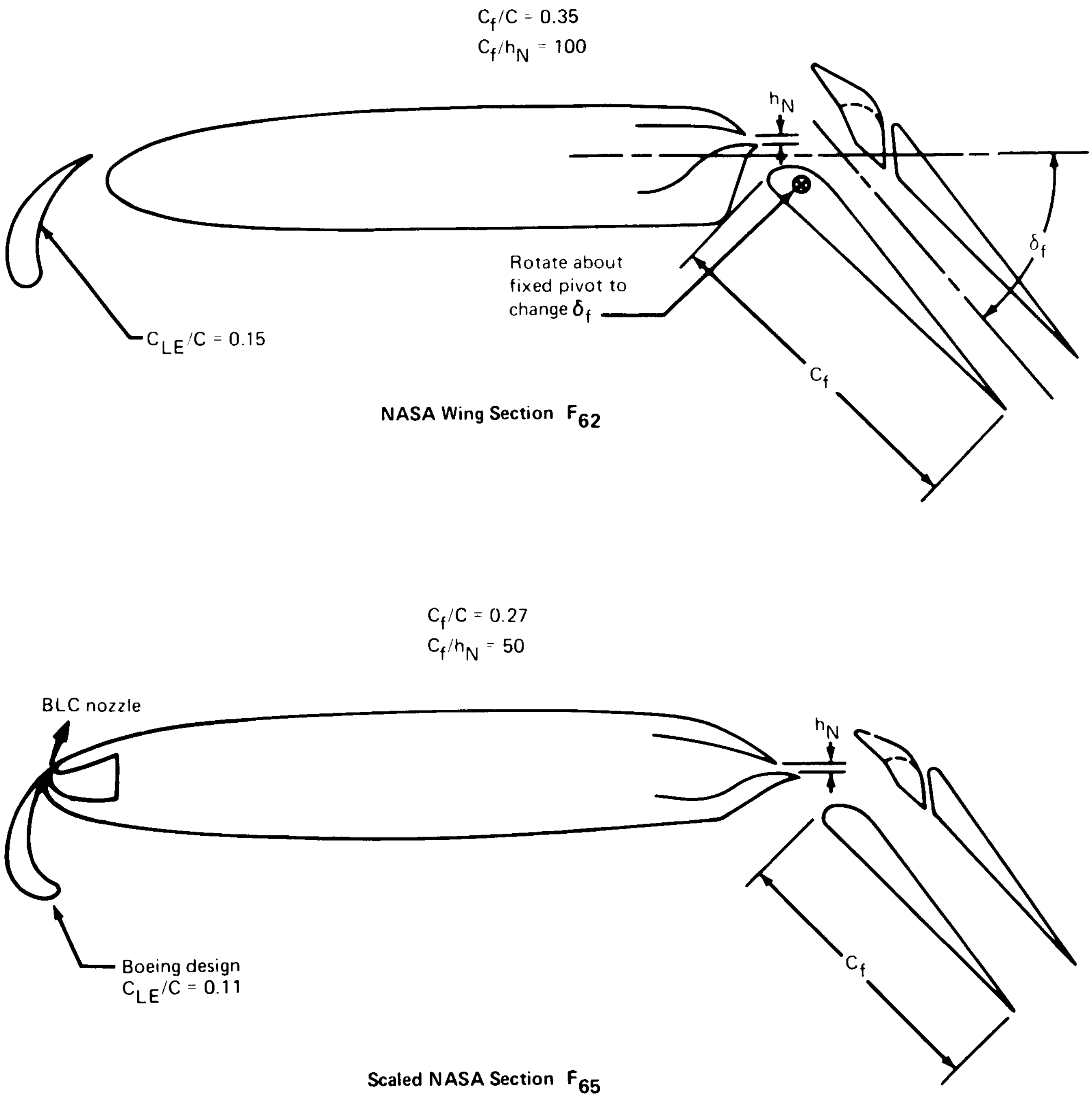

FIGURE 1.—SLOT NOZZLE CONFIGURATIONS TESTED

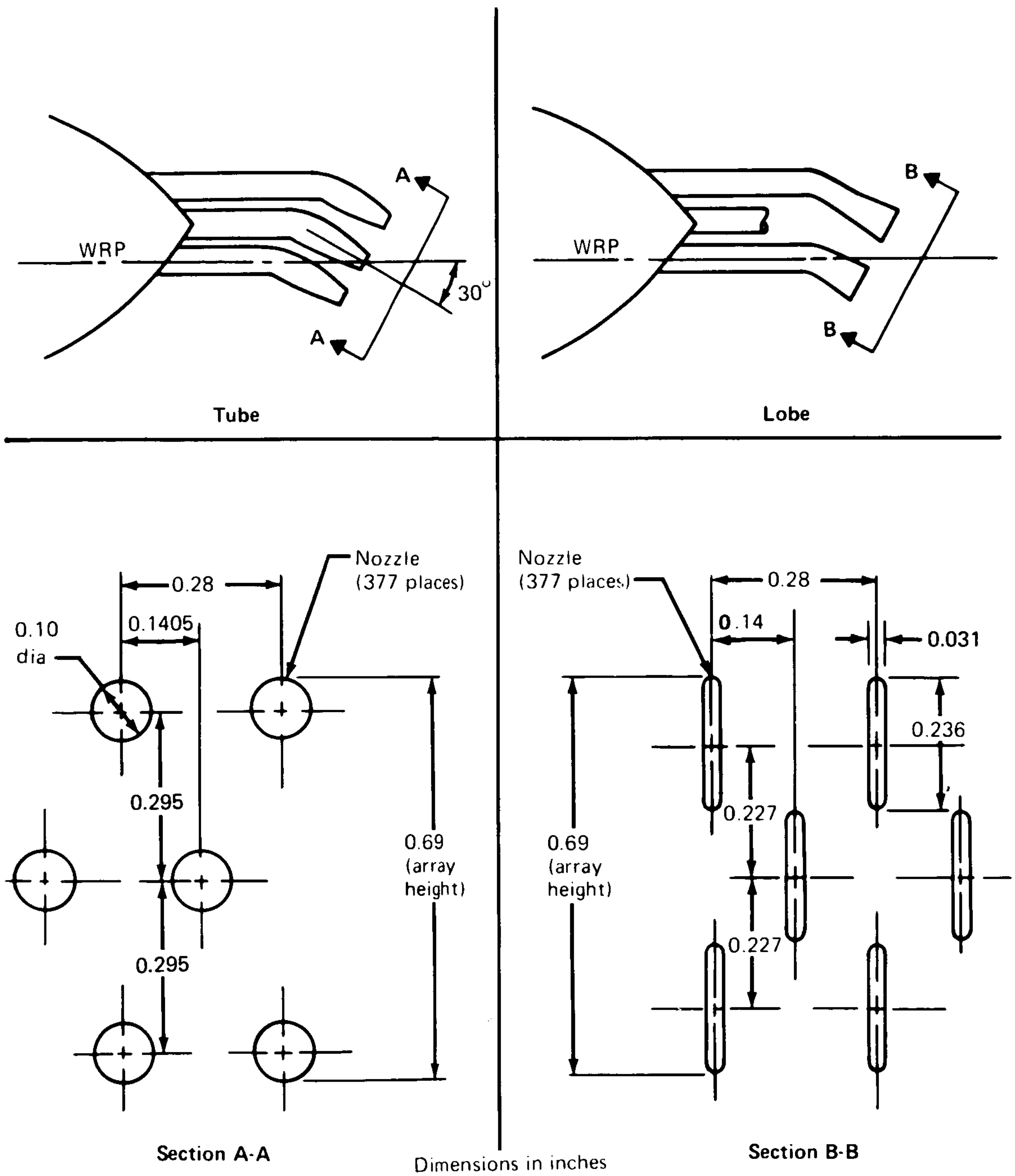

FIGURE 2.– MULTIELEMENT NOZZLE ARRANGEMENT

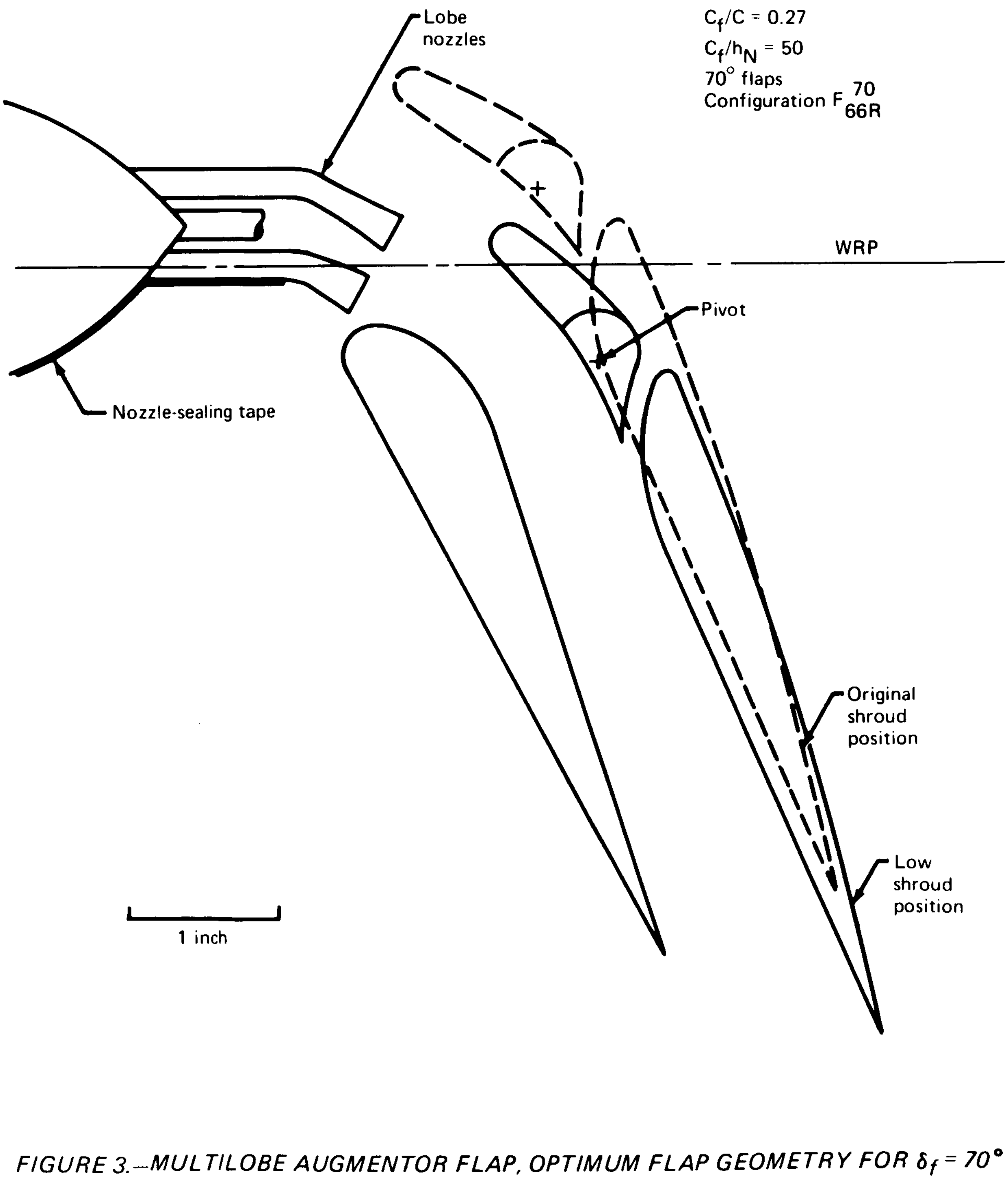

FIGURE 3.—MULTILOBE AUGMENTOR FLAP, OPTIMUM FLAP GEOMETRY FOR δ_f = 70°

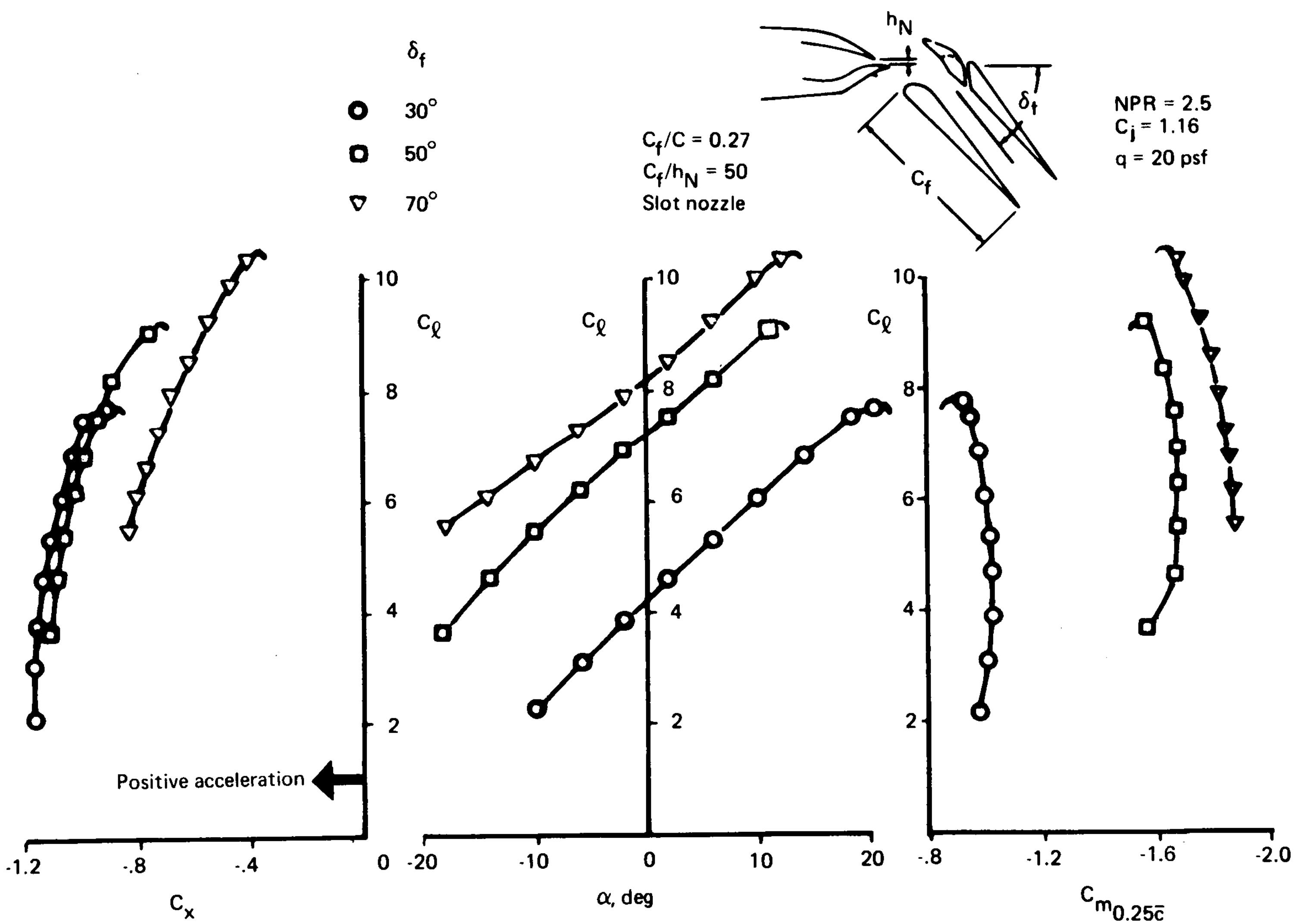

FIGURE 4.— REPRESENTATIVE AERODYNAMIC DATA FOR THE SCALED NASA SECTION AT $C_j = 1.16$

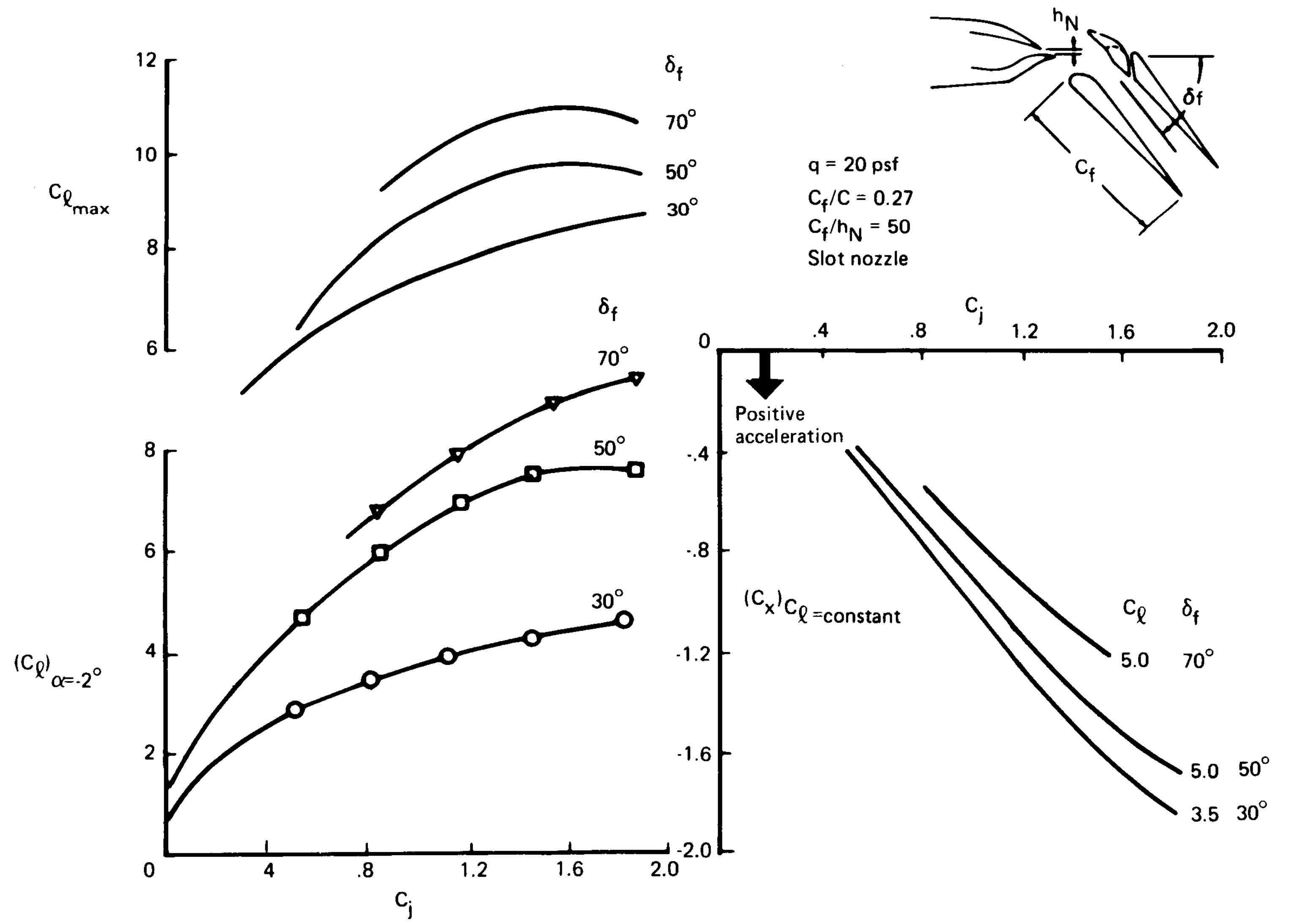

FIGURE 5.– VARIATION OF LIFT AND STREAMWISE FORCE WITH C_j FOR THE SCALED NASA SECTION

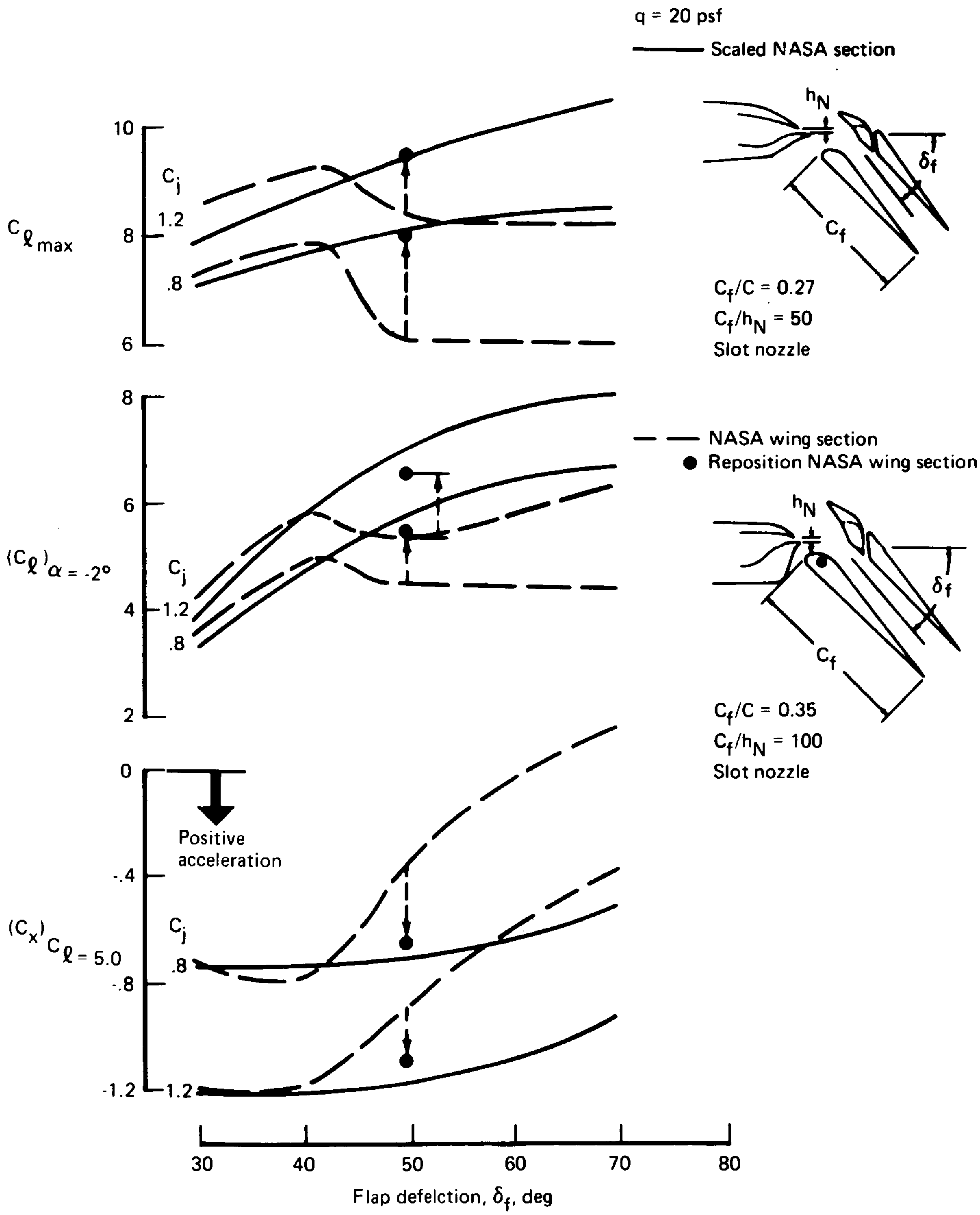

FIGURE 6.—COMPARISON OF FORCE DATA VARIATION WITH δ_f—NASA WING SECTION VERSUS SCALED NASA SECTION

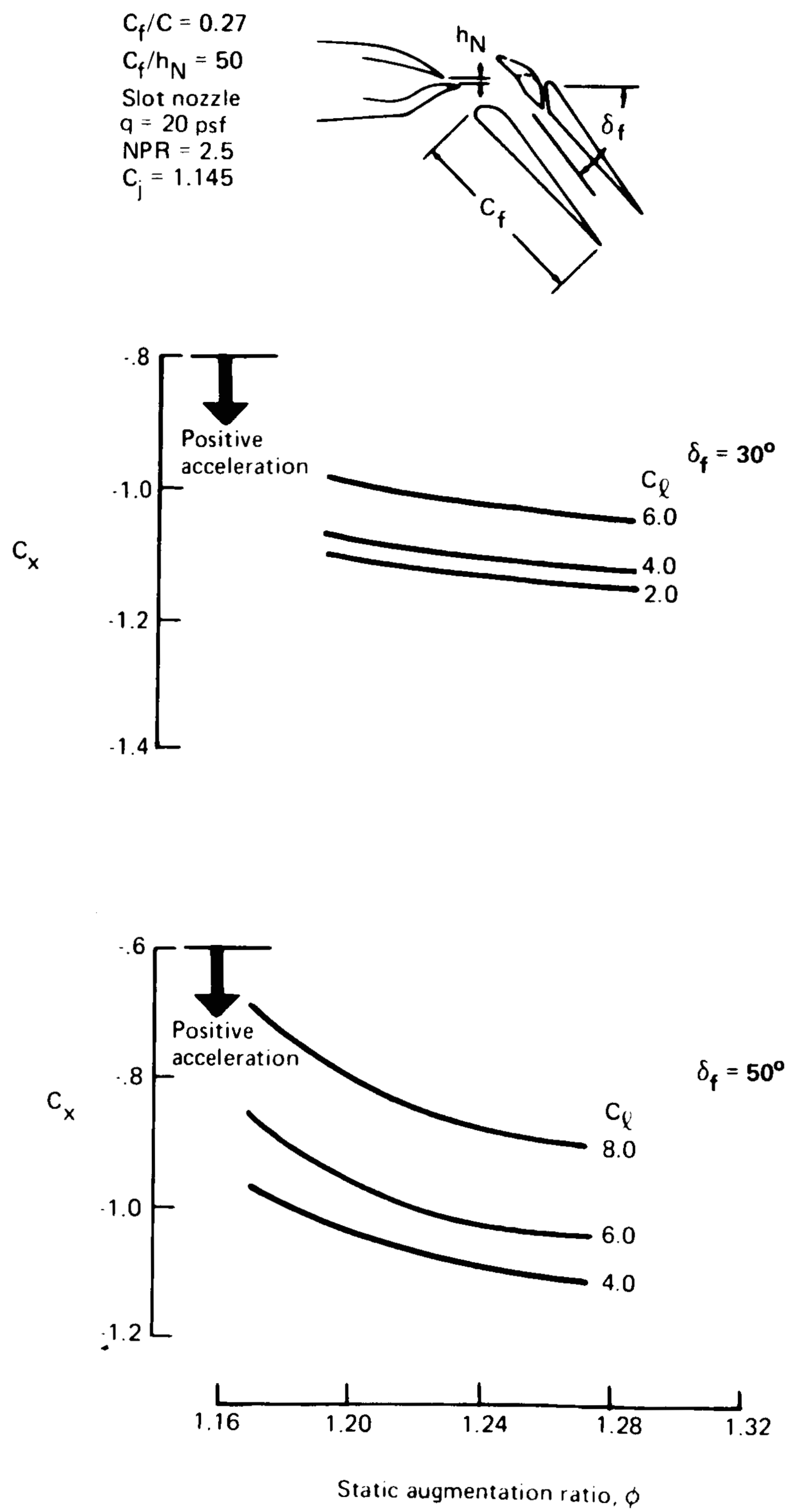

FIGURE 7.—EFFECT OF STATIC THRUST AUGMENTATION ON STREAMWISE FORCE AT FORWARD SPEED

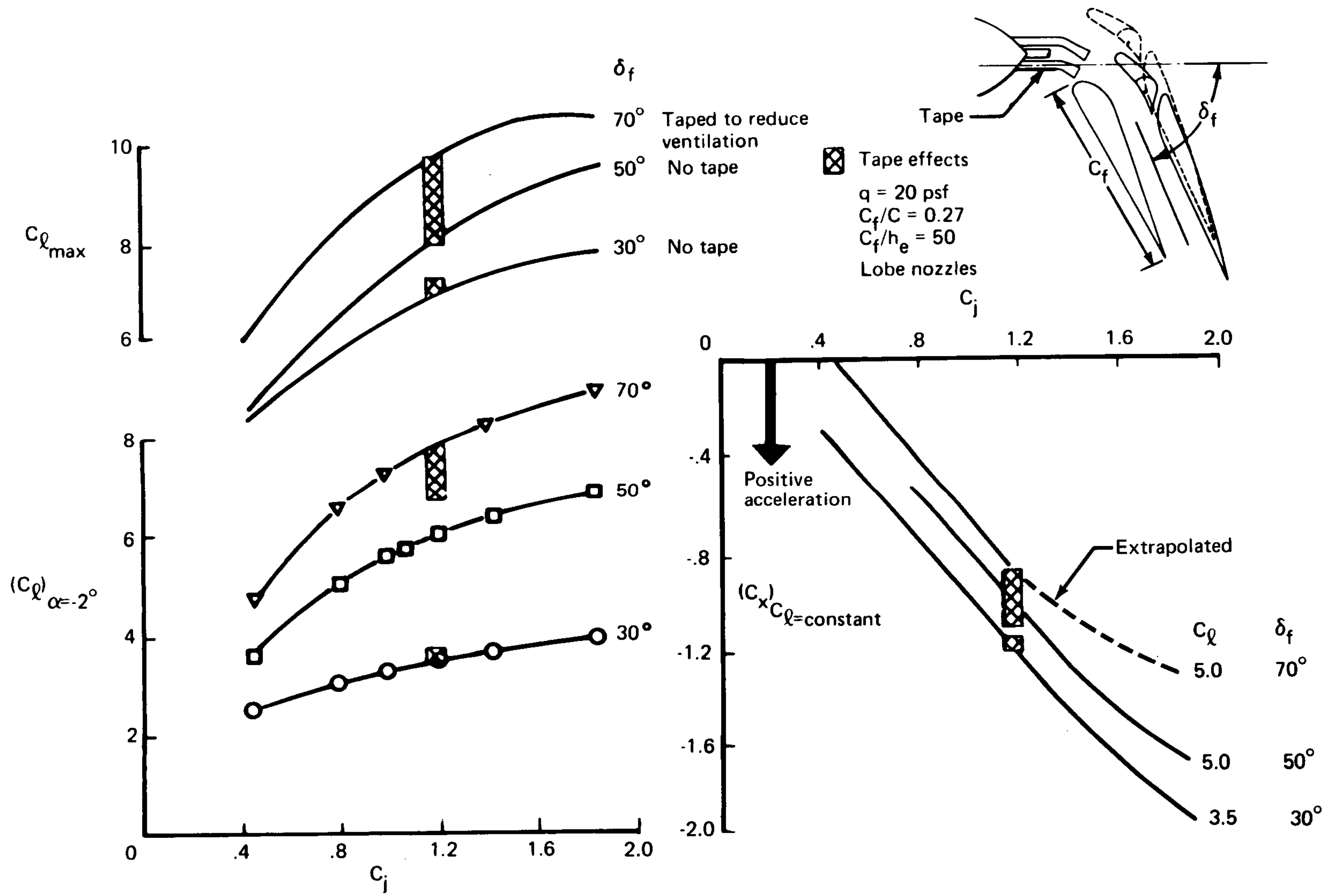

FIGURE 8.—VARIATION OF LIFT AND STREAMWISE FORCE WITH C_j FOR THE LOBE NOZZLE AUGMENTOR FLAP

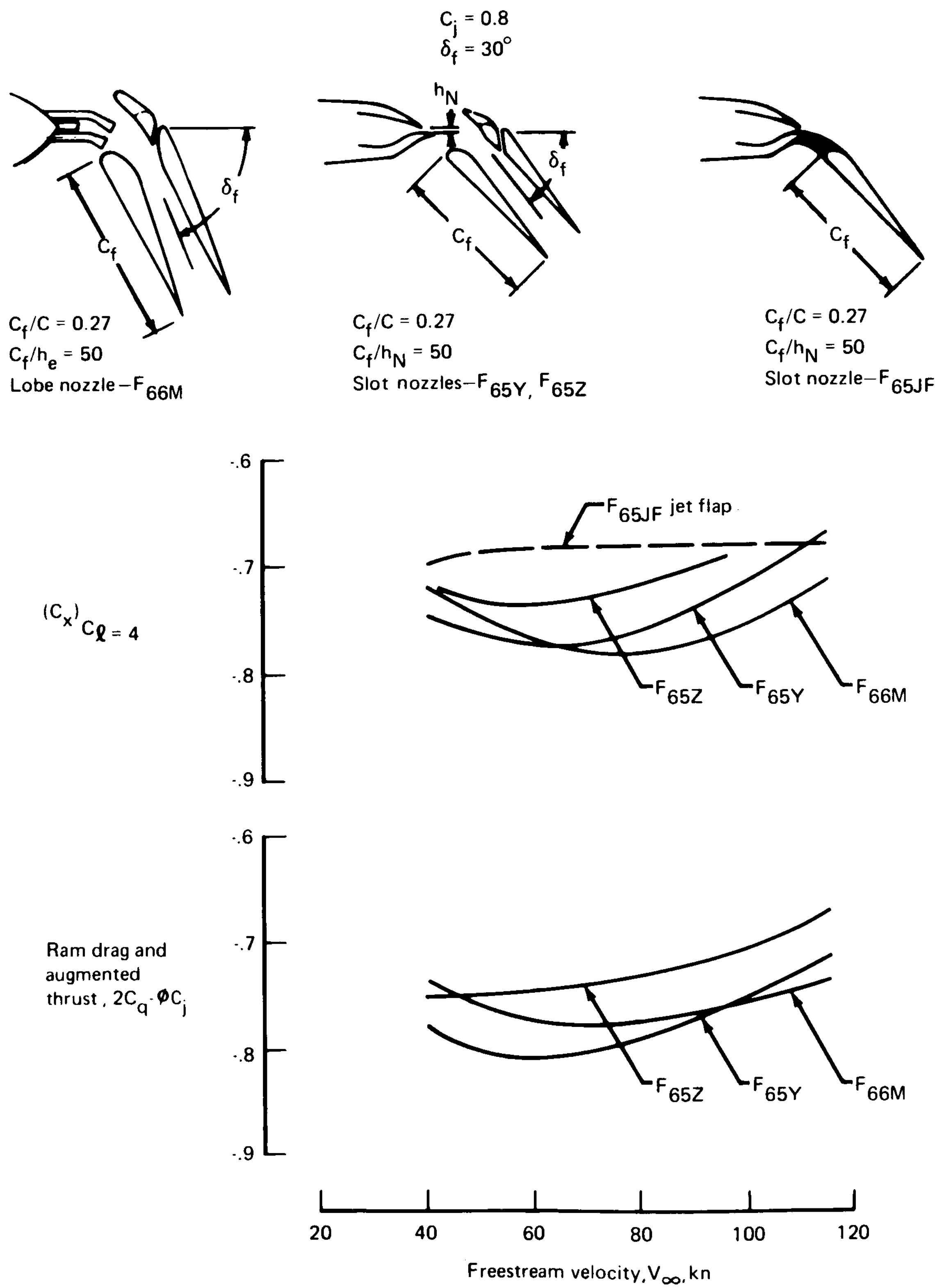

FIGURE 9.—EFFECT OF FORWARD SPEED AT CONSTANT C_j

2.0 INTRODUCTION

The aerodynamic development of the augmentor wing concept has been pursued by NASA and the de Havilland Aircraft of Canada, Ltd. (DHC) for a number of years. Recent emphasis on low noise levels for commercial STOL aircraft has focused attention on the fact that the augmentor wing has all the characteristics of an excellent ejector-type noise suppressor. The present program was initiated to develop, through analysis, design, static rig testing, wind tunnel testing, and design integration studies, an augmentor wing for a jet STOL transport aircraft having maximum propulsion and aerodynamic performance with minimum noise. This program consists of three basic elements:

1) System design and evaluation studies that were conducted to integrate the test results with the airplane design and reported in volume II.

2) Static rig tests to evaluate the noise and propulsion characteristics of various nozzle and flap configurations. The results are reported in volume III.

3) Two-dimensional wind tunnel tests to evaluate the aerodynamic performance of existing and new augmentor flap designs.

Previous experimental investigations were limited to quasi-two-dimensional (refs. 5 and 8) and three-dimensional (refs. 1, 6, and 7) wind tunnel tests of augmentor wing configurations with slot nozzles. The latest of these tests was conducted in the NASA Ames 40- by 80-ft wind tunnel with a swept wing airplane model (ref. 1). The results of this test formed the basis for the present system design studies. While the augmentor wing with slot nozzle demonstrated adequate aerodynamic performance, it would not meet the noise requirements for commercial STOL airplanes. New configurations with multielement nozzles were designed using a potential flow method described in reference 2 and developed during static rig tests. These configurations and those developed by NASA and DHC with slot nozzles were tested two dimensionally in the Boeing 3- by 8-ft wind tunnel. The effects of airspeed, nozzle thrust, leading edge flap geometry and blowing BLC, and variations in position and orientation of the augmentor flap elements were evaluated. The results are reported in this volume.

3.0 SYMBOLS AND ABBREVIATIONS

BLC	boundary layer control
BRWT	Boeing research wind tunnel
b	span, ft
C_μ	blowing momentum coefficient
C_D	drag coefficient, D/qS
C_d	sectional (local) drag coefficient
C_j, C_J	momentum or thrust coefficient, $c_j = \frac{\text{measured nozzle static thrust}}{qS} \times \frac{\dot{w} \text{ at } q \neq 0}{\dot{w} \text{ at } q = 0}$; all quantities measured at the same NPR
C_L	lift coefficient (L/qS)
C_l	sectional (local) lift coefficient
C_m	pitching moment coefficient, M/qSc
$C_{m_{0.25\,c}}$	pitching moment coefficient about quarter chord
C_P	pressure coefficient, $(P - P_\infty)/q$
C_q	mass flow coefficient, $\dot{w}/g\rho V_\infty S$
C_V	nozzle velocity coefficient
C_X	streamwise force coefficient
℄	reference centerline
c	wing (flaps up) chord, in.
$\bar{c}$	mean aerodynamic reference chord, in.
DHC	de Havilland Aircraft of Canada
F	engine thrust or augmentor primary nozzle thrust
F_R	resultant force, lb
g	gravitational constant, ft/sec^2

h_E	equivalent slot nozzle exit height, in.
h_N	nozzle height, in.
L	total lift ($L = C_L qS$), lb
LE	leading edge
l_e	augmentor exit height, in. (see fig. 17)
l_T	augmentor throat height, in.
l_Z	flap positioning dimension, in. (see fig. 17)
M	Mach number or pitching moment
M_j	jet Mach number
M_∞	freestream Mach number
NPR	nozzle pressure ratio
P	static pressure
P_A	atmospheric pressure, psf
q	dynamic pressure, psf
R_N	Reynolds number
S, S_W	wing reference area,
STOL	short takeoff and landing
T	thrust, lb
V_∞	freestream velocity
W	airplane or reference weight, lb
WCP	wing chord plane
$\dot{w}$	air weight flow, lb/sec
X	axial distance (downstream), in.
Y	spanwise coordinate, in.

Z	vertical coordinate, in.
z	flap positioning dimension, in. (see fig. 17)
α	wing angle of attack, deg
Δ	finite change in some parameter
δ	control surface deflection, deg
δ_f, δ_F	flap deflection angle with respect to the wing chord plane, deg
δ_N	flaps off primary jet deflection angle with respect to wing-chord plane, deg
θ	reference angle (diffuser or intake door), deg
θ_{diff}	augmentor diffuser angle, deg
θ_I	intake door reference angle, deg
ξ	skew factor of velocity profile
ρ	density, lb-sec^2/ft^4
ϕ	static augmentation ratio, $\frac{\text{measured resultant force, flaps on}}{\text{measured resultant force, flaps off}}$

Subscripts:

A, airpl	airplane
f	flap
E	equivalent, effective
LE	leading edge
j	jet
max	maximum
min	minimum
sec	secondary

∞	ambient, undisturbed condition
pri	primary
s	shroud
w	wing

4.0 TEST PROGRAM AND RESULTS

4.1 TEST PROGRAM

4.1.1 Facility and Installation

The test was conducted in the 3- by 8-ft test section of the Boeing low-speed research tunnel. The wing model, with 16-in. chord and 36-in. span, was mounted between two circular end plates of 3-ft diameter. These end plates were made completely flush to the sidewalls, free to rotate for angle-of-attack change, and mounted on the three-component balance pedestal. To ensure two-dimensional flow over the model, blowing boundary layer control was provided on sidewalls and end plates. Figure 10 shows the test section with model installed. The locations of BLC nozzles are indicated in figure 11.

4.1.2 Models

Four configurations of augmentor flap nozzles were tested. Two were slot nozzles used as a baseline, and two were multielement configurations developed on the static rig (vol. III) as optimum designs from the standpoint of noise and thrust augmentation. The four configurations were tested with the same midchord model section, but different combinations of leading and trailing edge sections.

The two augmentors with slot nozzles are shown in figure 12. The NASA wing section represents a streamwise section of the Ames swept-wing STOL model (ref. 1). As a result of sizing studies presented in volume II, the NASA section augmentor flap segments were scaled down to give a 0.27 c flap chord and increased slot height to give the desired thrust per wing area.

The two multielement nozzle augmentor flap systems (fig. 13), one of which had tube (circular) nozzles and the other lobe (rectangular) nozzles, were sized to meet the nominal criteria of the scaled NASA section (0.27 c flap chord and $C_f/h_E = 50$). Because of the difficulty of manufacturing the small nozzles to close tolerances, the nozzle areas were smaller than nominal. C_f/h_N (or C_f/h_E, using equivalent nozzle height) thus become 52 for the tube nozzles and 57 for the lobe nozzles. The value noted on the data plots, however, is the nominal value, $C_f/h_E = 50$. The nozzles were built with a jet turning angle of 30°, which previous tests showed to be more efficient for large flap deflections. The array area ratio (AAR) is the ratio of the enclosed area of the nozzle array to the nozzle area. The design AAR is 8, but because the manufactured nozzles were smaller than design, the AAR became 8.2 for the tube nozzles and about 9 for the lobe nozzles. The two nozzle arrangements are shown in figure 14. The internal contours of the augmentor flap assembly were developed from static rig tests described in volume III. The external contours were designed using a semiempirical method developed in task I and reported in reference 2.

Leading edge geometry is illustrated in figures 12 and 13. The 0.15 c leading edge slat was used only on the NASA wing section. The other three configurations incorporated the 0.11 c leading edge flap designed at Boeing for use with leading edge blowing boundary layer control. With the 0.11 c flap, a convergent, continuous slot ($h_N = 0.010$ in.) nozzle was incorporated for blowing nearly tangentially to the surface at the leading edge of the cruise airfoil.

4.1.3 Test Procedure

The test procedure was to carry out geometry optimization and then select the best configuration on the basis of static and q = 20 psf force data at a nominal design thrust level (NPR = 2.5 to 2.8). For the best configuration, a complete series of constant nozzle pressure ratio and varying angle-of-attack runs was then made. This procedure was repeated for every flap angle, except in the case of the NASA wing section.

Generally, nozzles were calibrated at the beginning and end of each augmentor wing test. The calibration included thrust and mass flow measurement at various nozzle plenum pressures. Spanwise uniformity of slot nozzle jet flow was checked by using a pitot probe traversed along the nozzle exit.

To examine flow separation over the shroud and at the intersection of the wing and end plate, tufts were attached at all interesting locations. The blowing rate of BLC at the intersection of wing and end plate required for two-dimensional flow was determined by observation of the tufts. Because three to four BLC nozzles were installed on each end plate, careful adjustment was required to obtain the best combination of nozzles pressures.

4.1.4 Test Data

The force and moment data were corrected for weight tares, airline tares, turntable BLC thrust, and solid blockage. Jet boundary corrections and jet blockage corrections were not applied. Standard two-dimensional wind tunnel wall corrections (vol. III), excluding wake blockage, were used. Test section dynamic pressure was corrected for front wall blowing.

Lift, drag, and pitching moment data were recorded using an external strain-gage balance located below the test section. The static calibrations of the force balance demonstrated repeatability of ±0.25% of the maximum model loads.

The majority of the wind-on data were obtained at a tunnel dynamic pressure of 20 psf with a corresponding Reynolds number, based on a chord of 16 in., of 1.1×10^6. The moment reference point is the 0.25 chord point of the wing reference chord. The basic force and moment data include both direct and induced thrust effects. All the data presented, except where noted, are without leading edge blowing.

The near-stall region of the two-dimensional augmentor wing model was characterized by flow unsteadiness and intermittent flow separation and reattachment. Consequently, it was difficult to obtain valid recorded balance data at the stall point. Balance data were recorded as close to stall as possible, and then continuous online plotter traces of the stall were made. Hence, the maximum lift coefficients presented have a degree of uncertainty associated with them, but it is thought to be small.

A high degree of flow two dimensionality was achieved with carefully tailored wall and end plate blowing BLC. Figure 15 shows a photograph of typical surface flow pattern developed with china clay on the repositioned NASA wing section. The test condition is for $C_j \approx 1.5$, $\alpha = -10°$, $\delta_f = 50°$, and a $C_l \approx 6.3$. Lines of flow separation are evident near the trailing edges of the leading edge slat and augmentor intake and the primary nozzle boattail area.

These lines are remarkably straight and parallel to the spanwise axis. A chordwise strip at 1/4 span was free of china clay to prevent clogging of static orifices. The effect of end plate blowing appears to be confined to 1 to 2 in. from the end plate.

A comparison of static thrust augmentation between a static rig model and a wind tunnel model* is shown in figure 16. The wind tunnel model is one-fifth the size of the static rig model. The static thrust augmentation ratio for the optimized configurations in the two test setups generally agreed well, but the positioning of the two "optimum" configurations, particularly the flap segments relative to the nozzle lip, was quite different. Similar comparisons cannot be made for configurations with multilobe nozzles, since there were several differences in lobe geometry of the two models.

4.2 AERODYNAMIC EVALUATION PARAMETERS

4.2.1 Geometry

Experience has shown that the aerodynamic performance of an augmentor flap is closely related to its static thrust augmentation characteristics. At static condition, the deflected augmentor flap may be considered a curved ejector. Therefore, it is not surprising that the results from the static test rig (vol. III) have shown that the static thrust augmentation ratio is a function of all the geometric parameters which govern the entrainment and mixing of the ejector flow. These parameters include:

- Throat area ratio (l_T/h_E)
- Mixing length (C_f/h_E)
- Diffuser angle
- Inlet geometry
- Location of primary nozzle exit
- Primary nozzle geometry

In addition to these parameters, the efficiency of a curved ejector depends upon the proper location of shroud surfaces relative to the primary jet. An empirical method has been developed by DHC (ref. 4) for the slot nozzle augmentors to predict a near-optimum position as a function of flaps-off jet path, flap coanda radius, and the desired jet deflection. The coanda surface location is characterized by l_Z and Z, defined in figure 17.

*The wind tunnel model data were not generated under the present contract. The augmentor flap segments shown have the same internal contour as flap A referred to in volume III of this report.

4.2.2 Thrust Coefficient and Augmentation Ratio

Thrust augmentation can only be identified at static condition. The static thrust augmentation ratio, ϕ, is defined as the measured resultant force of the augmentor wing divided by the measured resultant force with the flap system removed.

The significance of ϕ is illustrated by its relationship to aerodynamic performance. In general, increases in static thrust augmentation are manifested in streamwise force data at low flap angles. This is evident in figure 18, where variations of C_X at constant C_l with ϕ are shown for $\delta_f = 30°$ and $50°$. The variation of ϕ for the configurations having the same δ_f is generally due to small differences in throat area, diffuser angle, or flap position. The drag polars, not shown in the figure, are well behaved and do not cross except near stall. The change in streamwise force coefficient at a constant C_l represents a shift in the drag polar. Similar relationships between C_X and ϕ cannot be established at $\delta_f = 70°$.

The thrust coefficient, C_j is a primary parameter for correlating performance of powered lift systems. It is based on static calibration data of the primary nozzle without the flap system, and adjusted by the ratio of actual primary nozzle flow rate at forward speed to the calibration flow rate.

4.2.3 Lift and Streamwise Force Coefficients

The critical periods involving high noise levels occur during takeoff and landing. The performance of the various augmentor configurations was compared under conditions corresponding to the local wing lift coefficient, C_l, and flap momentum coefficient, C_j, expected during these conditions.

For the takeoff flap deflection, $\delta_f = 30°$, the streamwise force coefficient, C_X was generally evaluated at a constant C_l of 3.5. This local C_l was estimated from the following representative airplane takeoff conditions:

$V = 90$ kn

$W/S = 88$ lb/ft^2

$C_J/C_L = 0.28$

The local coefficient was estimated as follows:

$$C_{l_{local}} = C_{L_{airpl}} \times \frac{C_{l_{local}}}{C_{L_{airpl}}} = 3.2 \times 1.1 = 3.5$$

Furthermore, the equivalent two-dimensional C_j is estimated to be:

$$C_{j_{2\text{-}D}} = C_{J_{airpl}} \times \frac{\text{thrust through flap}}{\text{total fan thrust}} \div \frac{\text{flapped wing areas}}{\text{total wing area}}$$

$$= 0.9 \times 0.85 \div 0.72 = 1.06$$

The effects of configuration changes on C_l were evaluated at constant α. An angle of -2° was selected as representing the wing local angle of attack at the selected takeoff condition. These conditions are illustrated with representative two-dimensional data in figure 19.

For reasons similar to those given for the takeoff case, the higher flap deflections (δ_f = 40°, 50°, and 70°) were evaluated at conditions corresponding to the airplane on approach. The streamwise force coefficient, C_X, was evaluated at a constant C_l of 5.0 and the C_l data were evaluated at a constant α of -2°. These criteria were derived from a representative airplane approach condition where:

V = 76 kn

W/S = 85 lb/ft^2

C_J/C_L = 0.12

The equivalent two-dimensional C_j is estimated as:

$$C_{j_{2\text{-}D}} = C_{J_{airpl}} \times \frac{\text{thrust through flap}}{\text{total fan thrust}} \div \frac{\text{wing area flapped}}{\text{total wing area}}$$

$$= 0.55 \times \frac{0.85}{0.72} = 0.65$$

The sectional lift is given by:

$$C_{l_{local}} = C_{L_{airpl}} \times \frac{C_{l_{local}}}{C_{L_{airpl}}} = 4.5 \times 1.1 = 5.0$$

These conditions are illustrated with representative two-dimensional data in figure 20. It should be noted that the large negative values of C_X are due to the absence of induced drag.

Since the configuration changes in most cases show effects on lift and drag that vary with lift level due to shroud flow separation at high flap deflection, drag polars and C_l vs α curves are instructive. These data are generally shown for an NPR of about 2.5, as indicated by the system design studies. However, some variation was necessary to offset minor differences in nozzle area.

Although the various configurations are evaluated on the above criteria, the variation of maximum lift coefficient, $C_{l_{max}}$, is considered important. Where primary nozzle or augmentor configuration has a significant effect on the wing upper surface pressure distribution, $C_{l_{max}}$ may be expected to vary. Variations of $C_{l_{max}}$ have been evaluated both with respect to configuration changes and C_j changes.

4.3 SLOT NOZZLE AUGMENTOR FLAP CONFIGURATION TEST RESULTS

4.3.1 Principal Results

4.3.1.1 NASA Wing Section

Flaps-off nozzle calibration results are shown in figure 21. The nozzle losses are about 4%, and remained fairly constant with NPR. The jet deflected 11° down from the wing chord plane at NPR less than 3.0. It then increased with NPR and reached about 16°at an NPR of 3.5. This change has a significant effect on both static thrust augmentation and aerodynamic data, since it alters the effective coanda position.

This augmentor wing model was tested with four flap deflections (30°, 40°, 50°, and 70°) by rotating the augmentor flap assembly about a fixed pivot as in the NASA-Ames model. The intake door angle was set according to NASA test results (ref. 1). These configurations are referred to as the baseline configurations. Typical aerodynamic data at a C_j of 0.77 are shown in figure 22. Variations of $C_{l_{max}}$, C_l at $\alpha = -2°$, and C_X at constant C_l, with C_j, are shown in figure 23. The performance of the baseline configuration at $\delta_f = 50°$ and 70° was inferior to that at $\delta_f = 40°$. Similar trends are seen in the static augmentation data shown in figure 24.

Comparing the actual coanda position with the recommended position based on DHC experience (ref. 4), it became obvious that the flap coanda surface was about 0.05 in. too low at the high flap deflections (50°and 70°) and about 0.1 in. too high at $\delta_f = 30°$. Because of the time limitation, a partial geometry optimization process was carried out at $\delta_f = 50°$ only. The final setting, known as the repositioned configuration, incorporated a number of changes as illustrated in figure 25. Large improvements were obtained at both static and forward speed conditions, as shown in figures 22 through 24.

Because of turning loss, the static thrust augmentation is expected to decrease with increasing δ_f. The fact that ϕ values for the repositioned configuration at $\delta_f = 50°$ exceeded those for the baseline configuration at $\delta_f = 30°$ and 40° indicates the improvement potential at these lower angles. The values of ϕ for the repositioned configuration compared well with results published in reference 5 for a similar configuration.

The performance of the NASA wing section and the scaled NASA section are compared and discussed in section 4.3.2.

4.3.1.2 Scaled NASA Section

Flaps-off nozzle calibration results are shown in figure 26. The flow characteristics for this nozzle are similar to those shown in figure 21 for a narrower slot nozzle. The losses for the wider nozzle are about 3%, compared to 4% for the narrower nozzle. The jet deflection was 16°up to an NPR of 3.0 and increased to 25°at NPR = 3.5.

At each of the flap angles, 30°, 50°, and 70°, the model parts were repositioned to find the best configuration. For the final configurations, data at $C_j = 1.16$ are shown in figure 27 and variations of $C_{l_{max}}$, C_l at $\alpha = -2°$, and C_X at constant C_l, with C_j are shown in figure 28.

At $\delta_f = 70°$, the entire optimization process was devoted to minimizing flow separation over the shroud. Lowering the shroud as shown in figure 29 proved to be the only effective way. Thus, the results presented for $\delta_f = 70°$ are generally for the low shroud position. The effect of shroud position is discussed in section 4.3.2.

A unique characteristic of the augmentor flap is the fact that the increase in measured upstream force on the model can exceed the increase in primary nozzle thrust. This is apparent in figure 28, where the $|\partial C_X / \partial C_j|$ slopes, for $\delta_f = 30°$ and $50°$ are about 1.2.

The C_j required for flow attachment was determined on the basis of tuft observation. At $\delta_f = 50°$, the value is about 0.55, roughly six times that required for a typical plain blown flap. With the flow fully attached, the lift levels are in reasonable agreement with theoretical values (ref. 2).

The static thrust augmentation data of the scaled NASA section are presented in figure 30. At all three flap deflections, ϕ decreased with increasing NPR. The rate of change increased between NPR of 3.0 and 3.5 because of the change in flaps-off jet deflection. Values of ϕ for $\delta_f = 30°$ and $50°$ were similar; a value of 1.28 was achieved at NPR = 2.5. This is about 0.09 less than the corresponding value for the repositioned NASA wing section. The difference in ϕ resulting from the difference in the mixing length parameter, C_f/h_N, agrees well with ejector theory prediction.

4.3.2 Configuration Sensitivity Studies

The more significant effects of the geometric parameters introduced in section 4.2 are discussed in this section. Most of the data presented in this section were taken during the geometry optimization process.

4.3.2.1 Flap Chord and Mixing Length Ratios

Force data of the two slot nozzle augmentor flap configurations are compared in figures 31, 32, and 33. The two configurations differ in leading edge geometry and the flap chord and mixing length ratios, C_f/c and C_f/h_N. Results discussed in section 4.3.2.6 showed that the difference in leading edge geometry affected only $C_{l_{max}}$, so that the differences in C_X at constant C_l and C_l at $\alpha = -2°$ may be attributed to the effects of flap chord and mixing length ratio. A lift increment is expected for an increase in flap chord ratio, and an upstream force increment is expected with an increase in mixing length if it improves static thrust augmentation. The comparison in figures 31 through 33 showed that at $\delta_f = 30°$ the NASA wing section performed slightly better than the scaled NASA section, but at 50° even the repositioned configuration did not perform as well. Moreover, the relationship between ϕ and C_X at constant C_l discussed in section 4.2.2 does not hold in this comparison. These discrepancies have not been adequately explained from the available data. It is generally felt that the characteristics of the NASA wing section have not been adequately explored by extensive geometry optimization. However, this is not the objective of this study. The reason for testing the NASA wing section was to relate the performance of other configurations to this one, which was used in the large-scale three-dimensional wind tunnel test (ref. 1) and provided aerodynamic data used in the system integration studies. The emphasis in this study was to develop new configurations that meet the requirements derived from system design studies (vol. II).

The comparisons discussed above suggest that the wing sectional performance of the Ames phase VI model (ref. 1) was probably inferior to the performance of the scaled NASA section at flap angles above 50° and superior at angles below 50°.

4.3.2.2 Augmentor Shroud Position

The effect of shroud position on the force data is shown in figure 34 for $\delta_f = 70°$ and 50°. Lowering the shroud produced a large performance improvement at $\delta_f = 70°$ but a slight degradation at $\delta_f = 50°$.

At $\delta_f = 70°$, flow separation from the shroud upper surface persisted for all the configurations with high shroud position. The shroud was lowered in steps to the position shown in figure 29 before flow separation was eliminated at a reasonable C_j.

The static augmentation ratio decreased by about 0.20 at both flap deflections when the shroud was lowered. The typical effect of shroud position on ϕ is illustrated in figure 30 for $\delta_f = 70°$. At 50°, this effect contributed to changes in aerodynamic performance as discussed in section 4.2.2.

4.3.2.3 Augmentor Intake Door Angle

The flow conditions which exist over the upper surface of the intake and shroud were found to be sensitive to intake door angle, particularly at high flap deflection. Figure 35 presents lift and drag for two different intake door angles with the 0.27 c augmentor at $\delta_f = 70°$. For high nozzle thrust coefficients the more open intake door setting resulted in better performance; the opposite was true at low values of C_j. Sensitivity to intake door angle is partly due to the sharp leading edge of the door, which requires that the stagnation point be very close to the door leading edge to avoid flow separation. Although the static augmentation is higher with the wider intake door opening, shroud flow separation at low values of C_j tends to negate this advantage.

4.3.2.4 Flap Coanda Position

Static augmentation ratio is a strong function of the positioning of the flap with respect to the nozzle flow. Figure 36 shows the variation in augmentation ratio of the 0.27 c flap at $\delta_f = 30°$ as a function of the nondimensional vertical positioning of the flap. These data indicate that relatively small changes in the Z vertical distance have a large effect on augmentation ratio. The change in ϕ is reflected in the change in C_X, as shown in figure 18.

4.3.2.5 Augmentor Diffuser Angle

The static augmentation ratio is a function of the flap diffuser angle. If the diffuser angle is made too large, flow separation occurs and ϕ decreases. This point is illustrated by the data presented in figure 36 for the 0.27 c flap at $\delta_f = 30°$. Note that ϕ starts to decrease after a diffuser angle of 5° is reached. The effects of diffuser angle on ϕ and drag polars at q = 20 psf are shown in figure 37 for the NASA wing section with repositioned 50° flap. A 2° reduction in diffuser angle resulted in 5% to 10% improvement in C_X.

4.3.2.6 Wing Leading Edge Geometry

With a conventional flapped airfoil, a slotted leading edge flap generally produces higher drag and maximum lift than a sealed one. Figures 38 and 39 present some results of the effects of leading edge flap geometry on the lift, drag, and pitching moment of the scaled NASA augmentor flap at $\delta_f = 30°$. The results showed the change in maximum lift which can be attributed to both the geometry and the chord change. The change in drag is insignificant.

4.3.2.7 Wing Leading Edge Boundary Layer Control

The effects of leading edge blowing BLC on the lift, drag, and pitching moment of the 0.27 c flap at δ_f 30°, 50°, and 70° are shown in figures 40, 41, and 42, respectively. It is seen that leading edge BLC significantly increased the maximum lift coefficient, but had a significant effect on lift only at low angles of attack at $\delta_f = 70°$. The nose-down pitching moment increased with leading edge blowing, particularly at $\delta_f = 70°$. Drag decreased as a result of added momentum from leading edge blowing. Figure 43 shows maximum lift coefficient and thrust recovery, $(\Delta C_X)_{const\ C_l}/C\mu_{LE}$, as a function of leading edge blowing momentum coefficient for $\delta_f = 30°$, 50°, and 70°. Maximum lift continued to increase as the leading edge blowing was increased, but the blowing effectiveness diminished at $C\mu_{LE} > 0.10$. The ratio $(\Delta C_X)_{const\ C_l}/C\mu_{LE}$, indicative of the leading edge blowing thrust recovery, increased with $C\mu_{LE}$ at $\delta_f = 50°$ and 70°, but at $\delta_f = 30°$ a maximum exists at $C\mu_{LE} \approx 0.10$. Thrust recovery is generally less than 60%, which is comparable to values experienced by mechanical flapped or plain jet flapped airfoils. Thus, the interaction of leading edge blowing with the augmentor flap flow appears to be negligible.

4.4 MULTIELEMENT NOZZLE CONFIGURATION TEST RESULTS

4.4.1 Principal Results

The two multielement nozzles tested were the circular tube nozzle and the rectangular lobe nozzle. Flaps-off nozzle calibration data are shown in figures 44 and 45. The peak velocity coefficient, C_V, was 0.96 for the tube nozzle and 0.93 for the lobe nozzle. It had been expected from static rig test results that the lobe nozzle C_V would be lower than that of the tube nozzle and that both multielement nozzles would have a lower C_V than the slot nozzle ($C_V = 0.98$).

Both multielement nozzles had been designed and manufactured to have a 30° nozzle bend to preturn the flow. The actual flow turning angle for the tube nozzle was 31° (fig. 44), which was essentially constant with nozzle pressure ratio (NPR). The flow turning angle for the lobe nozzle was 32° at the low NPRs, but 30° at the high NPRs (fig. 45).

Taking into account the difference in nozzle exit area, h_E x span, and nozzle velocity coefficient, C_V, the thrust versus NPR variations are consistent between the tube and lobe nozzles.

Initial testing of both the tube and lobe nozzle augmentors was done with the augmentor flap installed at a deflection of 50°. The static augmentation ratios achieved with both nozzle configurations are given in figure 46. These ratios were attained with the intake door set at the optimum forward speed position. There was little difference in the static augmentation ratios of the two configurations. Figure 47 compares the lift, drag, and pitching moment characteristics at q = 20 psf and $C_j = 1.18$. The lobe nozzle augmentor gave slightly better performance than the tube nozzle augmentor. This is also seen at other nozzle blowing rates, shown in figure 48.

The lobe nozzles were tested at flap angles of 30°, 50° and 70°. At the 70° flap angle, as with previous slot nozzle configurations, it was necessary to make geometry changes to keep the flow attached on the intake and shroud. The result of these changes was to: (1) move the intake and shroud downstream relative to the flap (this is called the low shroud configuration), and (2) partially seal the space between the flap and the aft wing fairing below the nozzles, to increase the entrained flow around the intake and shroud (called the taped nozzle configuration). These changes are shown in figure 49. The effects of shroud position and nozzle taping will be discussed in sections 4.4.2.2 and 4.4.2.3.

The static augmentation ratio ϕ and force data at q = 20 psf, are shown in figures 50 through 52 for "optimized" configurations at δ_f = 30°, 50°, and 70°. The value of ϕ decreased with increasing NPR, as in the case of the slot nozzle augmentor, but at a slower rate. Since the flaps-off jet deflection was essentially independent of NPR, the loss of ϕ at high NPR was probably associated with viscous and shock losses rather than flap position. As noted in section 4.1.2, the nozzle areas were smaller than intended. To obtain the same C_j as in the case of the slot nozzle on the scaled NASA section, the NPR must be raised. Aerodynamic data at NPR = 2.8 are shown in figure 51. The corresponding ϕ was 1.32, 1.27, and 1.06 for δ_f of 30°, 50°, and 70°, respectively. The variation of $C_{l_{max}}$, $C_{l_{\alpha=-2°}}$ and $(C_X)_{const\ C_l}$ with C_j is shown in figure 52.

4.4.2 Configuration Sensitivity Studies

Preliminary testing was accomplished at δ_f = 50° with both the lobe and tube nozzles to select one configuration for more detailed studies. As reported in section 4.4.1, the lobe nozzle was selected for further testing. The optimization process used considered both the static and wind-on performance of the augmentor flap. Final configurations were selected on the basis of the best combined static and forward speed characteristics.

4.4.2.1 Flap Intake Door Angle

Proper positioning of the intake door angle has a significant effect on augmentor flap performance, both statically and at forward speed. Figure 53 shows the effect of removing the intake of the lobe nozzle augmentor at δ_f = 30° on the static augmentation ratio. The variation of ϕ with nozzle pressure ratio is similar with or without intake, but the level of ϕ increased by 0.06 with the intake removed. Figure 54 presents the effect of intake and intake door angle on the static augmentation ratio and aerodynamic lift and drag at NPR = 2.8 and δ_f = 30° for the lobe nozzle. For the range of intake door angles tested, improper door positioning is seen to have a significant effect on all of the parameters. The angle of -2° appears to be close to the optimum. Compared to intake off, this intake door setting gave about 0.15 higher C_l and 3% less net thrust.

4.4.2.2 Flap Shroud Position

The augmentor flap is sensitive to shroud flow separation at high flap deflections at forward speed. Figure 55 shows the effect of lowering the shroud trailing edge with respect to the flap trailing edge on the static augmentation ratio, lift, and drag for the lobe nozzle augmentor at $\delta_f = 70°$. Lowering the shroud promotes flow attachment over the shroud and results in a significant increase in lift and a decrease in drag, even though there is a sizeable reduction in the static augmentation ratio. For the data shown, the shroud was lowered 20% of the flap chord from its high position.

4.4.2.3 Nozzle Taping to Reduce Ventilation

The effect of reducing nozzle ventilation was investigated briefly when the lift level achieved with the lobe nozzle augmentor fell short of that achieved with the scaled NASA section. Ventilation was reduced by taping the gap between the lower row of tubes with tape, as shown in figure 56. At $\delta_f = 30°$, the effect of taping was to increase C_l slightly at a cost of reducing thrust both at static and at forward speed conditions. At $\delta_f = 70°$, taping resulted in substantial improvements in both lift and drag. The data demonstrating these effects at forward speed are shown in figures 57 and 58. The effect of taping on static augmentation ratio is shown in figure 59 for the "high shroud" configurations at $\delta_f = 30°$ and 70°.

Tuft observations at $\delta_f = 30°$ showed that the flow separation over the nozzle boattail upper surface was eliminated by restricting ventilation from below. From this flow phenomenon, one would expect a drag reduction. Since taping restricted ventilation and reduced the augmented thrust statically, the drag reduction was probably overshadowed by the reduction in augmented thrust. It is felt that the coanda position and throat area should be reoptimized when nozzle ventilation is restricted from below.

At $\delta_f = 70°$, although nozzle taping resulted in a loss of ϕ, the performance at forward speed was greatly improved by what can only be accounted for by a reduction in separated flow. Similar effects of nozzle taping may be expected at $\delta_f = 50°$, since shroud flow separation persisted up to a fairly high C_j.

4.5 COMPARISON OF MULTIELEMENT AND SLOT NOZZLE AUGMENTOR FLAPS TEST RESULTS

The multilobe nozzle augmentor configuration has demonstrated a higher thrust augmentation ratio and lower noise level than the slot nozzle augmentor during static rig tests. In this section, the aerodynamic performance of the lobe nozzle augmentor will be compared with that of the scaled NASA section. Typical force data shown in figures 27 and 51 for the scaled NASA section and the lobe nozzle augmentor, respectively, are superimposed in figure 60. The lobe nozzle augmentor has slightly lower lift, similar streamwise force at low lift, and more drag at high lift, i.e., more sensitivity to angle of attack, than the slot nozzle augmentor. Figure 61 shows a comparison of force data as a function of C_j. The lobe nozzle augmentor is seen to have lower lift at nearly all C_j's than the slot nozzle augmentor, but C_X's at the operational C_l (discussed in sec. 4.2) are quite comparable. For these comparisons, the lobe nozzle was sealed with tape to restrict ventilation from below only at $\delta_f = 70°$. Thus the large difference in lift level, C_l at $\alpha = -2°$, at $\delta_f = 50°$ would probably be greatly reduced if the lobe nozzle were taped.

The differences in $C_{l_{max}}$ are not critical to the augmentor wing STOL airplane being studied because leading edge blowing will be incorporated for such a duct-volume-limited wing design. Even without leading edge blowing, three-dimensional wind tunnel testing (ref. 1) has demonstrated ample stall margin during approach.

The static thrust augmentation ratios are compared in figure 62. At $\delta_f = 30°$, the untaped lobe nozzle augmentor was better than the scaled NASA section, but the difference was less than that shown by the results obtained on the static test rig (volume III). At $\delta_f = 70°$, the taped lobe nozzle augmentor had considerably higher ϕ than the scaled NASA section. Part of this difference could be attributed to the difference in the required primary jet turning angle, which was much greater for the slot nozzle than for the lobe nozzle augmentor.

In view of the large effects of nozzle taping, which was only briefly explored, one would expect the performance of the lobe nozzle augmentor to improve significantly with the proper extent of taping and with augmentor flap geometry optimized with respect to the taped nozzle configuration. On the basis of potential improvement and available comparative data, it is concluded that the aerodynamic performance of the lobe nozzle augmentor is comparable to that of the slot nozzle augmentor and that further development of the former is well worthwhile.

4.6 EFFECTS OF AIRSPEED VARIATION

4.6.1 Introduction

One of the principal advantages of the augmentor wing is its ability to augment the primary nozzle thrust. At static condition, a resultant force in excess of 1.4 times the primary nozzle thrust has been measured in static tests during the present program. Whether or not such thrust augmentation can be maintained at forward speed has a profound impact on the takeoff performance of an augmentor wing airplane. As in the case of an ejector, the net thrust is expected to decrease with increasing forward speed, primarily due to the inlet momentum or ram drag and the external drag. It is also possible that the ejector efficiency improves with forward speed. In addition, as for jet flaps, a high degree of the resultant force is translated into the streamwise direction as a thrust recovery. Thus, the effect of forward speed on the performance of an augmentor wing may be greater and more complex than that associated with mere Reynolds number variation. To reduce the amount of wind tunnel test data required to predict takeoff performance, a method is required to predict the aerodynamic performance over a range of forward speeds based on data obtained at one airspeed condition.

The difficulty in evaluating experimentally the thrust augmentation characteristics at forward speed arises from the fact that measured streamwise force represents the difference between thrust and drag. The identification of thrust and drag relies upon various simplifying assumptions. Previous experiments were performed with either three-dimensional (refs. 6 and 7) or quasi-two-dimensional models (ref. 8) which experienced large induced drag at high lift conditions. This introduced a large uncertainty in the data analysis. Also, data were not taken specifically to answer the question of airspeed effects. Statements suggesting that the augmented jet thrust is not affected by airspeed (ref. 6) were generally based on the evidence that C_L variation with C_j and augmentor exit total pressure profiles are reasonably independent of airspeed. A clear indication and explanation of the variation of streamwise force of an augmentor wing with airspeed is lacking.

The present investigation has been conducted with a test setup that ensures a high degree of two-dimensionality. The plenum pressures for the various wall and end plate BLC slots were adjusted for each forward speed, first by matching the blowing momentum coefficient or (M_j^2/M_∞^2) and then tuning on the basis of flow visualization. The latter involves fine adjustment of individual nozzle pressures to achieve uniform flow separation or reattachment over the shroud upper surface when C_j is varied.

The approach taken to evaluate the thrust augmentation characteristics of an augmentor wing as a function of forward speed is to use the forward speed characteristics of a plain jet flap as a base. The plain jet flap is chosen because its characteristics are well understood and considerable experience has accumulated in applying wind tunnel data to predict airplane performance. The difference in the forward speed effects for the two configurations forms the basis for modifying the established method used for jet flap airplanes so that it applies to augmentor wing airplanes.

The data addressed to the airspeed effects were taken primarily on typical takeoff configurations, i.e., $\delta_f = 30°$. These configurations include two augmentors of scaled NASA section (F-65Y and F-65Z) and one jet flap (F-65JF), all with slot nozzles, and another augmentor with a multilobe nozzle. All these configurations have a 0.27 c flap chord. The augmentor (F-66M) with the lobe nozzle (untaped) is shown in figure 13. The F-65Y and F-65Z augmentors used the same model parts but different spacing between the shroud and the flap to give l_T/h_N of 7 and 11, respectively. The jet flap configuration, F-65JF, is F-65Y with the shroud and intake removed and the flap gap sealed. The slot nozzle is the same one used for all F-65 augmentor flaps, but the slot height has been increased slightly as a result of final adjustment to achieve uniform slot height. The nozzle calibration curves shown in figure 63 are similar to those shown in figure 26.

The data runs were made by maintaining constant primary nozzle pressure ratio, wall blowing rates, and airspeed while pitching the model through a range of α to adequately define the polar shape, minimum drag (maximum thrust), and maximum lift. A summary of data runs addressed to the airspeed effects is tabulated in table 1.

4.6.2 Results and Discussion

4.6.2.1 Static Performance

Figure 64 shows the variation of static thrust augmentation with NPR for augmentors F-65Y, F-65Z, and F-66M and plain jet flap F-65JF. For the jet flap there was a 5% thrust loss which is nearly independent of NPR. Augmentation ratios for all the augmentors show various degrees of dependence on NPR, and always decrease with increasing NPR. The lobe

TABLE 1.—SUMMARY OF PITCH RUNS FOR AIRSPEED EFFECT STUDY

Configuration	δ_f	q, psf	NPR (Nominal)
Plain jet flap (F_{65JF}) with slot nozzle	30°	6 12 20 30 45	1.2, 1.6, 2.0, 2.3 1.6, 2.0, 2.3, 2.8 1.0, 1.6, 2.0, 2.3, 3.0, 3.5 1.6, 2.0, 2.3, 3.0 1.6, 2.0, 2.3, 3.0, 3.5
Scaled NASA section augmentor flap ($F_{65Y}\ \frac{\ell t}{h_N} = 7$) with slot nozzle	30°	As above	As above
Scaled NASA section augmentor flap ($F_{65Z}\ \frac{\ell t}{h_N} = 11$) with slot nozzle	30°	As above	As above
Lobe nozzle augmentor flap (F_{66M})	30°	As above	As above
NASA wing section baseline augmentor flap (F_{62}) with slot nozzle	30° 40° [a]50°	10 20 10 20 10 20	2.0, 3.0 1.25, 1.6, 2.0, 2.5, 3.0, 3.5 1.6, 2.0, 2.5, 3.0, 3.5 1.0, 2.0, 2.5, 3.0, 3.5 1.6, 2.0, 2.5, 3.0 2.0, 2.5, 3.0, 3.5
Scaled NASA section augmentor flap (F_{65}) with slot nozzle	30° 50°	5 10 20 40 5 10 15 20 30 40	2.5 2.5 1.0, 1.6, 2.0, 2.5, 3.0, 3.5 2.5 2.5 2.5 2.5 1.0, 1.6, 2.0, 2.5, 3.0, 3.6 2.5 2.5

[a]Repositioned

nozzle augmentor showed the least dropoff in augmentation ratio with increasing NPR. At NPR = 2.5, it achieved an augmentation ratio of 1.33 compared to values of 1.265 and 1.235 for the F-65Y and F-65Z augmentors, respectively.

The entrainment characteristics of the augmentors are compared in figure 65. The secondary weight flow, w_{sec}, was computed on the basis of the measured resultant force and the augmentor exit velocity profile shape, which is characterized by a skew factor, ξ. For a rectangular profile, ξ is unity. It becomes less than one for any nonuniform velocity profile. The values of ξ are about 0.986 for the lobe nozzle augmentor, and 0.963 and 0.914 for the F-65Y and F-65Z slot nozzle augmentors, respectively. A comparison of exit total pressure profiles of the three augmentor configurations at forward speed is shown in figure 66. The profile for F-65Z showed a possibility of flow separation from the shroud lower surface, which explains its lower augmentation ratio while entraining more air than F-65Y. The relationship between the skew factor and the augmentation ratio is in full agreement with simplified ejector theory, which shows that the thrust augmentation improves with the uniformity of the exit velocity (ref. 9).

The entrainment ratio, $\dot{w}_{sec}/\dot{w}_{pri}$, attained with the lobe nozzle augmentor was about 0.6 greater than that of the slot nozzle augmentor; however, it was still significantly less than the theoretical value, as shown in figure 65. F-65Y represents a near-optimum configuration for this augmentor flap with slot nozzle. The entrainment ratio is about 0.4 less than the theoretical value. (The theoretical value is computed by a method similar to that described in reference 10.)

4.6.2.2 Aerodynamic Performance Comparison

The maximum lift, lift level ($\alpha = -2°$), pitching moment, and streamwise force coefficients at $C_l = 3.5$ are compared in figure 67 for the augmentors F-65Y and F-65Z, and the jet flap, all with slot nozzles at q = 20 psf. Both augmentors gave higher $C_{l_{max}}$, nose-down pitching moment, and net thrust than the jet flap at a given C_j. However, at C_j less than about 0.6, the augmentors generally gave lower lift and higher drag than the jet flap (see also fig. 68) because of incipient flow separation from the shroud upper surface. The differences in attachment C_j are apparent from the $C_{l_\alpha} = -2°$ curves in figure 67. The fairing of these curves at low C_j follows similar curves in figure 68 where the force data at $\alpha = 2°$ taken at all airspeeds are included. Both C_l and C_X for the jet flap and C_l for the augmentors correlate well with C_j. However, the variation of C_X with C_j for the augmentors appears also to depend on airspeed.

At flap deflections greater than 30°, a limited amount of data taken with the NASA wing section at q = 10 and 20 psf (fig. 69) showed that even C_l variation with C_j became increasingly dependent on airspeed as flap deflection increased.

From figures 67 and 68 it is also apparent that the augmentor with better static thrust augmentation also performed better at forward speed. The augmentor F-65Y had lower drag and nose-down pitching moment at a given C_l and lower attachment C_j than F-65Z.

The aerodynamic performance of the lobe nozzle augmentor flap is compared with that of the slot nozzle augmentor flap in section 4.5.

4.6.2.3 Effect of Airspeed on Drag Polars

Figure 70 shows drag polars at $C_j = 0.8$ for augmentors and jet flap with slot nozzle. Each polar was interpolated from data taken at a fixed airspeed. For the jet flap, polars at various airspeeds lie within a C_X band of 0.02. This is about the size of the experimental uncertainty interval. For the two augmentors, the bandwidths are about 0.05 if the q = 45 polars are excluded. The variation of C_X with airspeed at a fixed C_l is shown in figure 71. For the jet flap, C_X at a fixed C_l is essentially independent of airspeed. For the augmentors, a minimum generally occurs between a q of 10 and 15 psf.

To explain the variation of C_X with airspeed at constant C_l, a drag equation is proposed:

$$C_X = -\phi C_j + 2C_q + F(C_l,C_j) + C_{Di}$$

where

$$2C_q = \frac{2\dot{w}_{sec}}{g\rho_\infty V_\infty S_{ref}} \text{ and } C_{Di} = \frac{C_L^{\ 2}}{\pi AR + kC_j}$$

are the ram drag and the vortex drag of a three-dimensional jet flapped wing, respectively. The drag polars of the augmentor flap F-65Y were found to be sensibly approximated by parabolas with values of $\partial C_X/\partial C_l^2$ varying from 0.003 to 0.004. Such low values of $\partial C_X/\partial C_l^2$ indicate that the effective aspect ratio was very high and two-dimensional conditions were indeed closely approached. Therefore, C_{D_i} may be neglected.

Both ϕ and $\dot{w}_{sec}$ in the drag equation are based on static test data. The function $F(C_l,C_j)$ represents all the viscous effects at forward speed including thrust recovery, mixing of the jet with the external stream, and external drag of the augmentor shroud. This function also accounts for changes in ejector characteristics, i.e., $\Delta\phi$ and $\Delta\dot{w}_{sec}$, with airspeed. In the absence of flow separation over an "optimized" augmentor configuration, the value of $F(C_l,C_j)$ is expected to be smaller than ϕC_j or $2C_q$. At $C_j = 0.8$, the values of NPR, ϕC_j and $2C_q$ are tabulated below.

	q(psf)	6	12	20	30	45
F-65Y	ϕC_j	1.082	1.072	1.049	1.007	0.933
	$2C_q$	0.29	0.262	0.252	0.245	0.222
	NPR	1.25	1.55	1.99	2.57	3.45
F-65Z	ϕC_j	1.057	1.020	1.000	0.985	0.900
	$2C_q$	0.302	0.275	0.270	0.263	0.23
	NPR	1.25	1.55	1.99	2.57	3.45
F-66M	ϕC_j	1.076	1.073	1.069	1.052	1.000
	$2C_q$	0.337	0.302	0.292	0.287	0.262
	NPR	1.33	1.68	2.20	2.82	3.83

At a constant C_j, NPR increases with airspeed, so that ϕ and entrainment ratio are both decreasing. Note that the values of ϕC_j or $2C_q$ in all cases varied monotonically with the dynamic pressure, whereas curves of C_X vs q for the augmentors (in fig. 71) showed a minimum. The combination of $2C_q - \phi C_j$ (except for F-65Z) also has a minimum value. The lines representing $2C_q - \phi C_j$ for the two slot nozzle augmentors are compared in figure 72 with the C_X vs q curves of figure 71. The spacing between the two lines of $-\phi C_j + 2C_q$ and the shape of these lines agreed reasonably well with the experimental data except for F-65Z at high q values. The C_X levels of these lines indicate that $F(C_l,C_j)$ must increase with C_l, starting from a negative value to a positive value. It also appears that $F(C_l,C_j)$ is approximately independent of airspeed, which suggests that polars at various airspeeds may be generated from test data at static and at one forward-speed condition. This tentative conclusion is probably invalid when the ejector characteristics change markedly with airspeed as in the case of a "nonoptimum" configuration.

For the lobe nozzle augmentor, the effect of airspeed on the drag polar is similar to that of the slot nozzle augmentors. The variation of C_X with q for F-65Y is compared with that of F-66M in figure 73. Also shown is a comparison of $2C_q - \phi C_j$ for the two configurations. For F-66M the correlation between $2C_q - \phi C_j$ with the experimental data is satisfactory, although not as good as for F-65Y.

The rate of change of C_X with C_j at a constant C_l is sometimes used to evaluate the thrust recovery characteristics or thrust effectiveness (defined in sec. 1.3.1) of propulsive wings such as the jet flap. The variation of C_X with C_j is usually linear in the jet flap regime where flow separation is absent. The present data permit plotting C_X vs C_j at constant C_l in two ways: by keeping q constant and by maintaining constant thrust or NPR. The slope, $\partial C_X/\partial C_j$, obtained in either way is differentiated by a subscript indicating the quantity held constant. The slopes $(\partial C_X/\partial C_j)_{V_\infty}$ and $(\partial C_X/\partial C_j)_{NPR}$ at $C_l = 3$ are shown in figure 74 for the augmentors and the jet flap. The accuracy in determining the slope is usually not better than ±0.01; therefore, bands rather than lines are shown in the figure. In general, the slope is not noticeably affected by the lift coefficient. The lobe nozzle augmentor has the best thrust effectiveness, i.e., the greatest values of $|\partial C_X/\partial C_j|$. The jet flap has the lowest value – $|\partial C_X/\partial C_j|_{V_\infty} = |\partial C_X/\partial C_j|_{NPR} = 0.915$. The slope $|\partial C_X/\partial C_j|_{V_\infty}$ of the augmentors diminishes with increasing airspeed; only its value at q = 8 to 10 psf matches the value of $|\partial C_X/\partial C_j|_{NPR}$.

4.6.2.4 Airspeed Effects at Constant NPR

During takeoff, the NPR remains essentially constant while airspeed increases. Figure 75 shows the airspeed effects on lift and drag at $\alpha = -2°$ and NPR = 2.0 and 2.3. The forces are divided by the primary nozzle thrust, which remains constant for a given NPR. Thus, the vertical scales represent forces experienced by the wing. The difference in lift between the slot nozzle augmentors and the jet flap becomes apparent as airspeed increases. This is due to the effect of C_j on C_l discussed in section 4.6.2.2. The difference in lift vanishes at NPR above 2.5. To eliminate the influence of lift, the data are replotted for constant C_l (3 and 5) at NPR = 2.3 in figure 76. The drag variation and the differences between the configurations are similar at either constant α or constant C_l.

Compared to the jet flap, the more rapid rate of drag increase with airspeed can be attributed largely to ram drag which is manifested in the pressure distribution of an ejector and, therefore, included in the profile drag of the augmentor flap system. Qualitative evidence is provided by an examination of the static pressure distributions and flap trailing edge total pressure profiles.

The streamwise force on the model is composed of the jet reaction and the external pressure and skin friction forces. The change of streamwise force with q at a fixed NPR is due primarily to a change in external pressure force. The rate of change in pressure forces acting on the wing and the flap with airspeed depends mainly on the general flow field around the model, which should be similar for the jet flap and for the augmentor as long as α, C_l, C_j, and δ_f are reasonably well matched. Available static pressure data are insufficient for a quantitative analysis. The static pressure distributions over the F-65Y augmentor flap, shroud, and intake for $\alpha = -2°$, NPR = 2.0 and various q values are presented in figure 77. The static pressure (in psig) is plotted against the distance normal to the wing chord plane so that the areas under the curves represent streamwise forces (except for a small α correction). The dashed lines in the figure denote the aft-facing surfaces. The plots show that the flap experienced a drag force which increased with q due to the increased pressure on its lower surface. The shroud experienced a thrust which diminshed with q because of the increased suction on its upper surface. The intake experienced a thrust at static condition, which changed to drag at the lowest q tested (6 psf), and this drag increased rapidly with q. These changes in pressure drag are primarily due to the relationship between the relatively constant internal flow field (between flap and shroud) and the q-induced changes in the external flow field. The force commonly referred to as ram drag is imposed on the airframe through these pressure changes.

Total pressure profiles at the augmentor exit measured on the static test stand have shown large spanwise variation, i.e., integrated momentum flux varied ±20%. Therefore, the single total pressure rake located at 1/4 span in the present test cannot provide data for quantitative anlaysis. But interesting trends, demonstrating qualitatively the airspeed effects on jet mixing, have been observed. Figures 78 and 79 show the jet total and static pressure profiles at the trailing edges of the augmentor F-65Y and the jet flap, respectively, for NPR = 2.0, $\alpha =$ $-2°$, and q values varying from 0 to 45 psf. For the augmentor, the total pressure profile was nearly triangular with the peak well centered between the flap and the shroud at static condition. With increasing q, the peak shifted slightly toward the flap but the shape and the peak value were little affected. For the jet flap, typical wall jet profiles were formed with the peak located about 0.07 in. from the flap surface. With increasing q, the peak location was unchanged but the peak pressure increased faster than the freestream total pressure. The consistency of these trends is illustrated in figure 80 by plots of maximum total pressure versus q at NPR = 1.6, 2.0, and 2.3 for both slot nozzle augmentors F-65Y and F-65Z and the jet flap at $\alpha = -2°$.

The total pressure data suggest a fundamental difference in the effects of forward speed for the jet flap and for the augmentor flap. For the jet flap, the jet is exposed at forward speed to the high local velocity at the flap knee or near the nozzle exit due to increased circulation. Thus, the jet peak velocity decay rate is reduced at forward speed. For an "optimized" augmentor, the mixing and entrainment of the jet must adjust to the exit pressure field subject to the constraint of duct geometry. Since the exit pressure varies only slightly with forward speed, the entrained mass flow and consequently the velocity of the jet external stream or ejector secondary flow must remain relatively constant. The change in secondary stream (including main wing boundary layer) total pressure is less than 0.5% of the jet total pressure for the conditions of interest. These considerations lead to the conclusion that the effect of airspeed on the ejector internal flow is small. The supervelocity due to increased circulation must occur mainly over the wing, the intake, and the shroud.

Exit total pressure profiles for the lobe nozzle augmentor (F-66M) at several airspeeds are presented in figure 81. The effect of airspeed on the exit flow is similar for either lobe or slot nozzle augmentors.

5.0 CONCLUSIONS AND RECOMMENDATIONS

Extensive two-dimensional wind tunnel testing of four augmentor flap configurations was carried out at the 3- by 8-ft Boeing low-speed research tunnel. Analysis of the test results led to the following conclusions:

- For low and moderate flap deflections ($30° \leq \delta_f \leq 50°$), augmentor flap configurations which have the best static performance generally have the best forward speed characteristics. However, at high flap deflections augmentor flap configurations which produce the best static performance do not usually produce the best forward speed characteristics.

- Proper positioning of the augmentor flap with respect to the primary nozzle jet path is extremely important for achieving good overall performance.

- Sectional aerodynamic characteristics of the NASA phase VI swept augmentor wing were probably superior at δ_f less than 50° and inferior at δ_f greater than 50° to those of the scaled-down NASA section.

- The aerodynamic characteristics of the multilobe and the multitube nozzle augmentors are similar at $\delta_f = 50°$.

- Lift and drag levels achieved with the multielement lobe nozzle configuration compare favorably with those obtained with the slot nozzle configuration. It was necessary to restrict the lower surface flow through the multielement nozzle to achieve comparable levels at high flap deflections.

- Upper surface flow separation on augmentor flap shrouds at forward speed for $\delta_f = 70°$ can be avoided only by lowering the shroud with respect to the flap.

- Both leading edge geometry and leading edge boundary layer control primarily affect maximum lift for an augmentor flap. The interaction between leading edge blowing and the augmentor flap flow field appears to be negligible.

- Variations of C_l and C_X with C_j are essentially independent of airspeed and nozzle pressure ratio for the plain jet flap at $\delta_f = 30°$.

- For the augmentor flap, variation of C_l with C_j is generally independent of airspeed and nozzle pressure ratio at takeoff flap setting of 30°; at higher flap angles this is no longer the case.

- For the augmentor flap at $\delta_f = 30°$, variation of C_X with C_j is influenced by the airspeed and the nozzle pressure ratio. Based on the static thrust augmentation and ram drag computed from entrained secondary air, the airspeed effects on the streamwise force can be approximated.

- For the jet flap, the mixing of the primary jet with the air stream was significantly influenced by the airspeed, whereas for the augmentors, the mixing process is quite independent of airspeed for both lobe and slot nozzles.

An important discovery is the large favorable effect of reducing multilobe nozzle ventilation from below. This effect has not been explored in depth. The results indicate that the performance of the multilobe augmentor flap could be improved by finding the best nozzle ventilation arrangement and optimizing the flap geometry with respect to it. Since restricting nozzle ventilation from below could also have an effect on noise, further study is recommended to seek the best compromise between aerodynamic and acoustic performance.

Two-dimensional wind tunnel testing has proven to be an efficient way to develop complex powered high-lift configurations. Because of the complexity of multielement nozzle augmentor flap configurations, only a limited number and range of configuration variables have been investigated. In view of the encouraging results obtained in this study, continued development of such a powered lift concept appears warranted.

The Boeing Company
P.O. Box 3707
Seattle, Washington 98124, June 5, 1972

REFERENCES

1. M. D. Falarski and D. G. Koenig, "Aerodynamic Characteristics of a Large Scale Model with a Swept Wing and Augmented Jet Flap," NASA Ames TM-X62, 029, April 1971.

2. *Design Integration and Noise Study for a Large STOL Augmentor Wing Transport,* Task I Report, D6-60139, The Boeing Company, July 1971.

3. A. Pope, *Wind Tunnel Testing,* Second Edition, John Wiley & Sons, Inc., New York, 1954.

4. F. L. Gilbertson and R. H. Love, *Augmentor Optimization Tests Leading to Ames Phase 4 Configuration,* DHC-DIR-69-7, The de Havilland Aircraft of Canada, Ltd., September 1969.

5. J. L. Harris, *Phase 3 Test Results for Augmentor Wing Model WTBA, Vol. I: Test Data,* DHC-DIR-68-23, October 1968.

6. D. Koenig, V. Corsiglia, and J. Morelli, "Aerodynamic Characteristics of a Large-Scale Model With an Unswept Wing and Augmented Jet Flap," NASA TN D-4610, 1968.

7. D. B. Garland, *Report on the Phase 3 Tests of the DHC Augmentor-Wing Model in the 40 x 80 Wind Tunnel at Ames Research Center,* Vol. II, DHC-DIR-67-42, November 1967.

8. J. L. Harris, *Phase 3 Test Results for Augmentor Wing Model WTBA, Vol. II: Analysis and Results,* DHC-DIR-68-24, December 1968.

9. Theodore von Karman, "Theoretical Remarks on Thrust Augmentation," *Reissner anniversary volume,* J. W. Edwards, ed., 1949, pp. 461-468.

10. R. B. Fancher, "Low Area Ratio Thrust Augmenting Ejectors," AIAA paper no. 71-576, 1971.

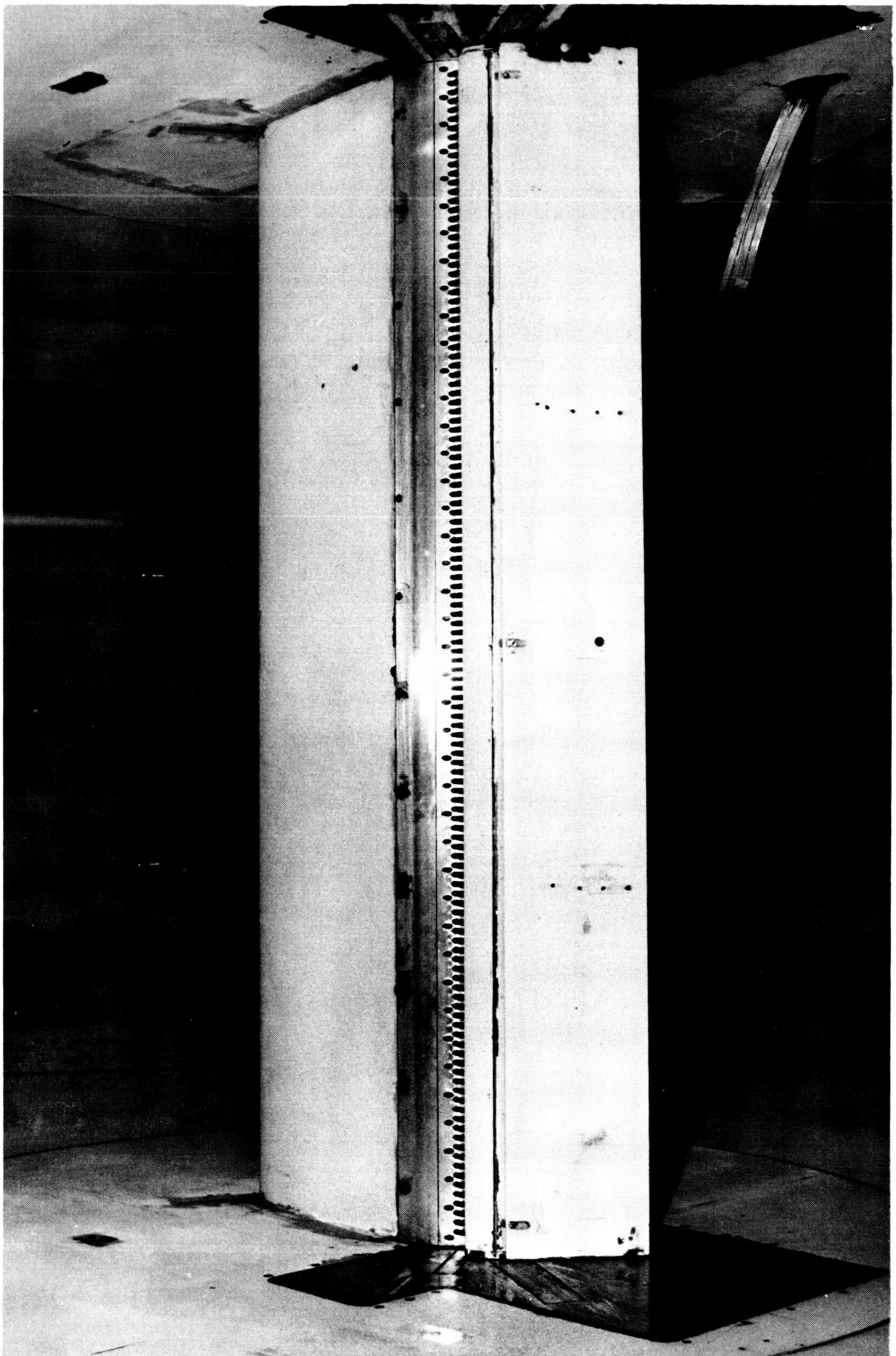

FIGURE 10.—TWO-DIMENSIONAL WIND TUNNEL TEST SECTION WITH AUGMENTOR FLAP MODEL

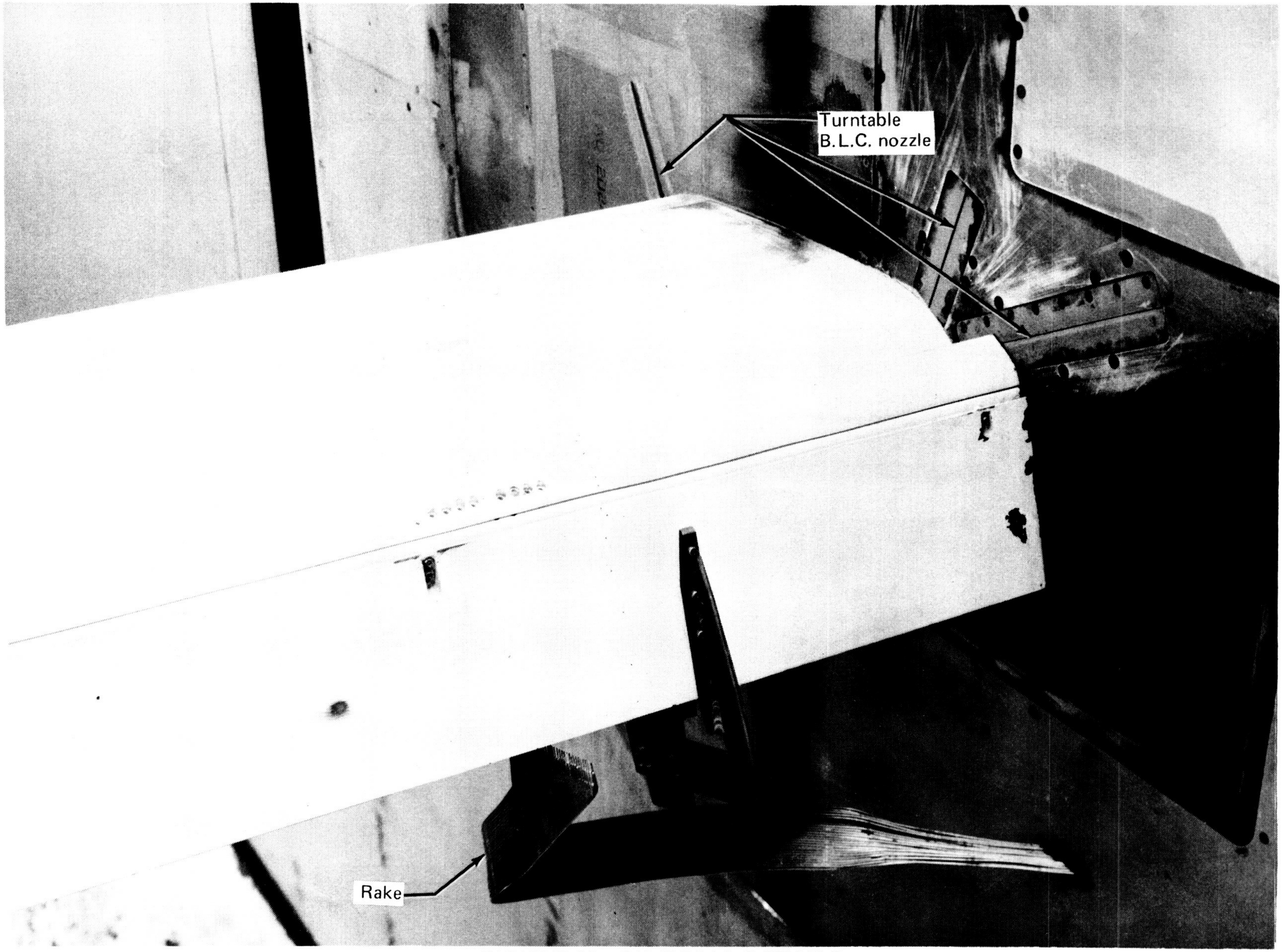

FIGURE 11.–SIDEWALL DETAILS

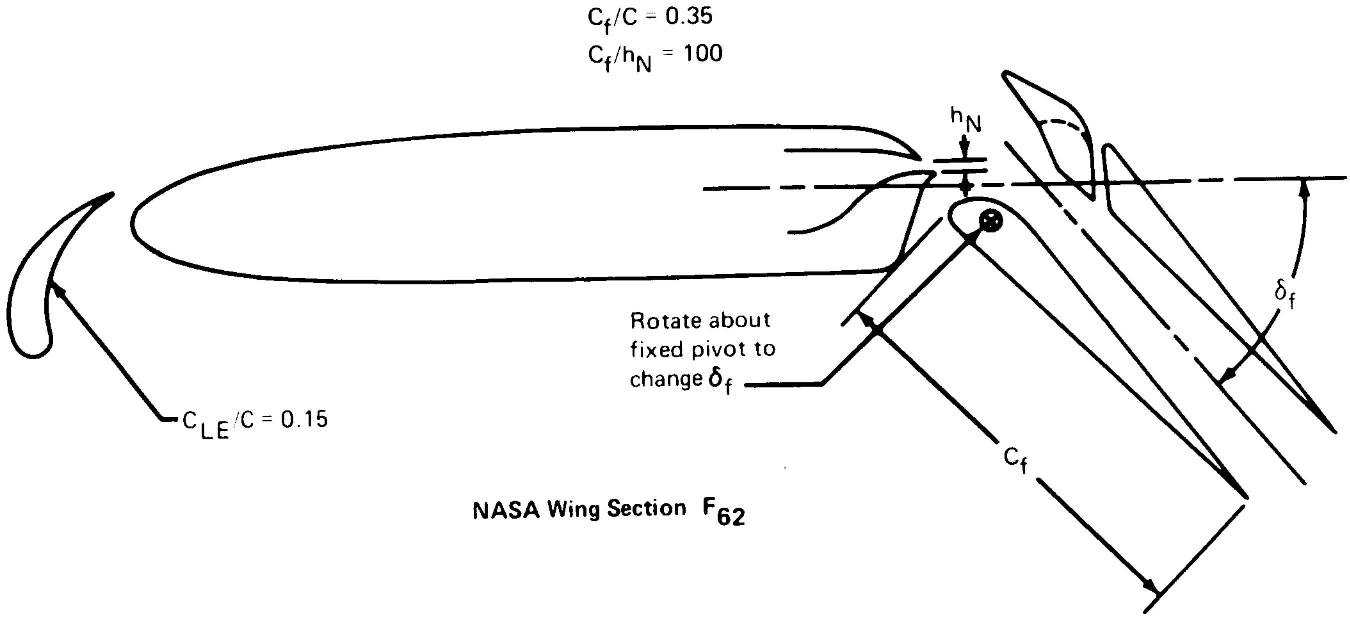

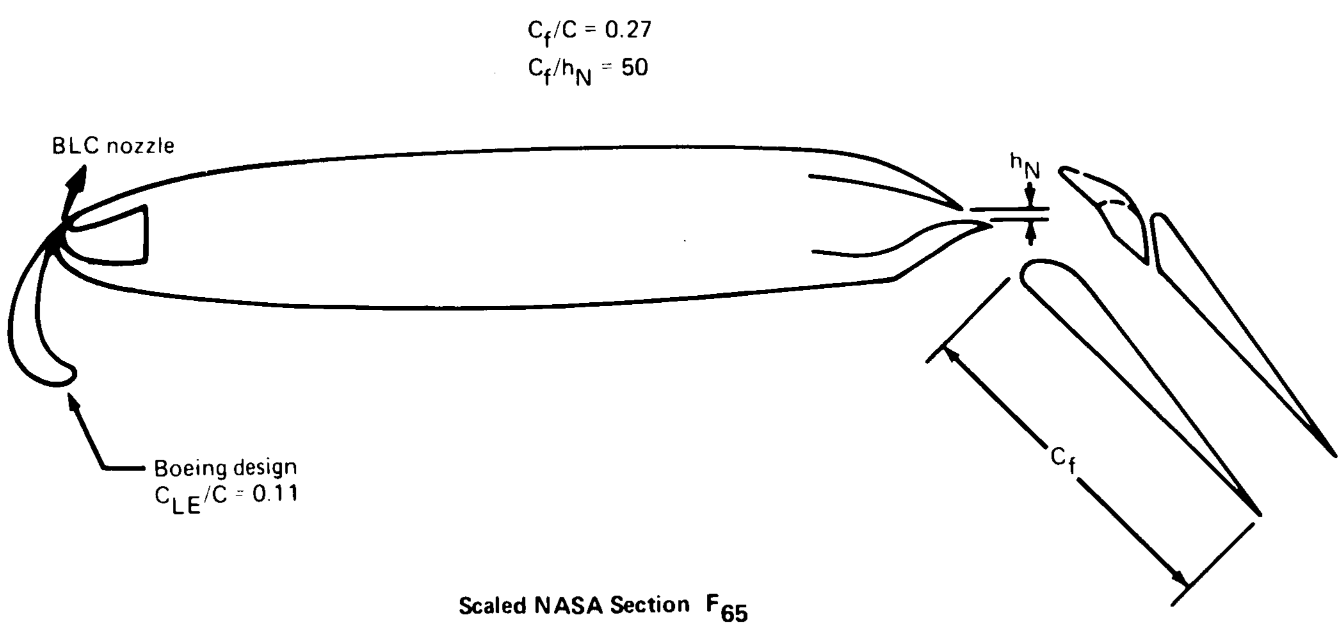

FIGURE 12.—SLOT NOZZLE CONFIGURATIONS TESTED

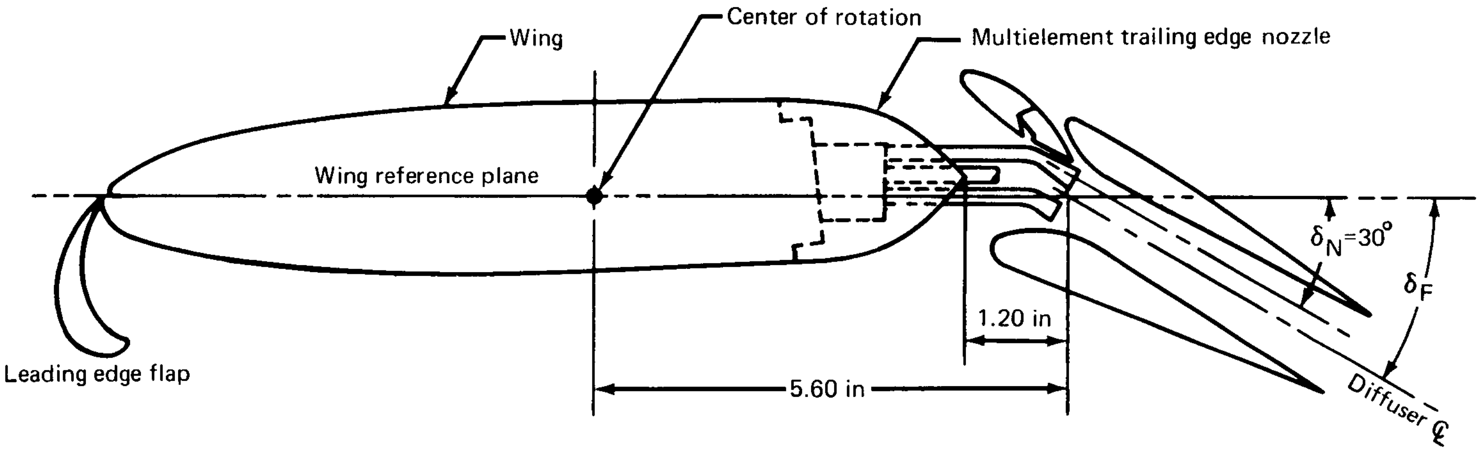

Lobe Nozzle Augmentor

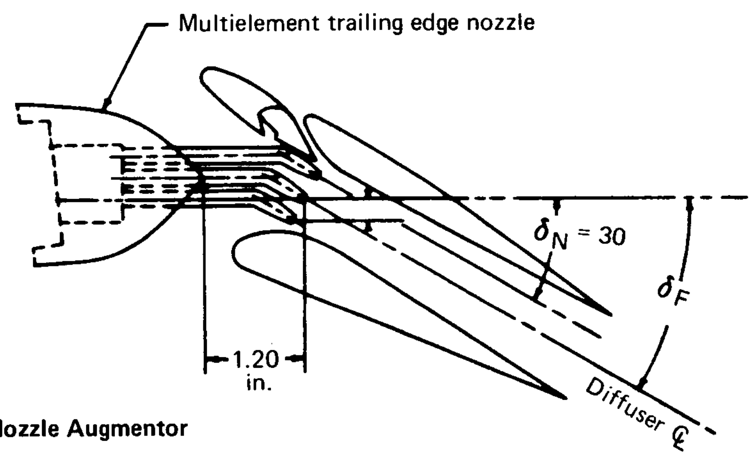

Tube Nozzle Augmentor

FIGURE 13.—MULTIELEMENT NOZZLE AUGMENTOR CONFIGURATIONS

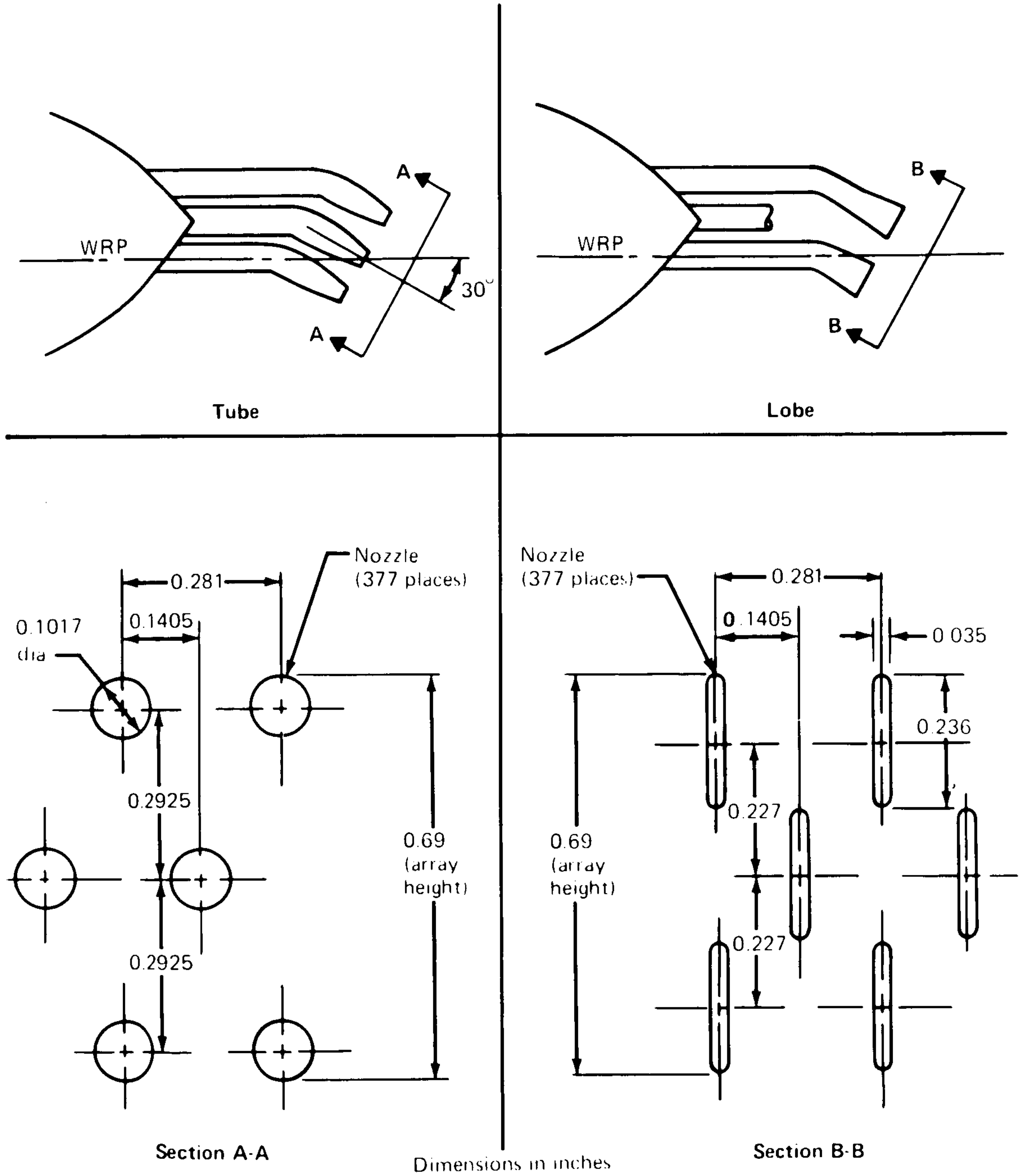

FIGURE 14.–MULTIELEMENT NOZZLE ARRANGEMENT

FIGURE 15.—TYPICAL MODEL UPPER SURFACE FLOW PATTERN DEVELOPED WITH CHINA CLAY

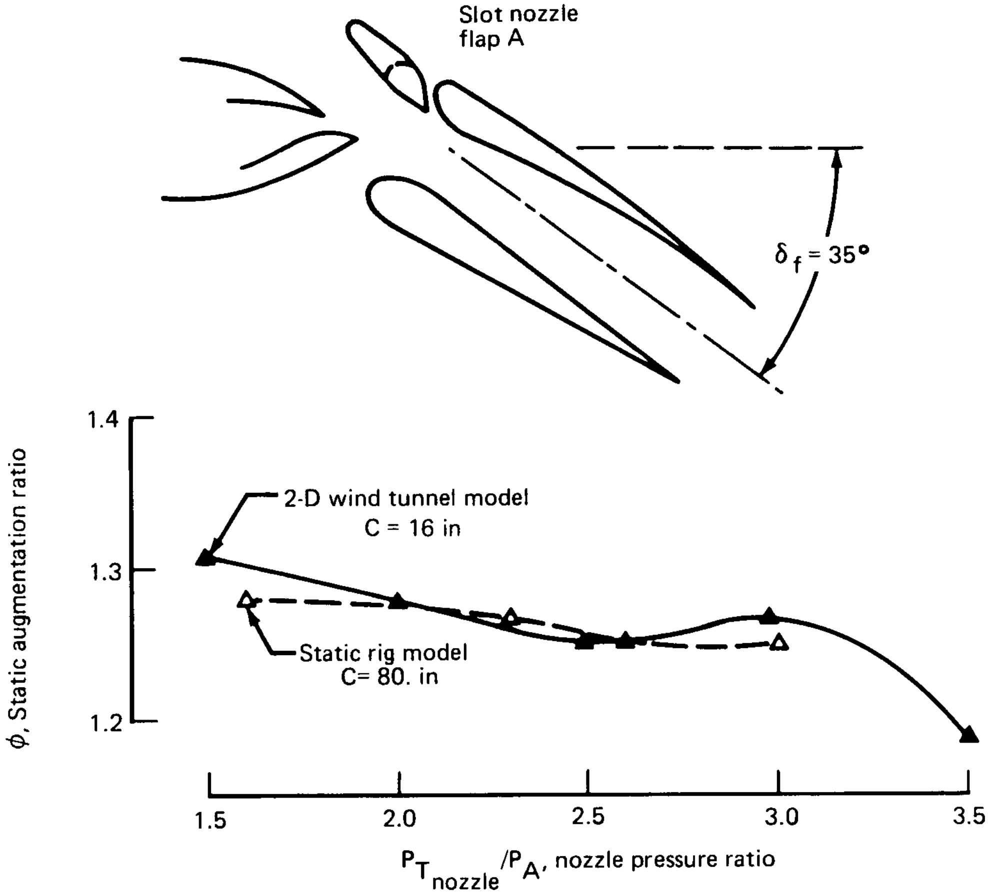

FIGURE 16.—COMPARISON OF STATIC RIG AND TWO-DIMENSIONAL WIND TUNNEL MODEL STATIC THRUST AUGMENTATION RATIO

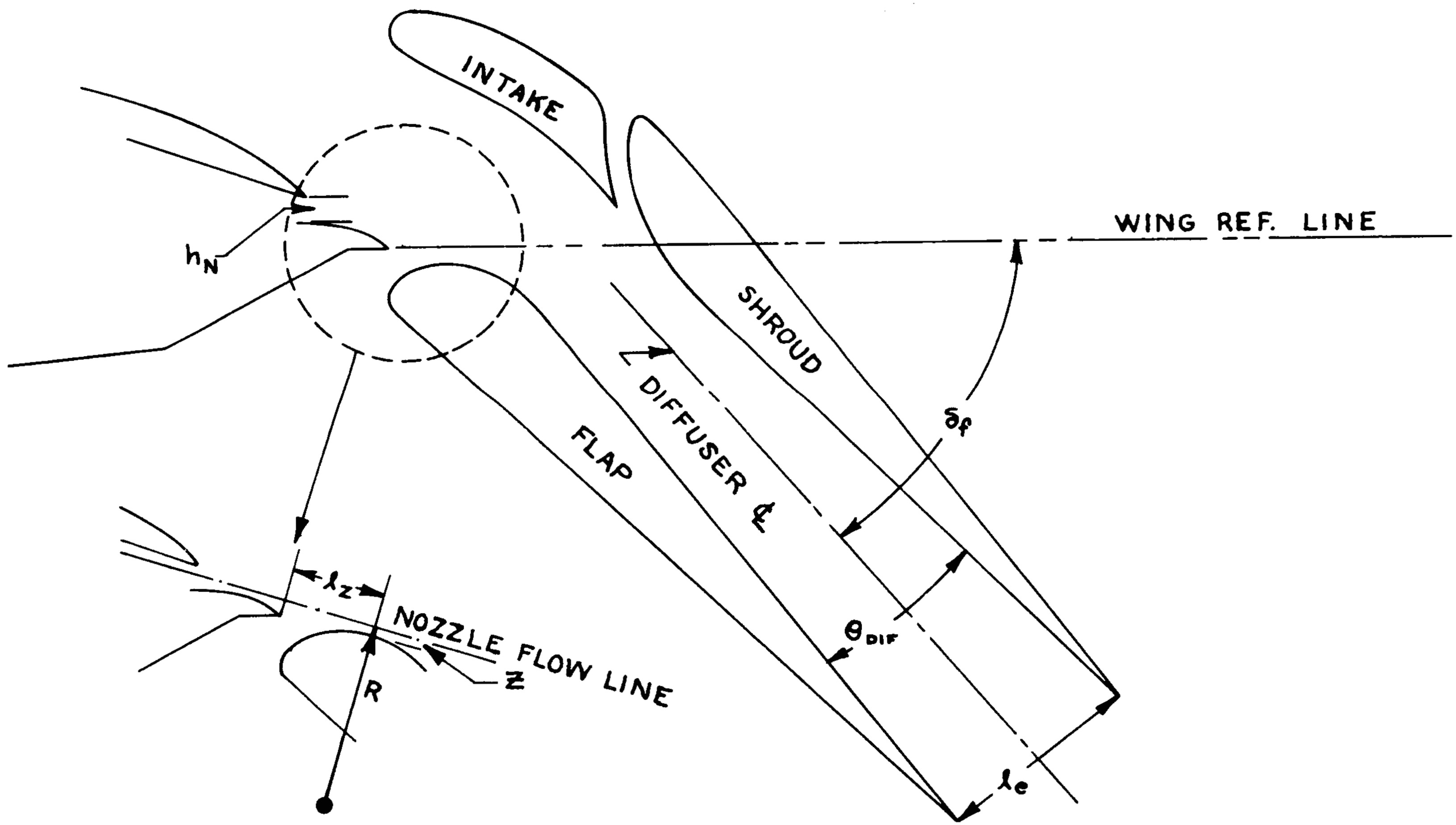

FIGURE 17.–DEFINITION OF GEOMETRY PARAMETERS

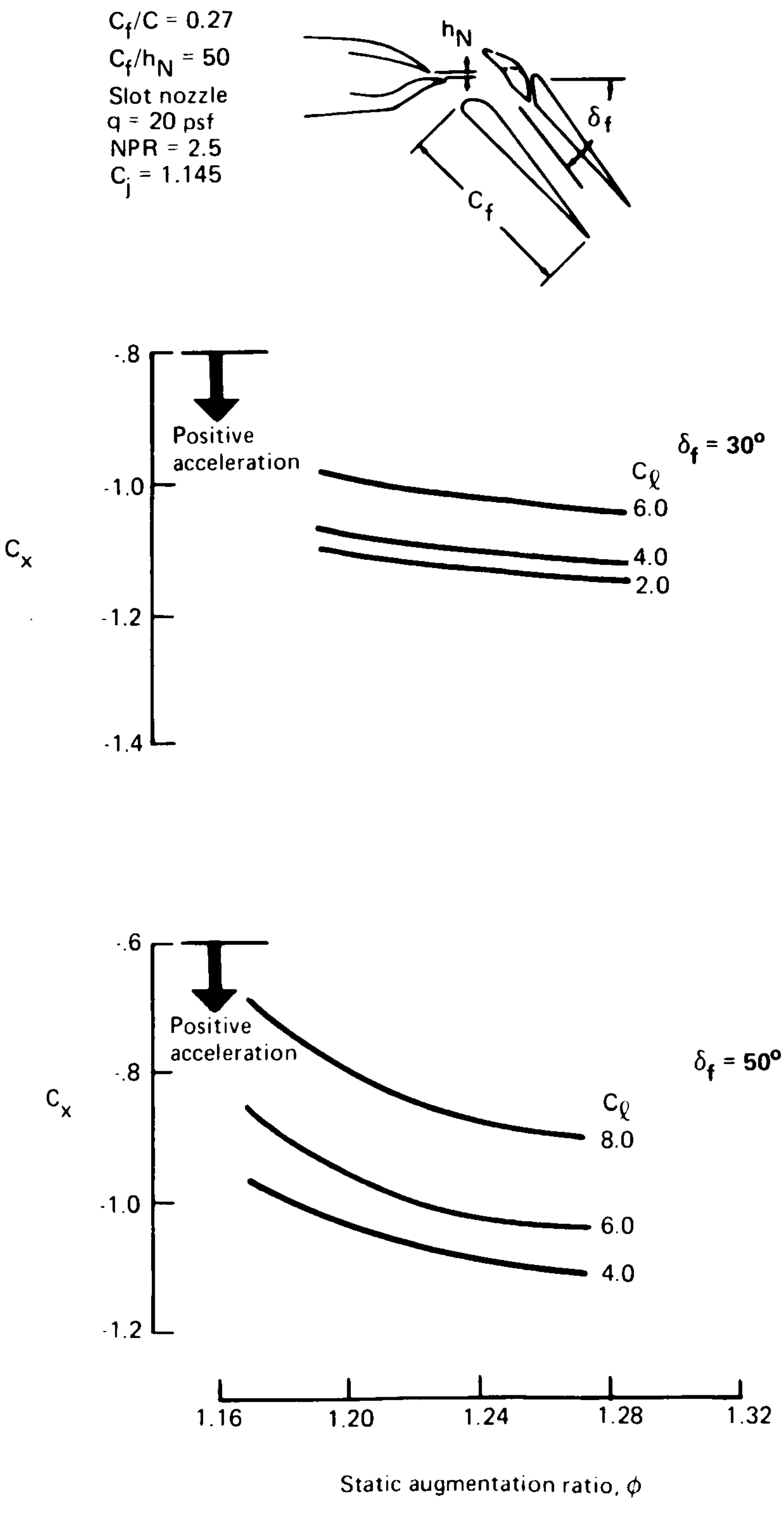

FIGURE 18.—EFFECT OF STATIC THRUST AUGMENTATION ON STREAMWISE FORCE AT FORWARD SPEED

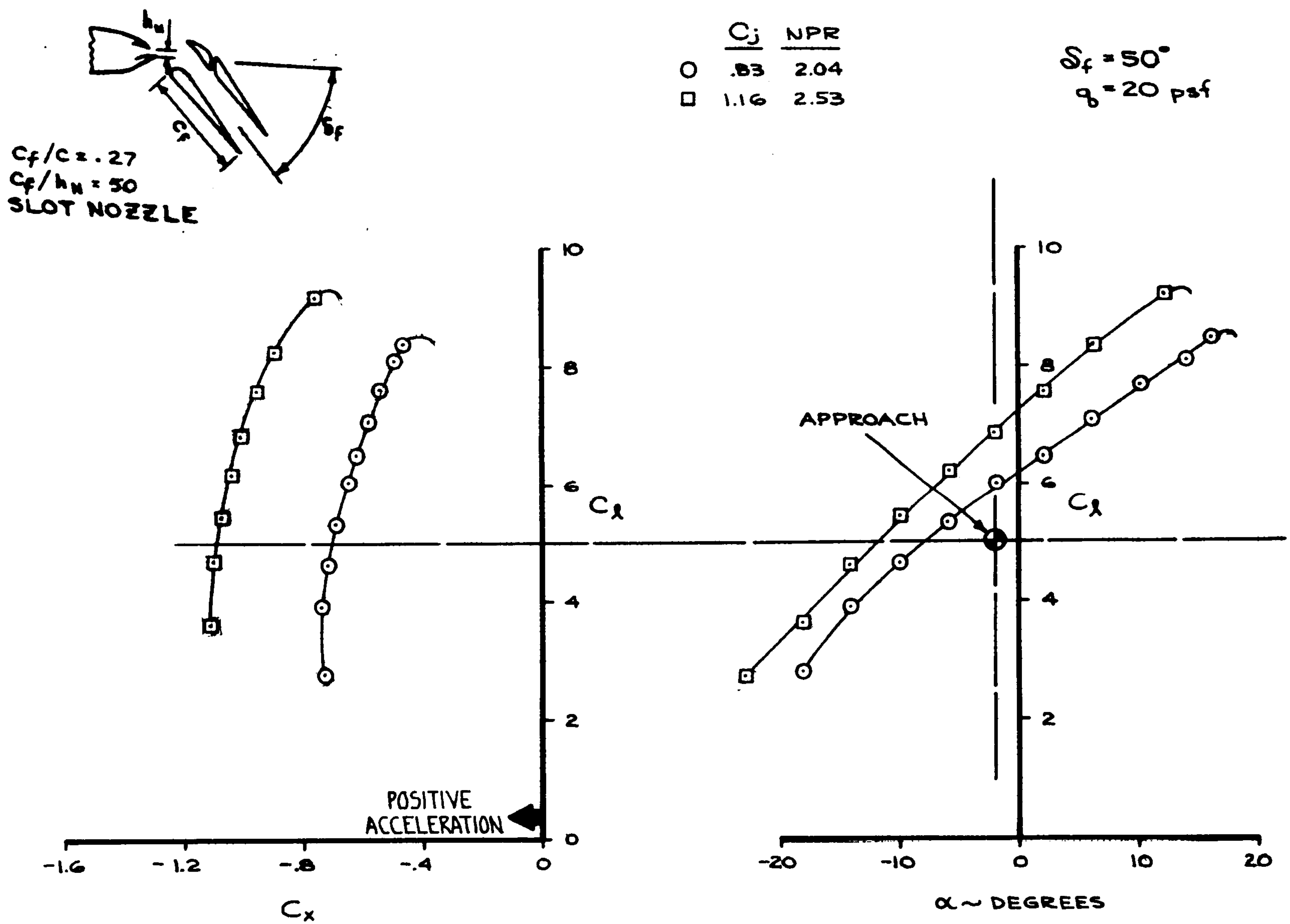

FIGURE 19.– REPRESENTATIVE LIFT CURVES AND DRAG POLARS FOR $\delta_f = 50°$

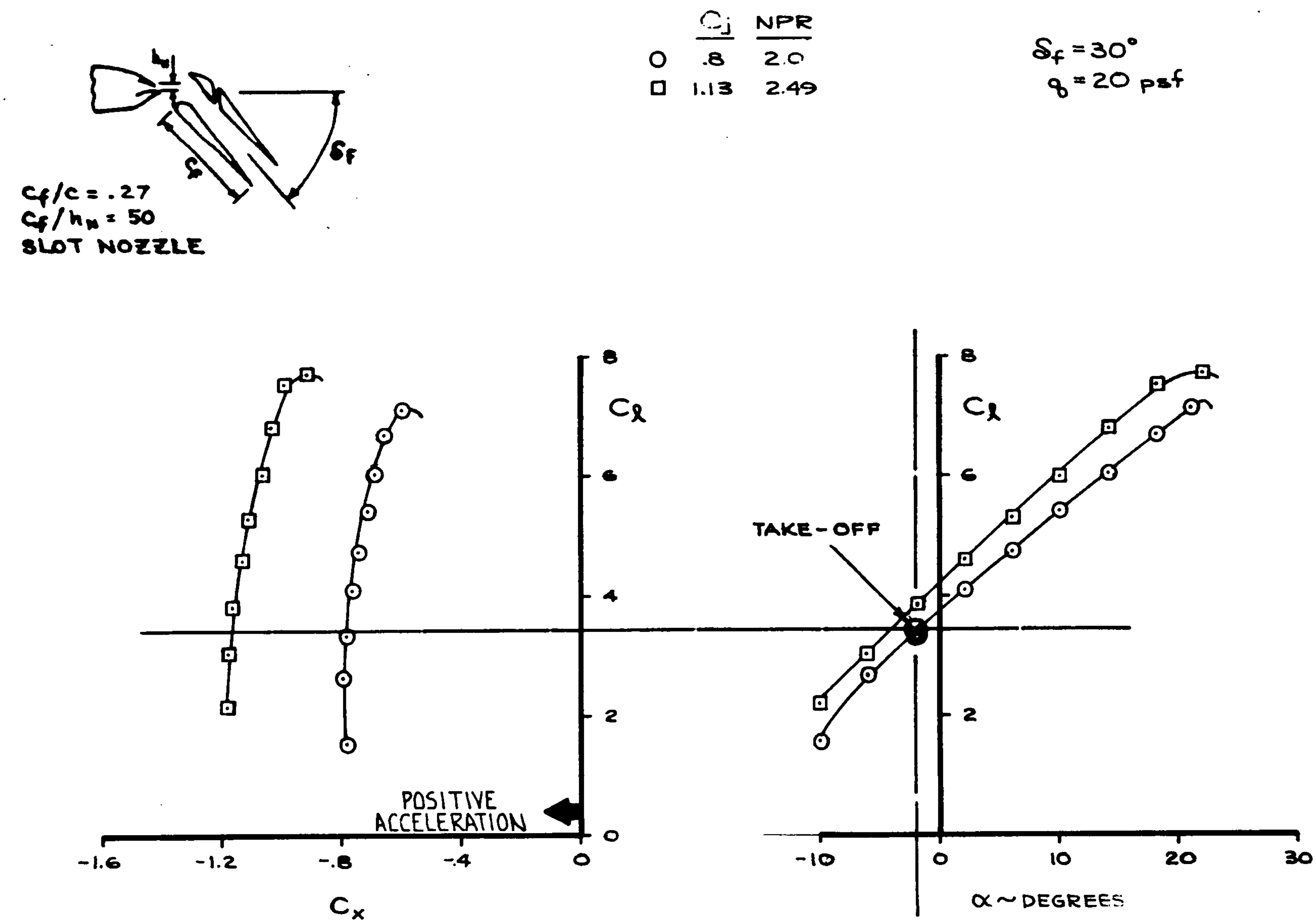

FIGURE 20.—REPRESENTATIVE LIFT CURVES AND DRAG POLARS FOR $\delta_f = 30°$

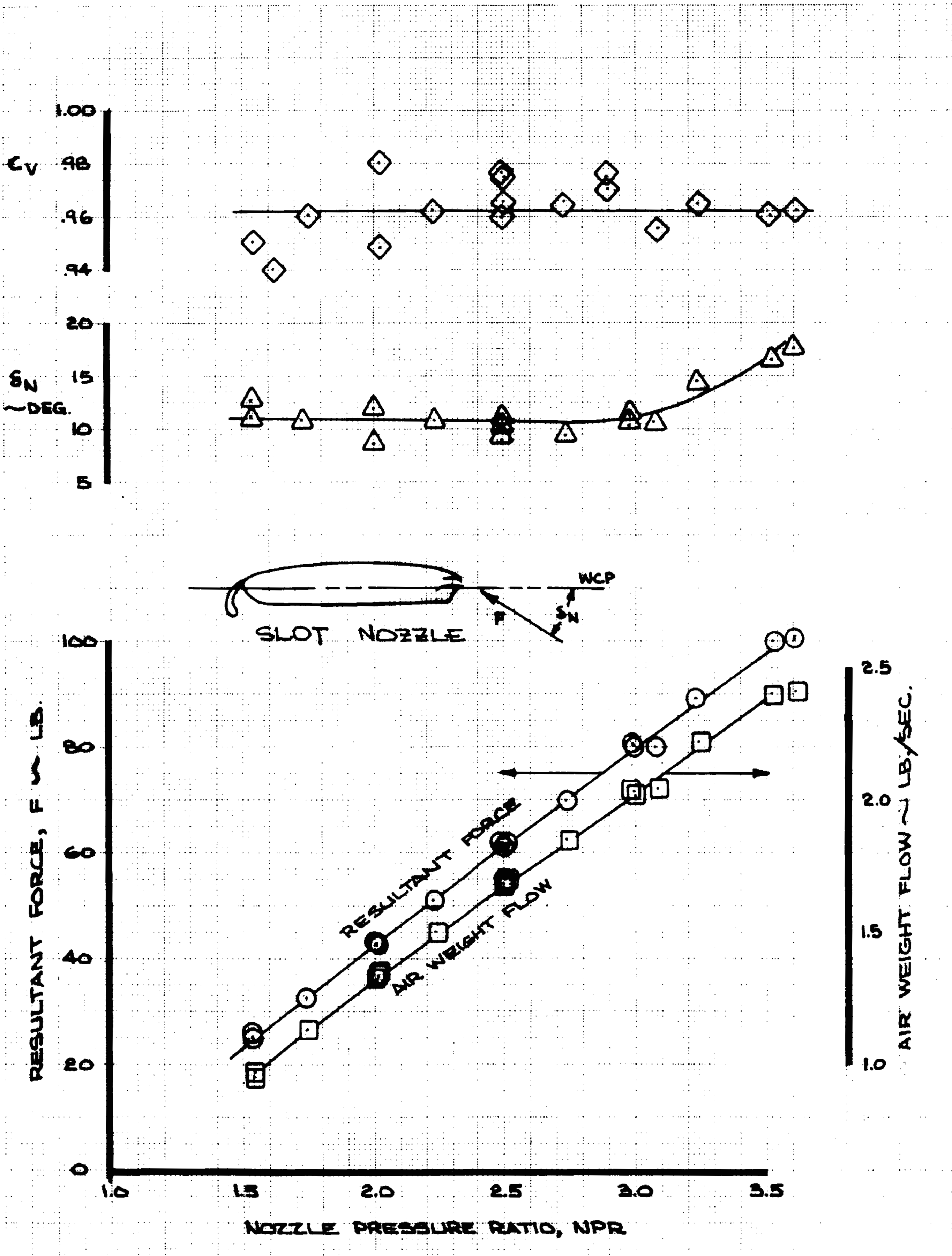

FIGURE 21.—NOZZLE CALIBRATION RESULTS FOR h_N = 0.054-IN. SLOT NOZZLE USED FOR NASA WING SECTION

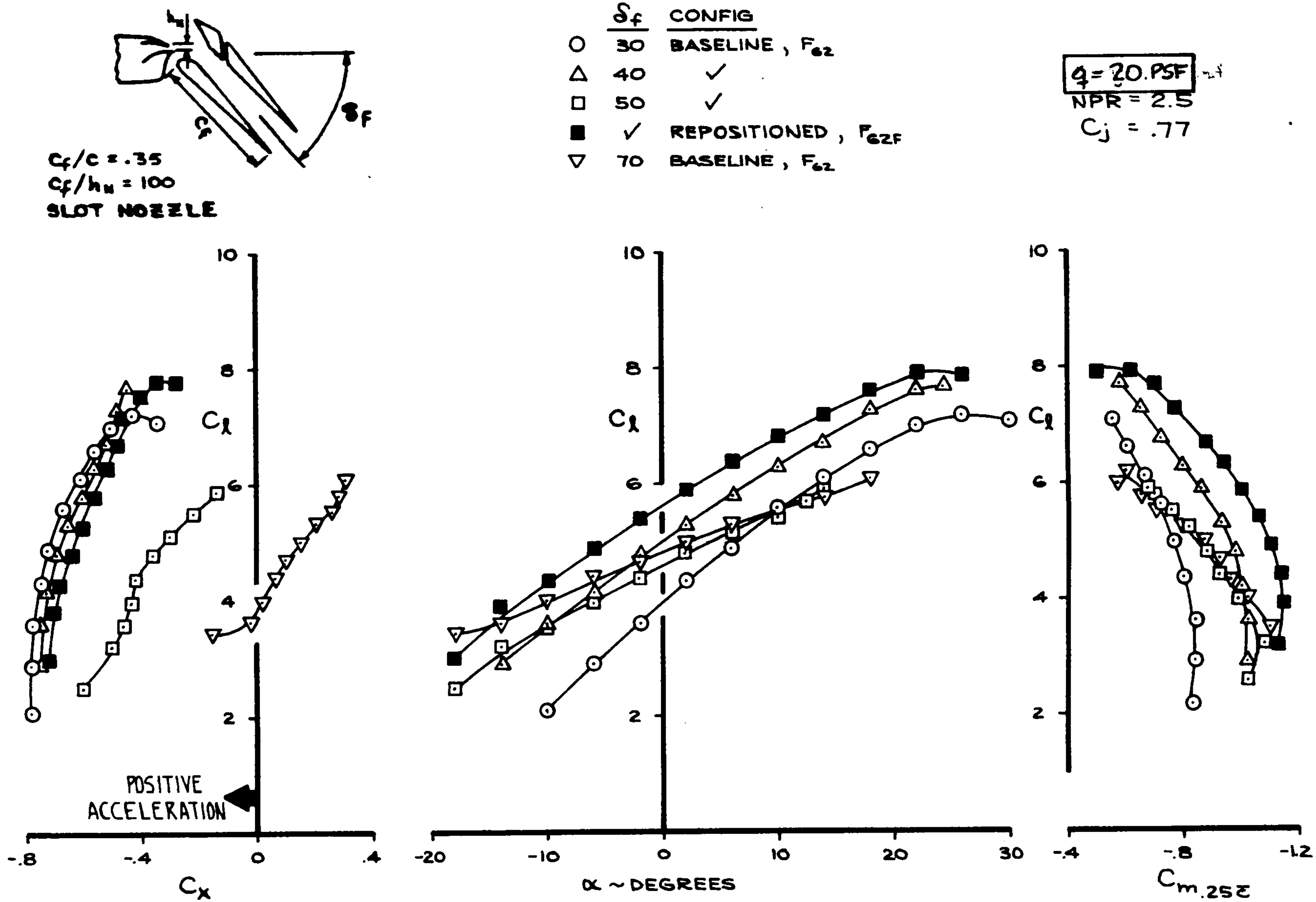

FIGURE 22.—REPRESENTATIVE AERODYNAMIC DATA FOR THE NASA WING SECTION AT $C_j = 0.77$

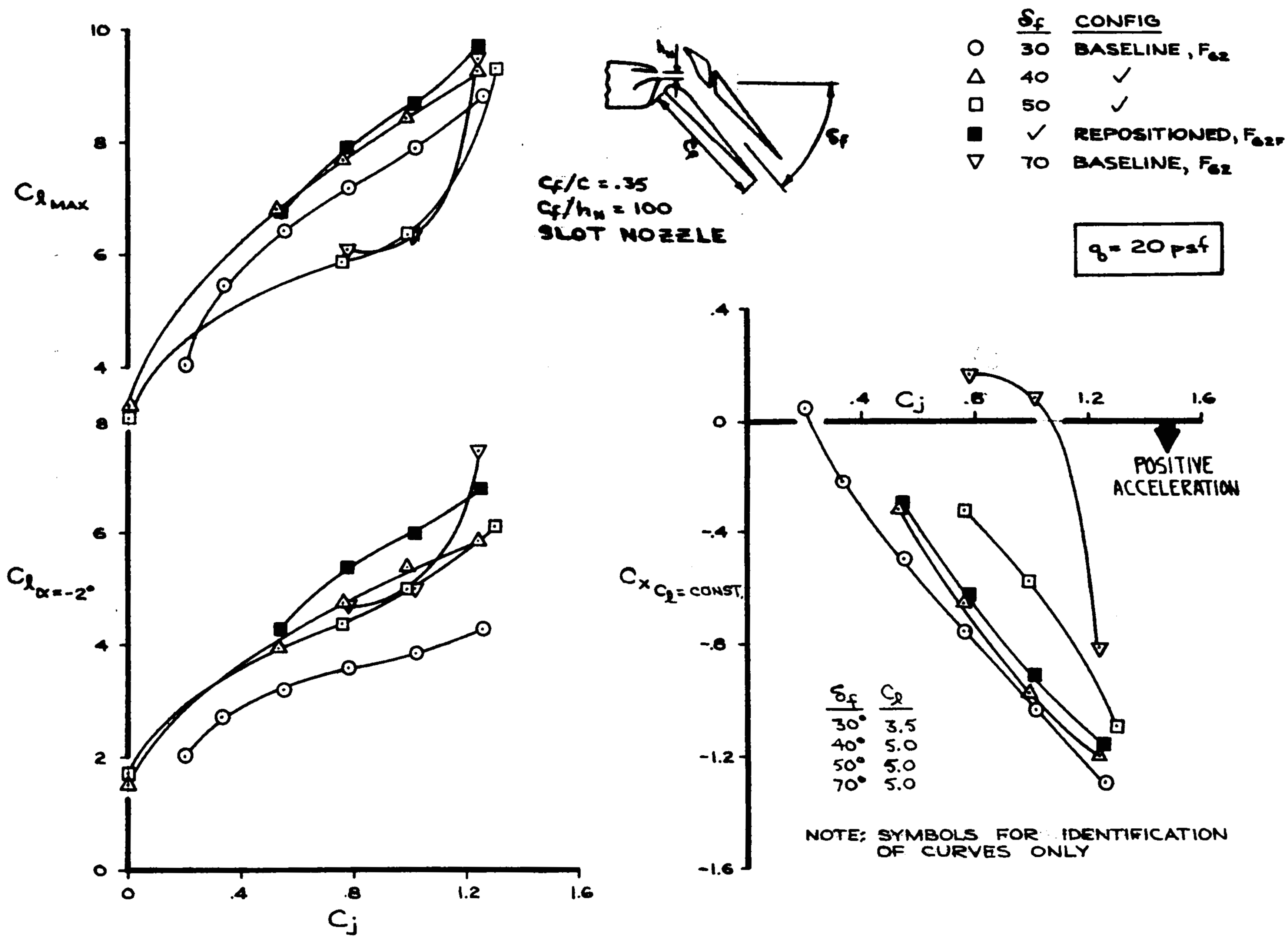

FIGURE 23.—LIFT AND STREAMWISE FORCE VARIATION WITH C_j FOR NASA WING SECTION

C2

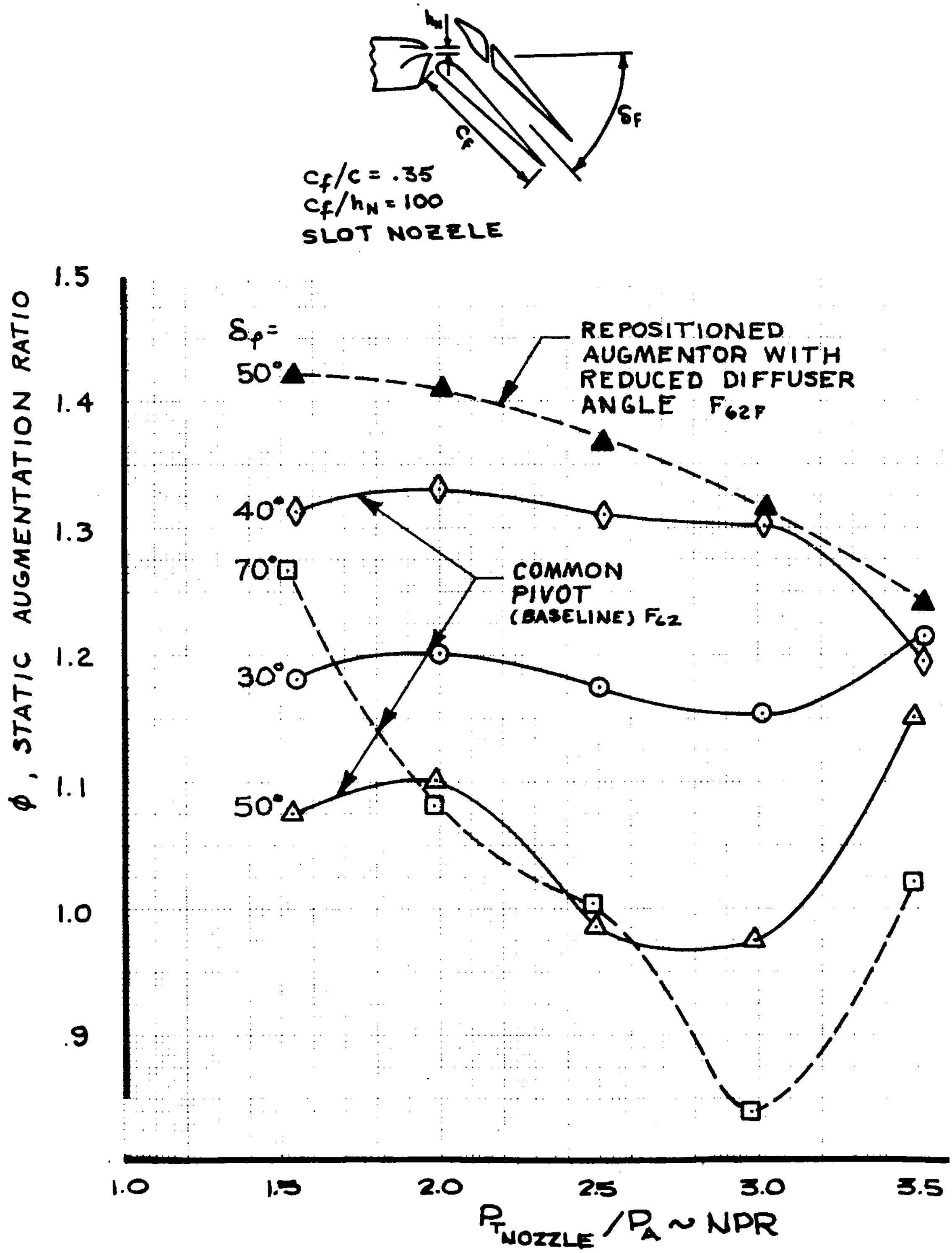

FIGURE 24.–STATIC THRUST AUGMENTATION RATIO FOR THE NASA WING SECTION AUGMENTOR

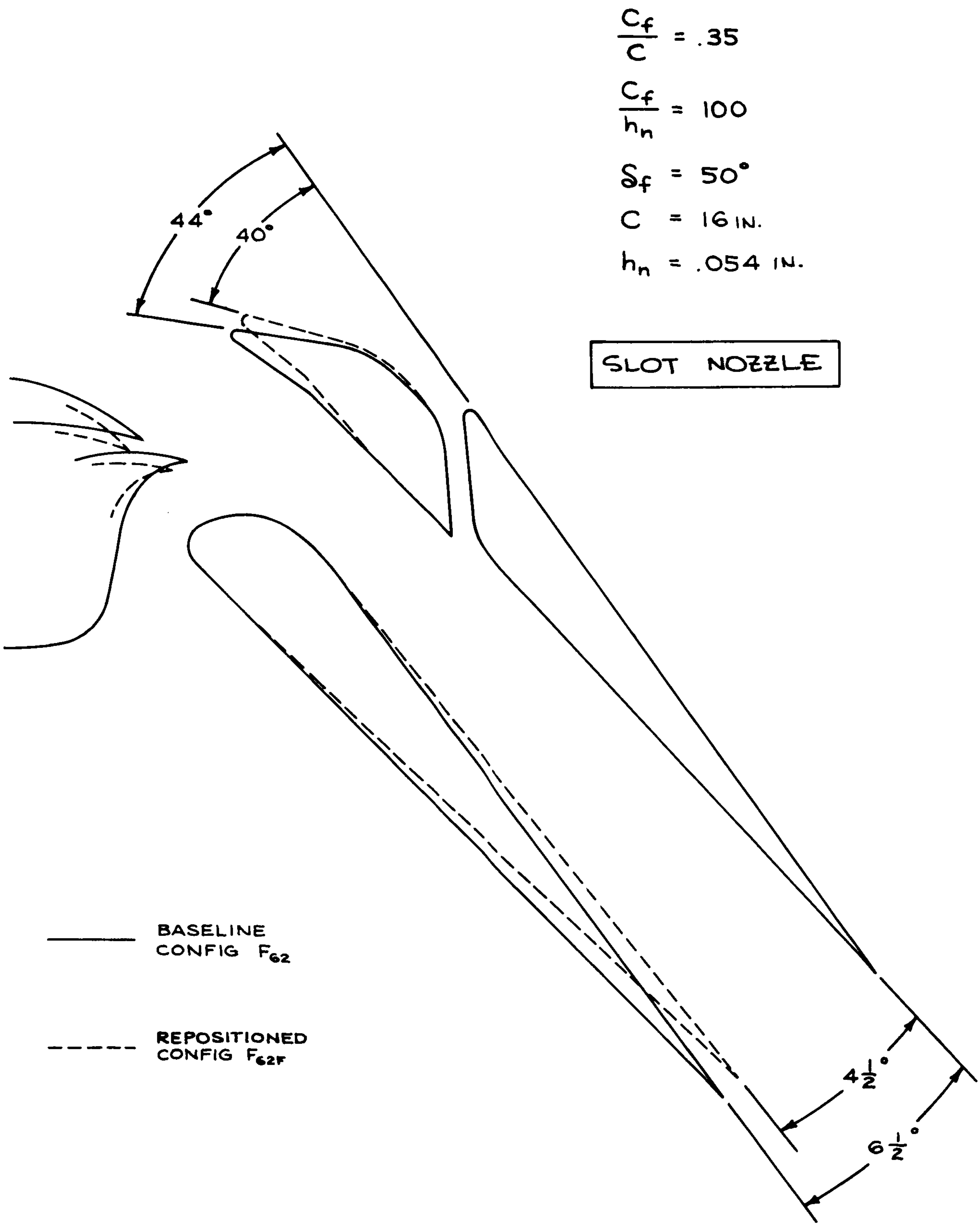

FIGURE 25.—NASA WING SECTION BASELINE AND REPOSITIONED CONFIGURATIONS

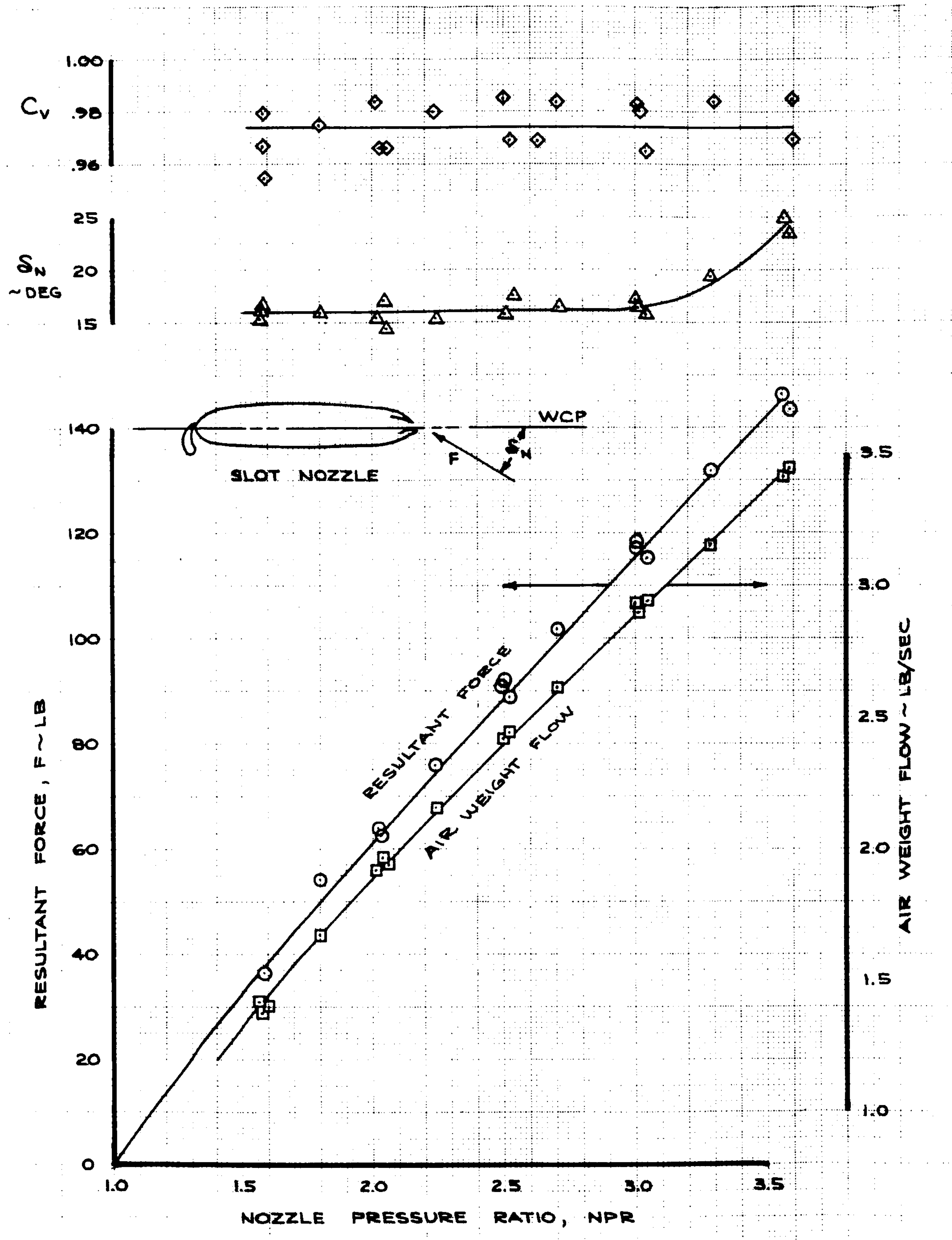

FIGURE 26.–NOZZLE CALIBRATION RESULTS FOR h_N = 0.085-IN. SLOT NOZZLE USED FOR SCALED NASA SECTION

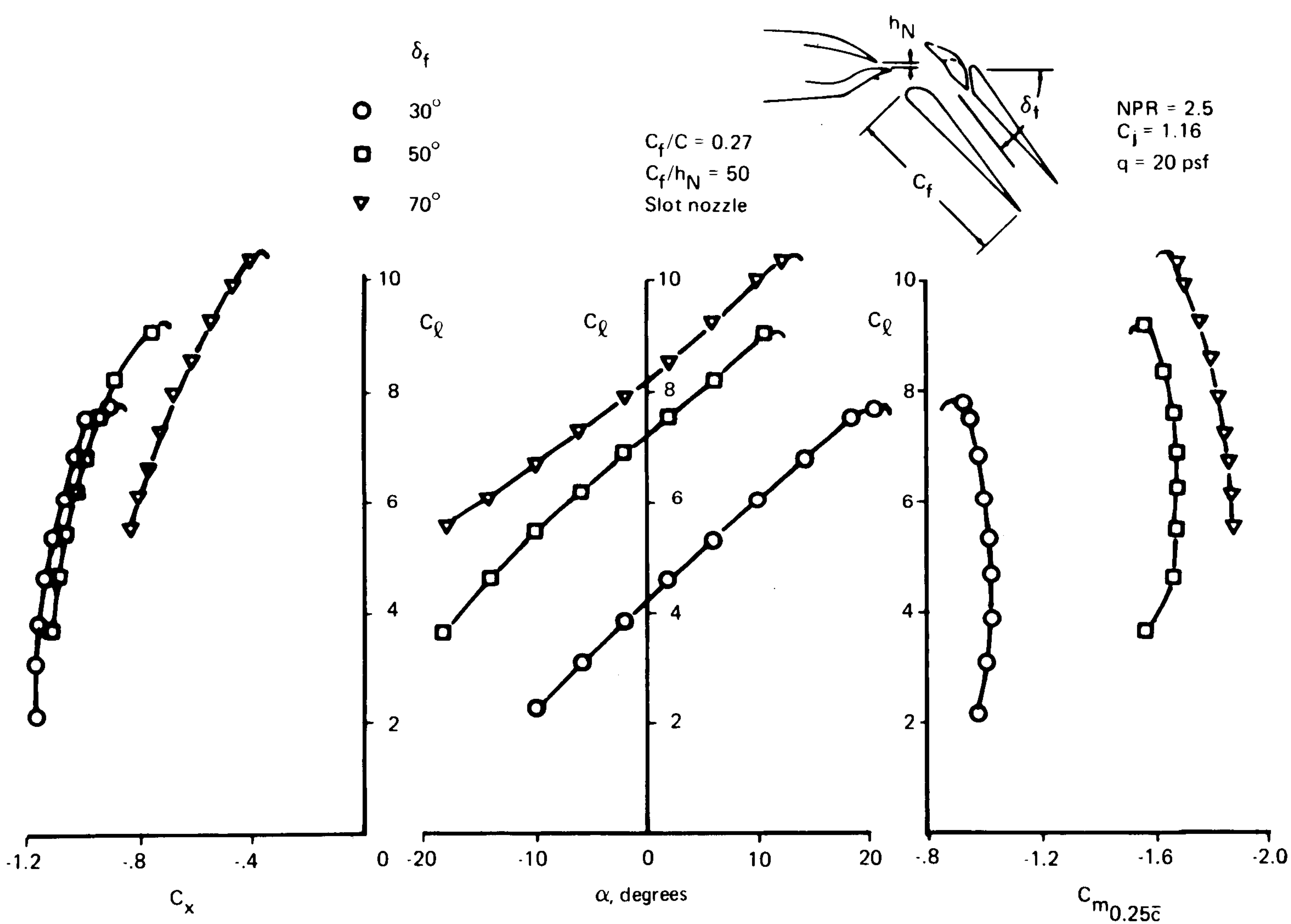

FIGURE 27.–REPRESENTATIVE AERODYNAMIC DATA FOR THE SCALED NASA SECTION AT $C_j = 1.16$

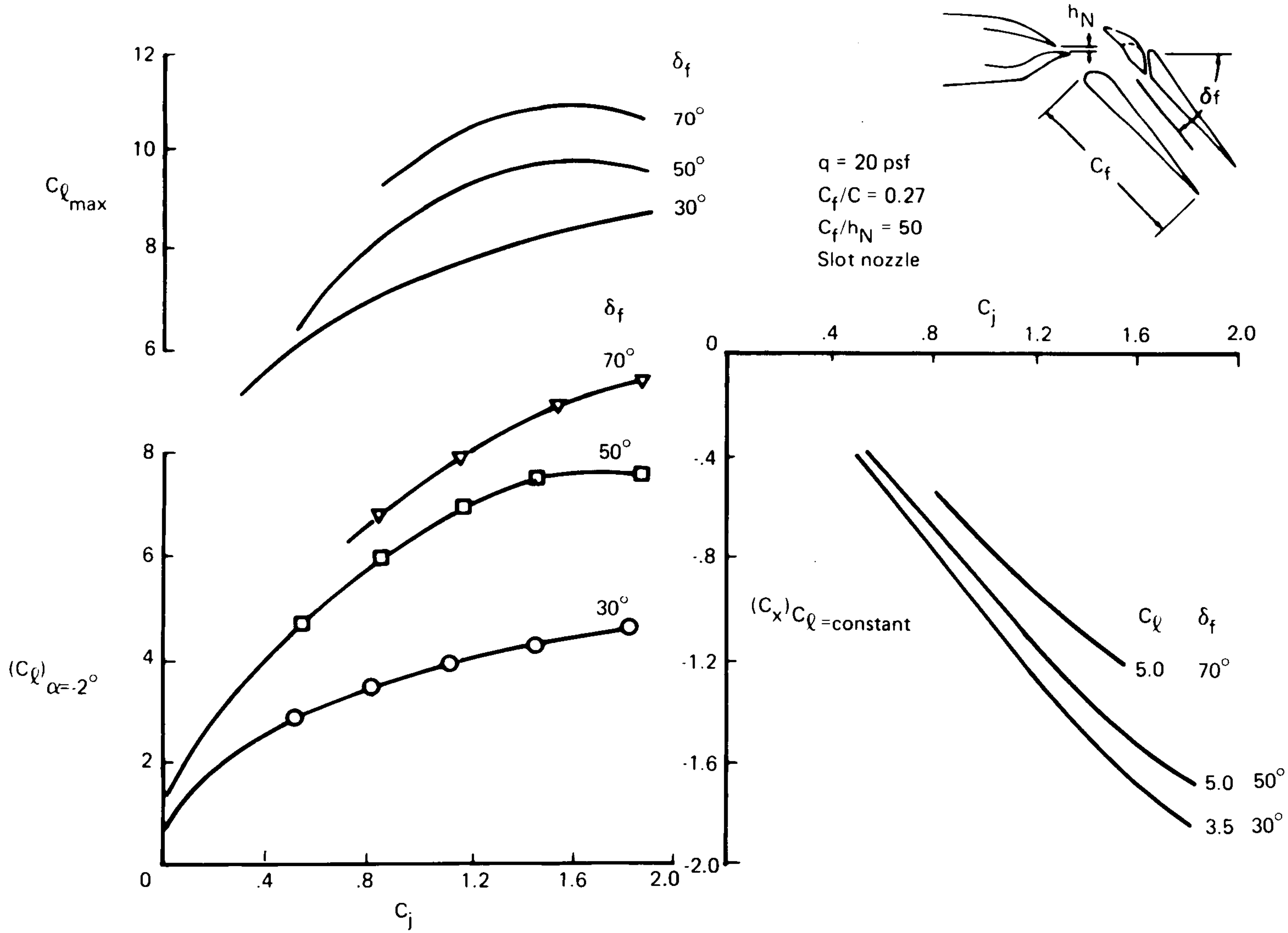

FIGURE 28.—VARIATION OF LIFT AND STREAMWISE FORCE WITH C_j FOR THE SCALED NASA SECTION

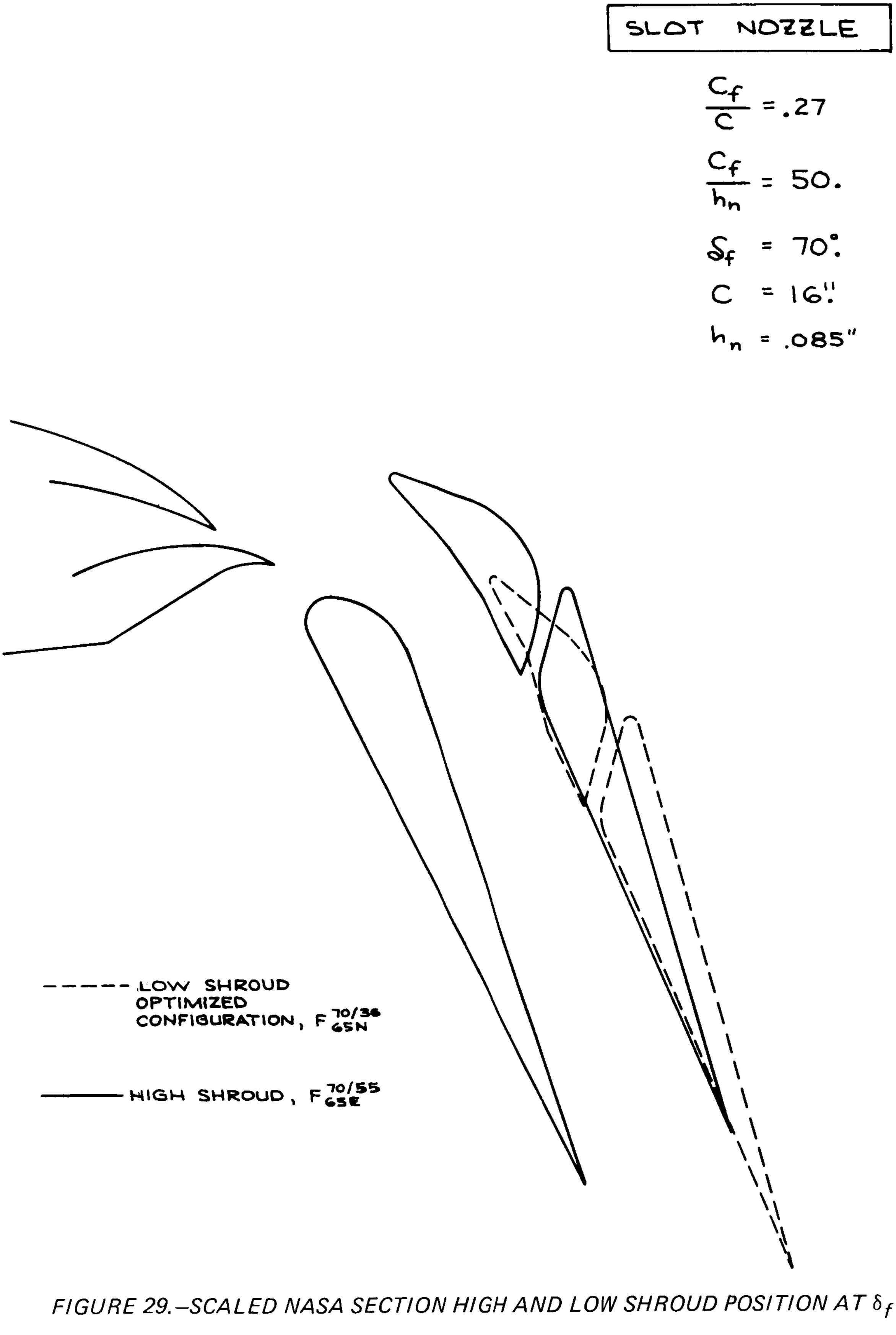

FIGURE 29.—SCALED NASA SECTION HIGH AND LOW SHROUD POSITION AT $\delta_f = 70°$

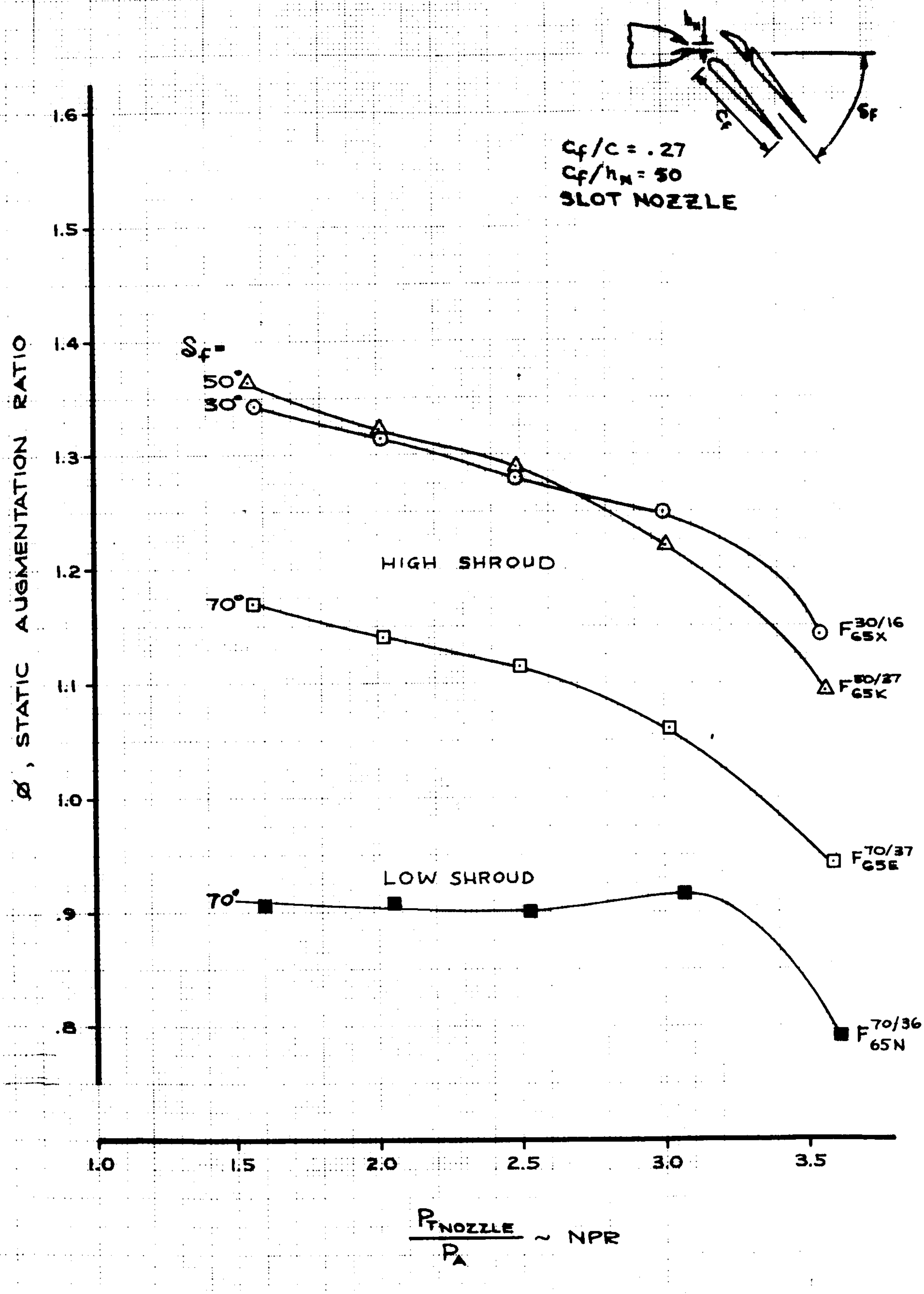

FIGURE 30.–STATIC THRUST AUGMENTATION RATIO FOR SCALED NASA SECTION

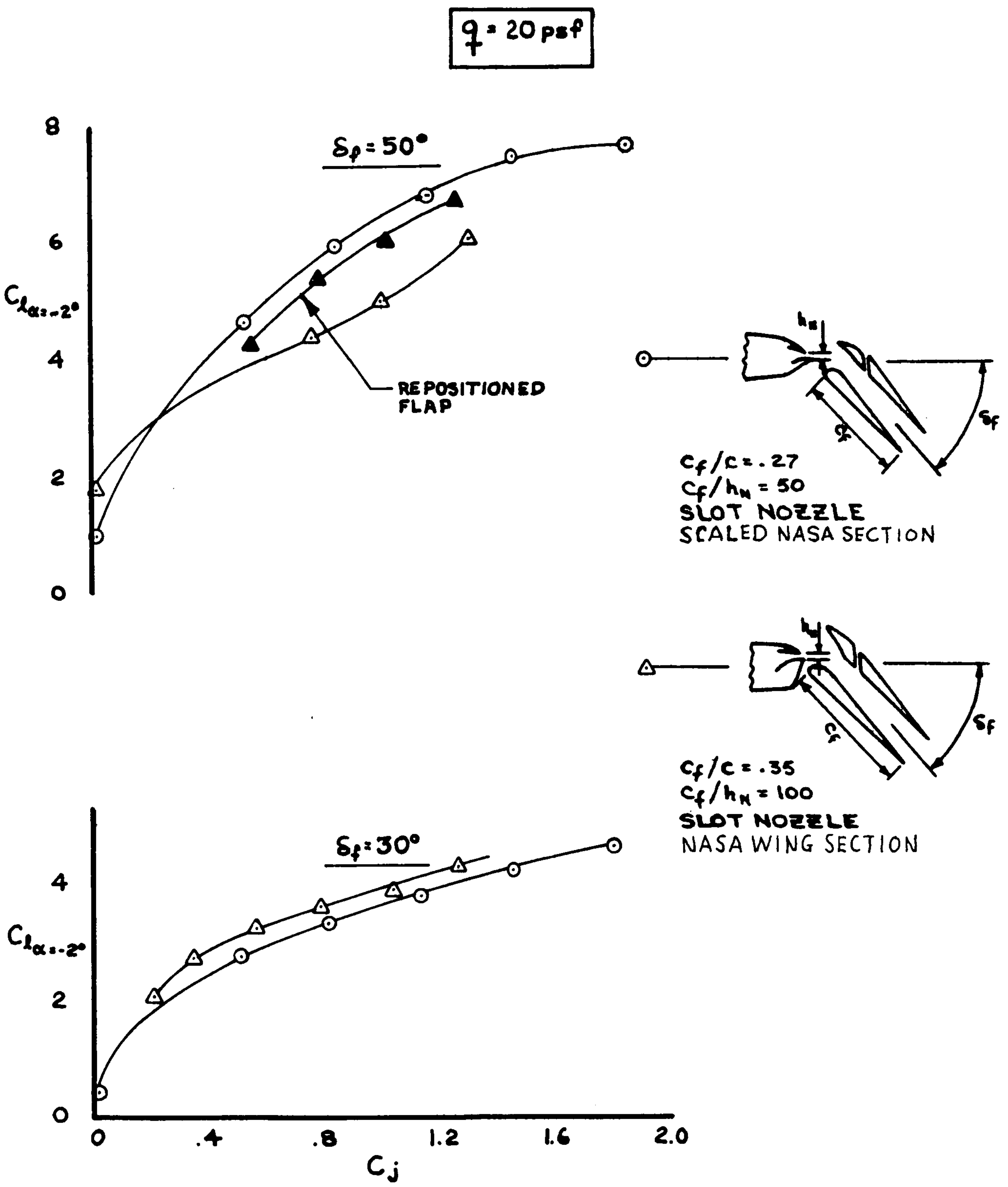

FIGURE 31.—LIFT LEVEL VARIATION WITH C_j FOR NASA WING SECTION AND SCALED NASA SECTION

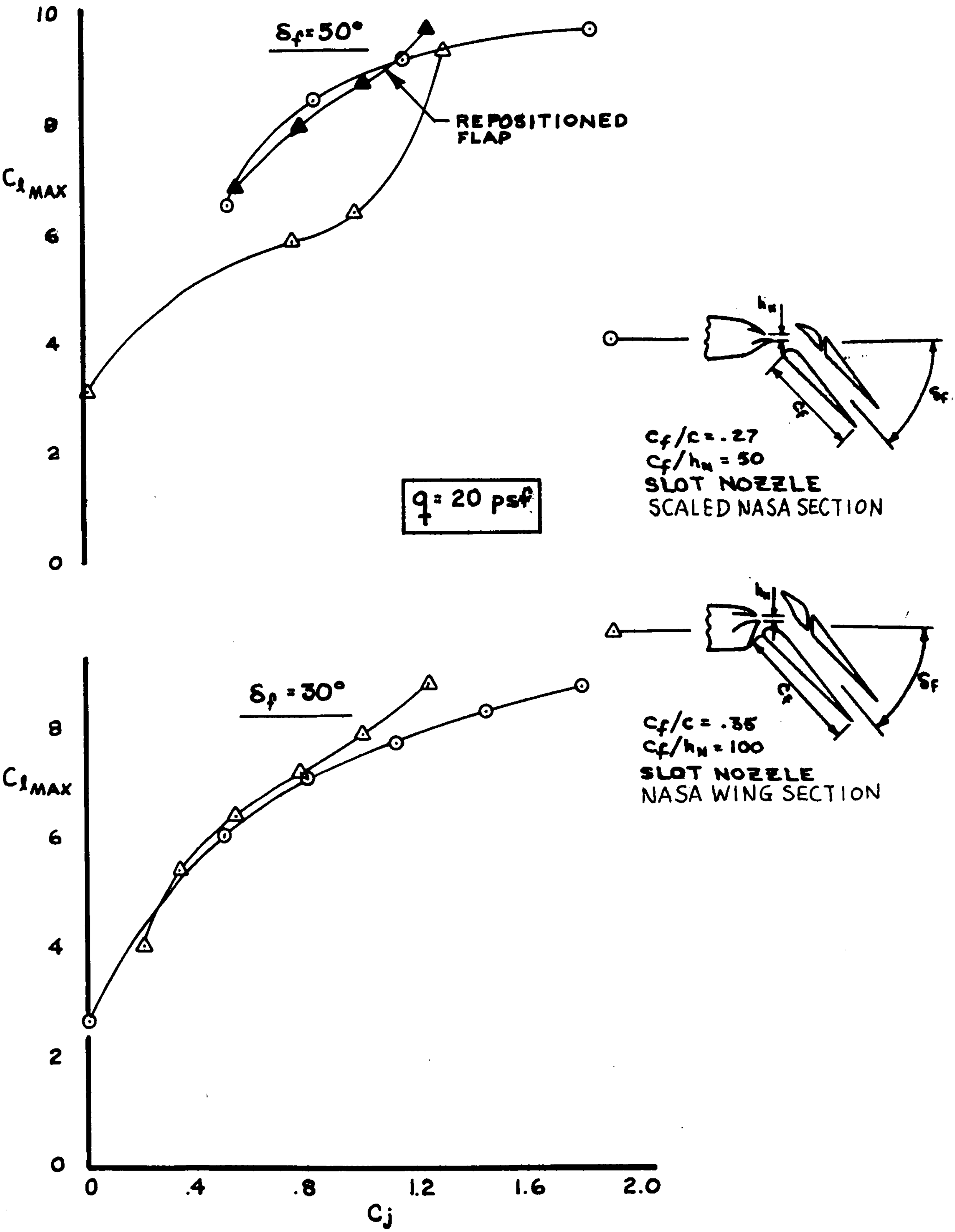

FIGURE 32.–COMPARISON OF MAXIMUM LIFT WITH C_j FOR NASA WING SECTION AND SCALED NASA SECTION

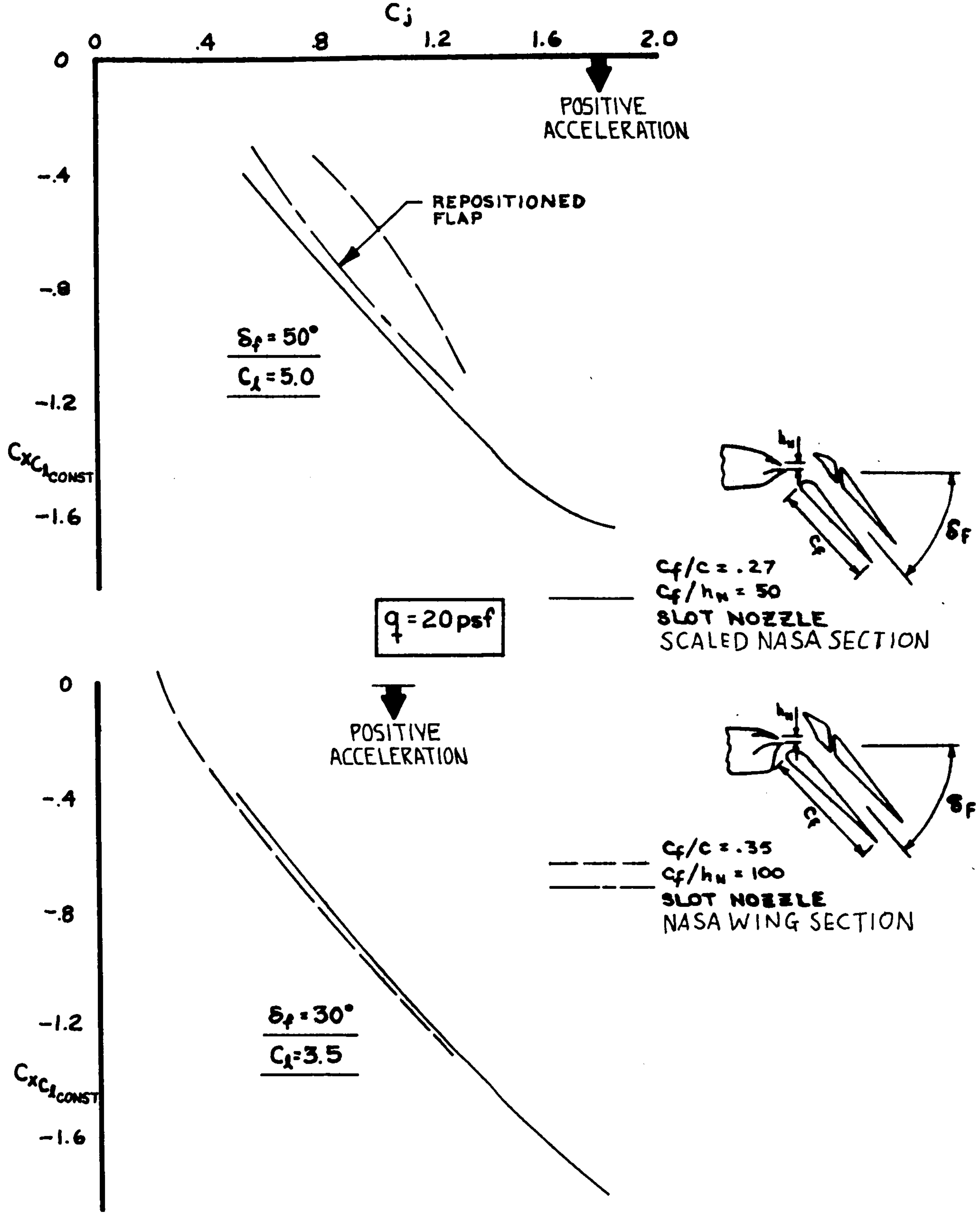

FIGURE 33.—COMPARISON OF STREAMWISE FORCE VARIATION WITH C_j FOR NASA WING SECTION AND SCALED NASA SECTION

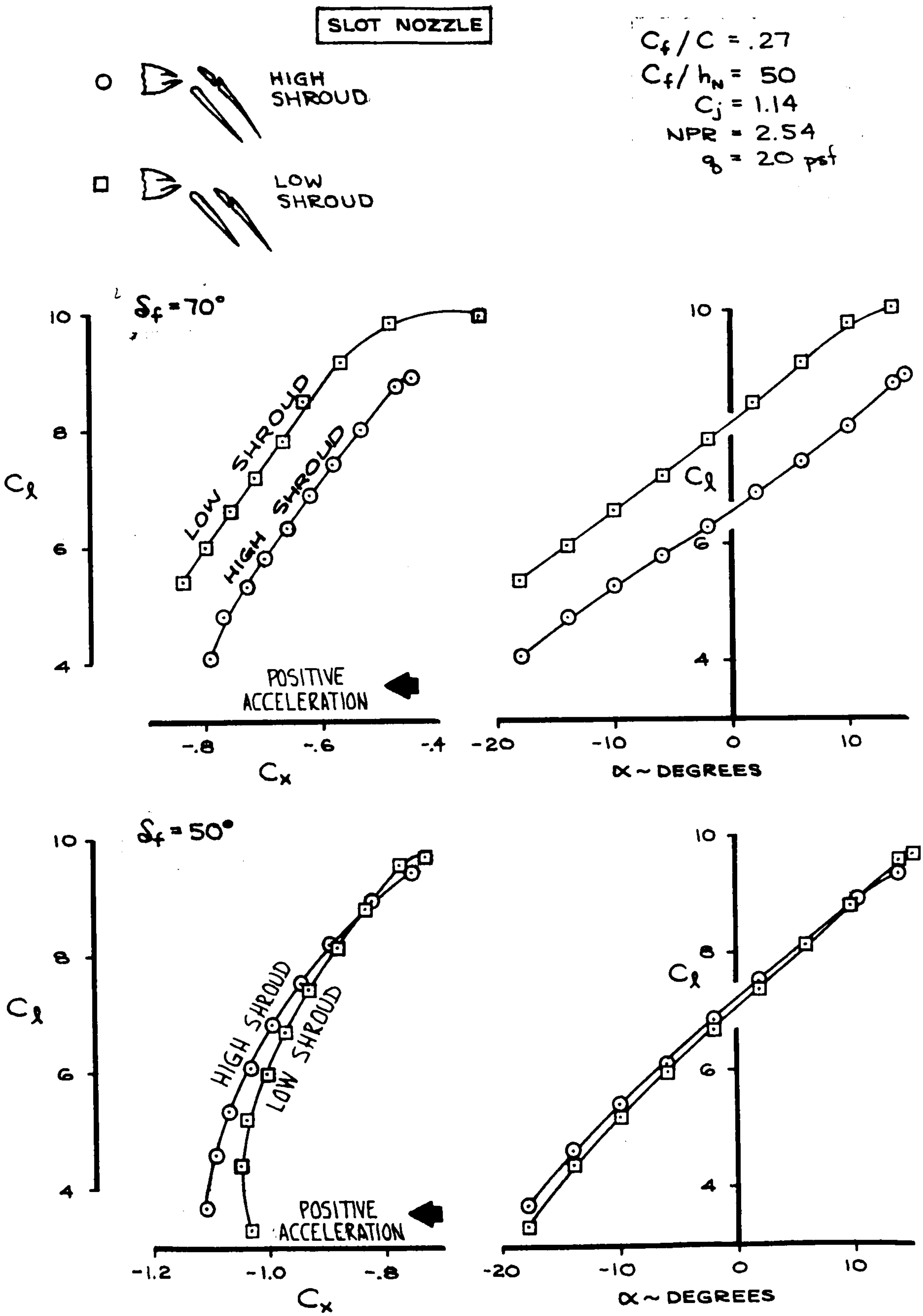

FIGURE 34.—EFFECT OF SHROUD POSITION

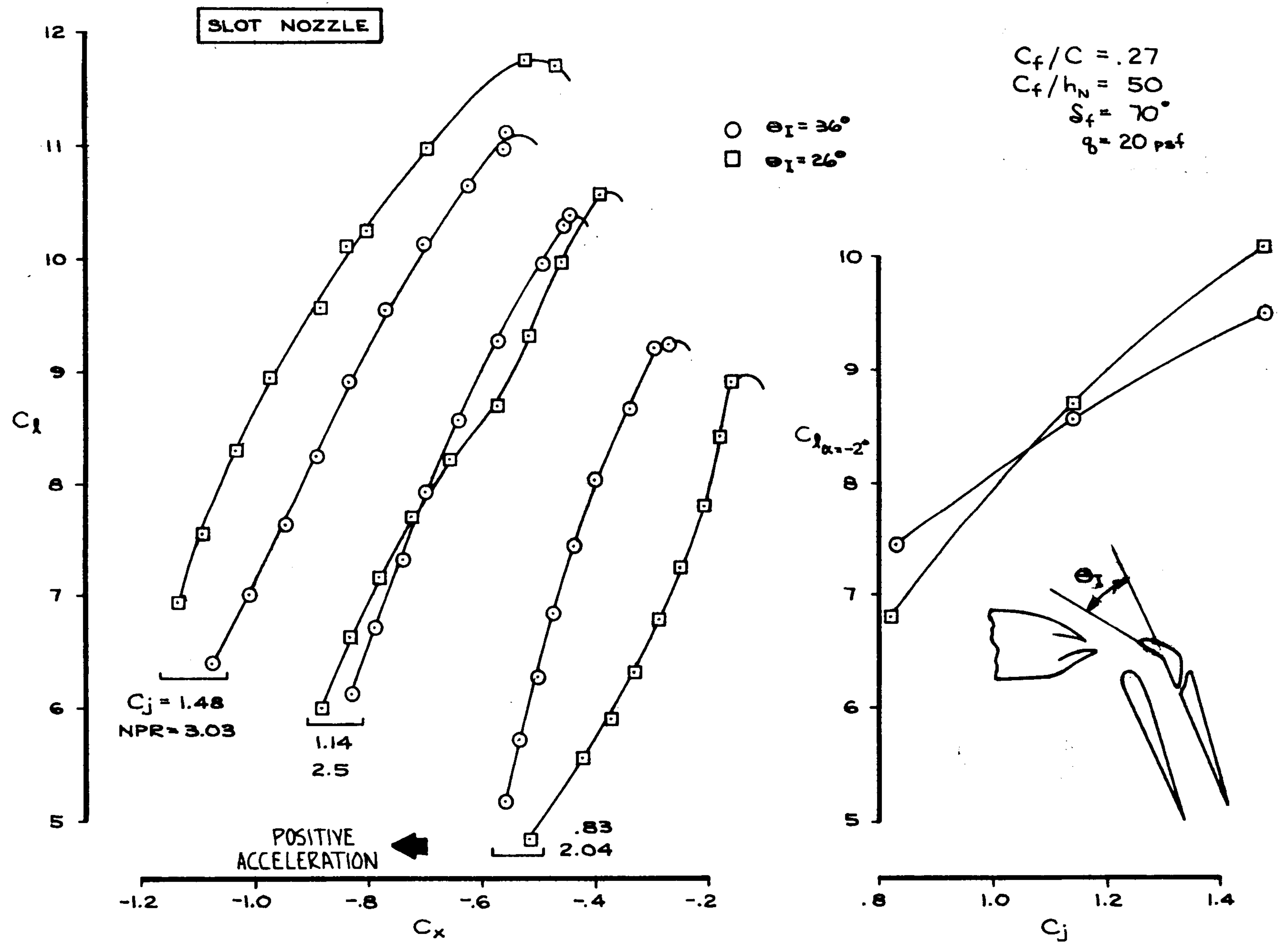

FIGURE 35.—EFFECT OF INTAKE DOOR ANGLE

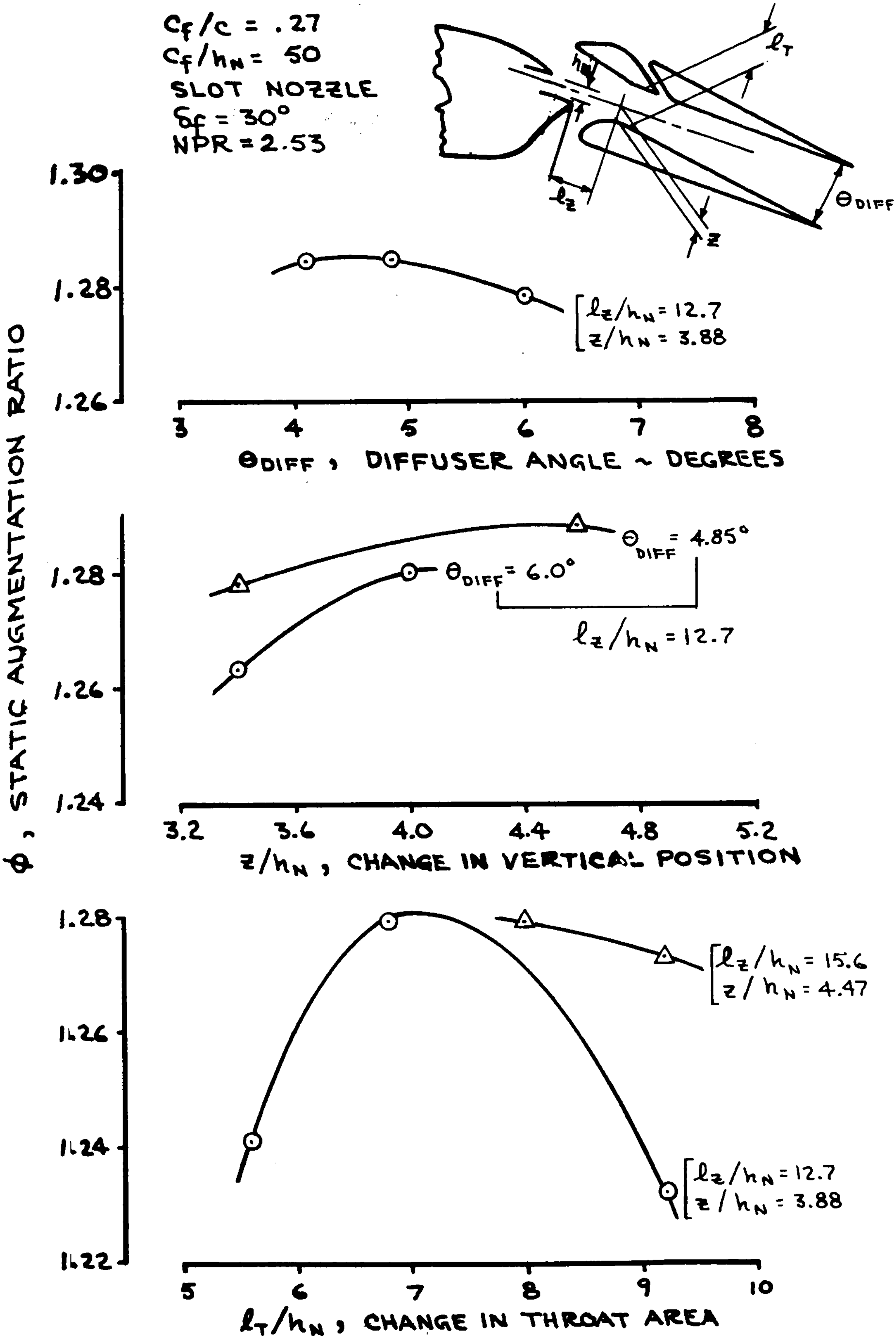

FIGURE 36.—EFFECT OF AUGMENTOR FLAP GEOMETRY ON STATIC THRUST AUGMENTATION RATIO FOR SCALED NASA SECTION

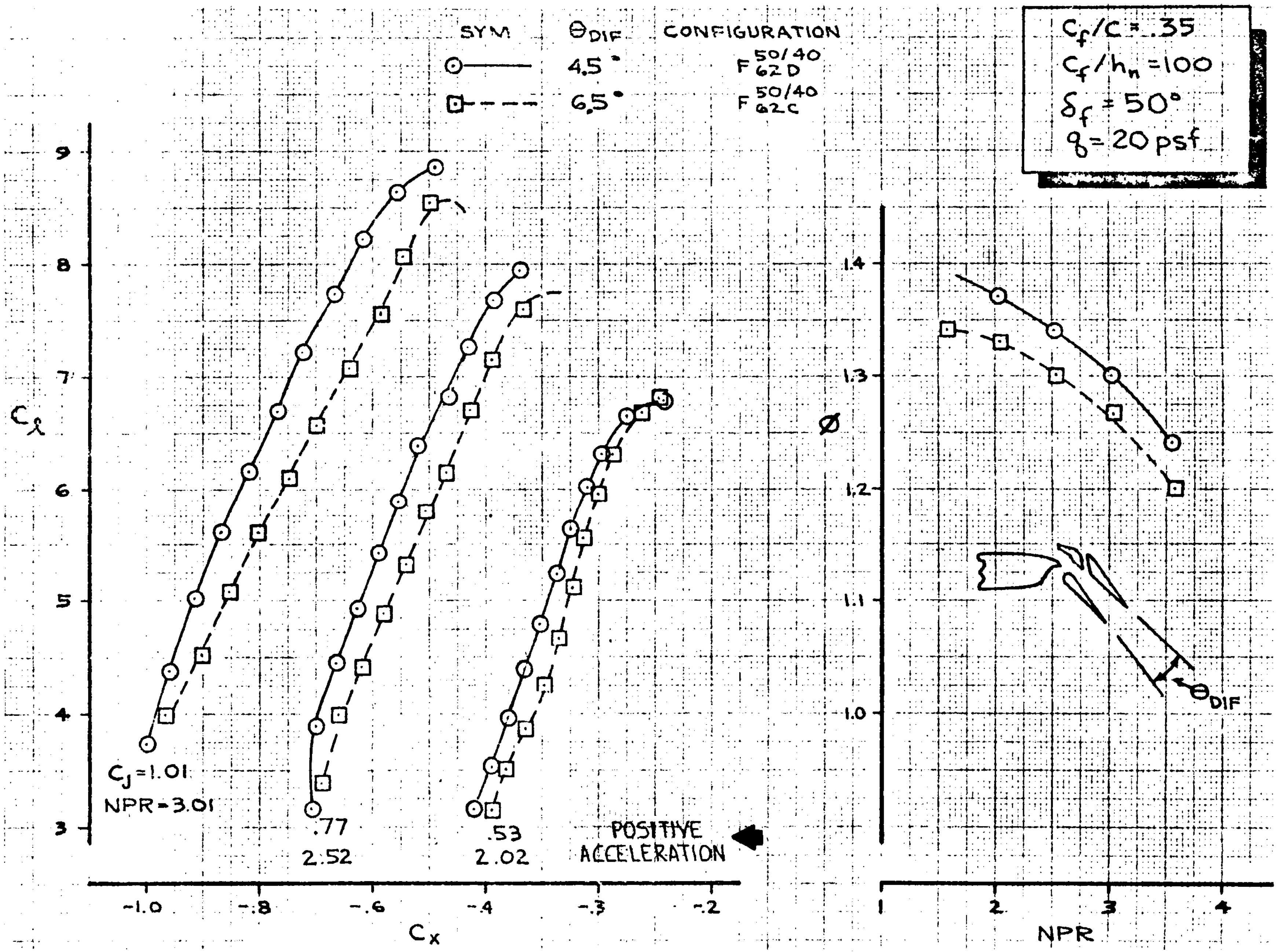

FIGURE 37.—EFFECTS OF DIFFUSER ANGLE FOR NASA WING SECTION AT $\delta_f = 50°$

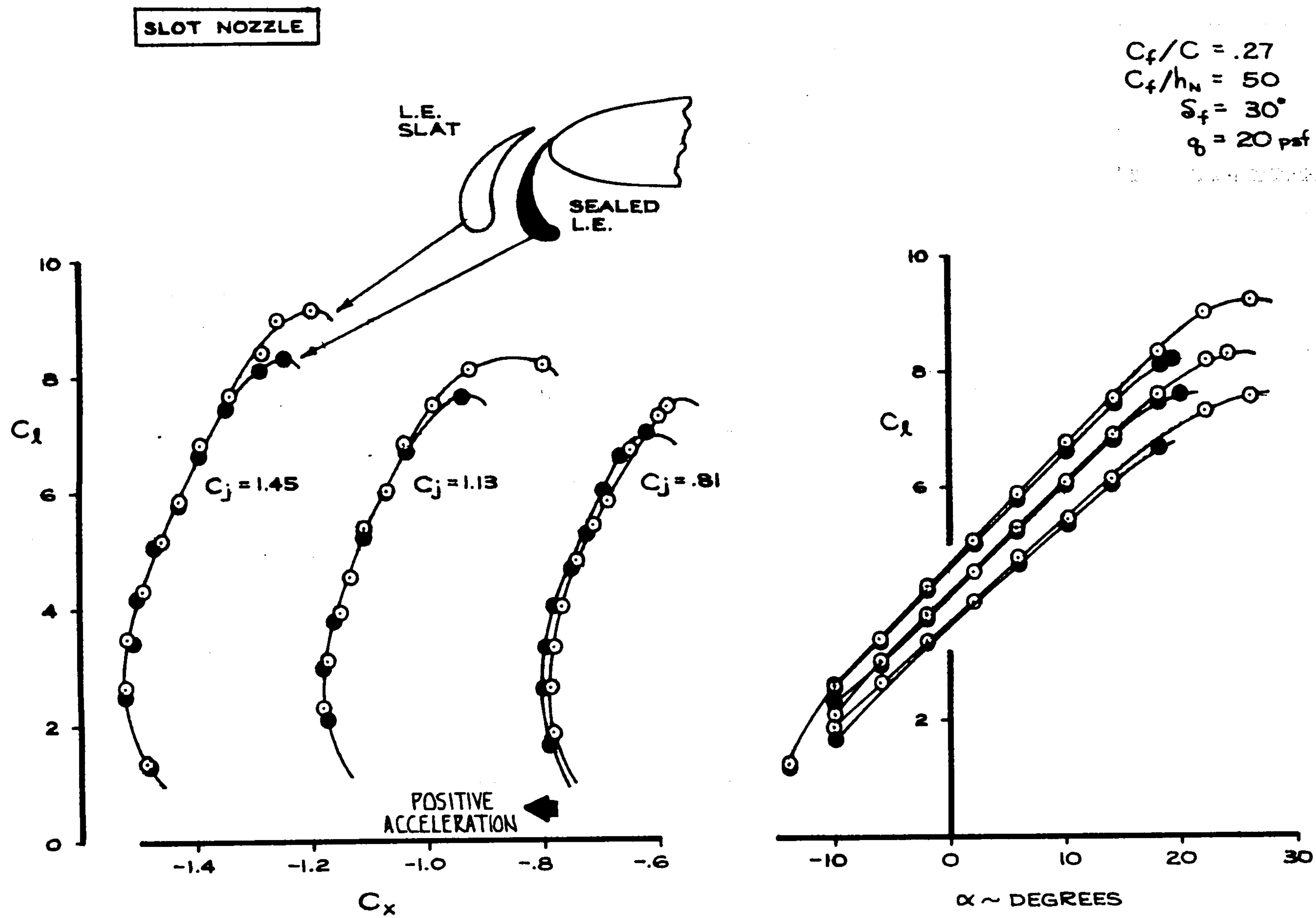

FIGURE 38. —SEALED AND UNSEALED LEADING EDGE DEVICE COMPARISON FOR SCALED NASA SECTION, LIFT, AND STREAMWISE FORCE

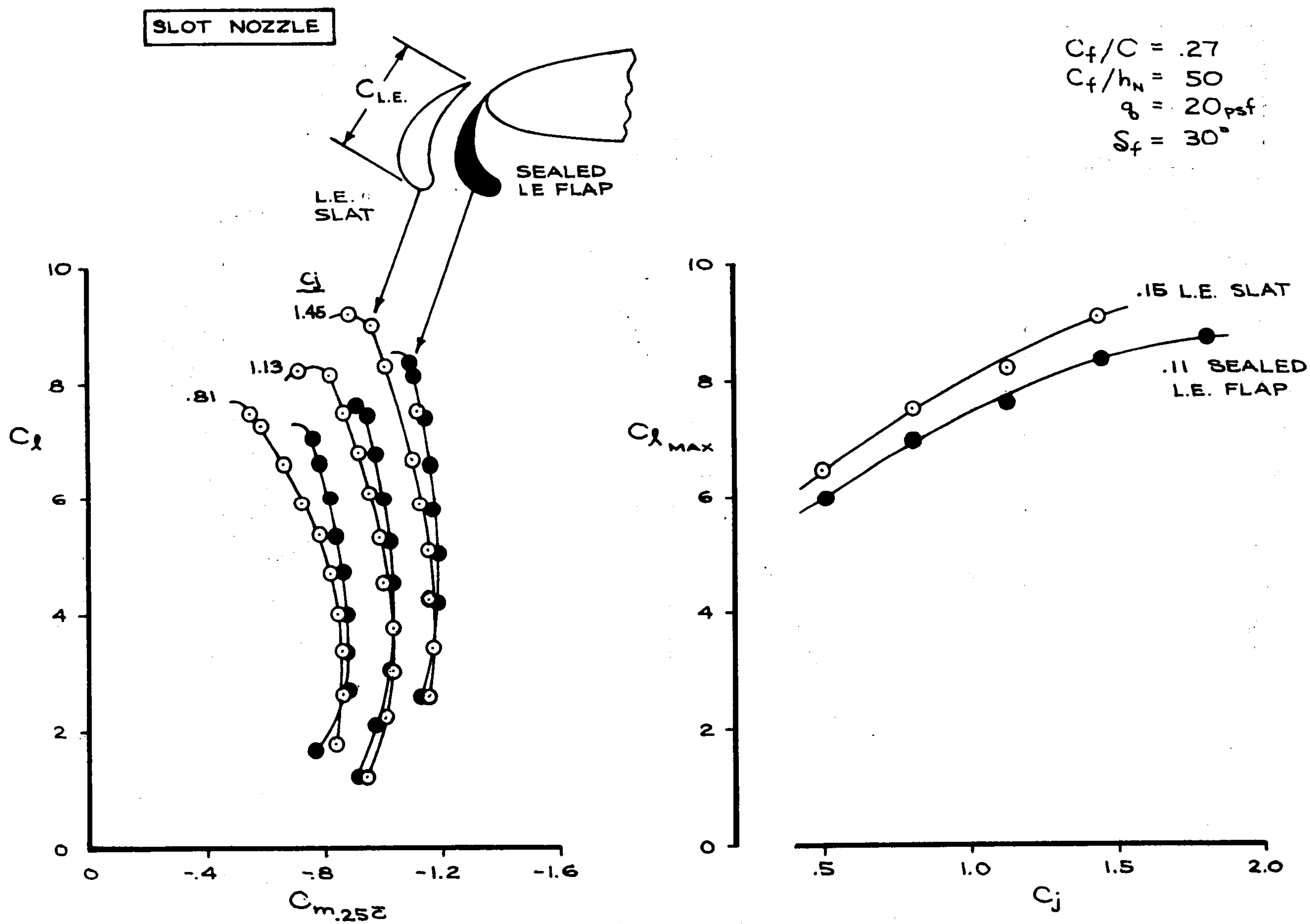

FIGURE 39.—SEALED AND UNSEALED LEADING EDGE DEVICE COMPARISON FOR SCALED NASA SECTION, MAXIMUM LIFT AND PITCHING MOMENT

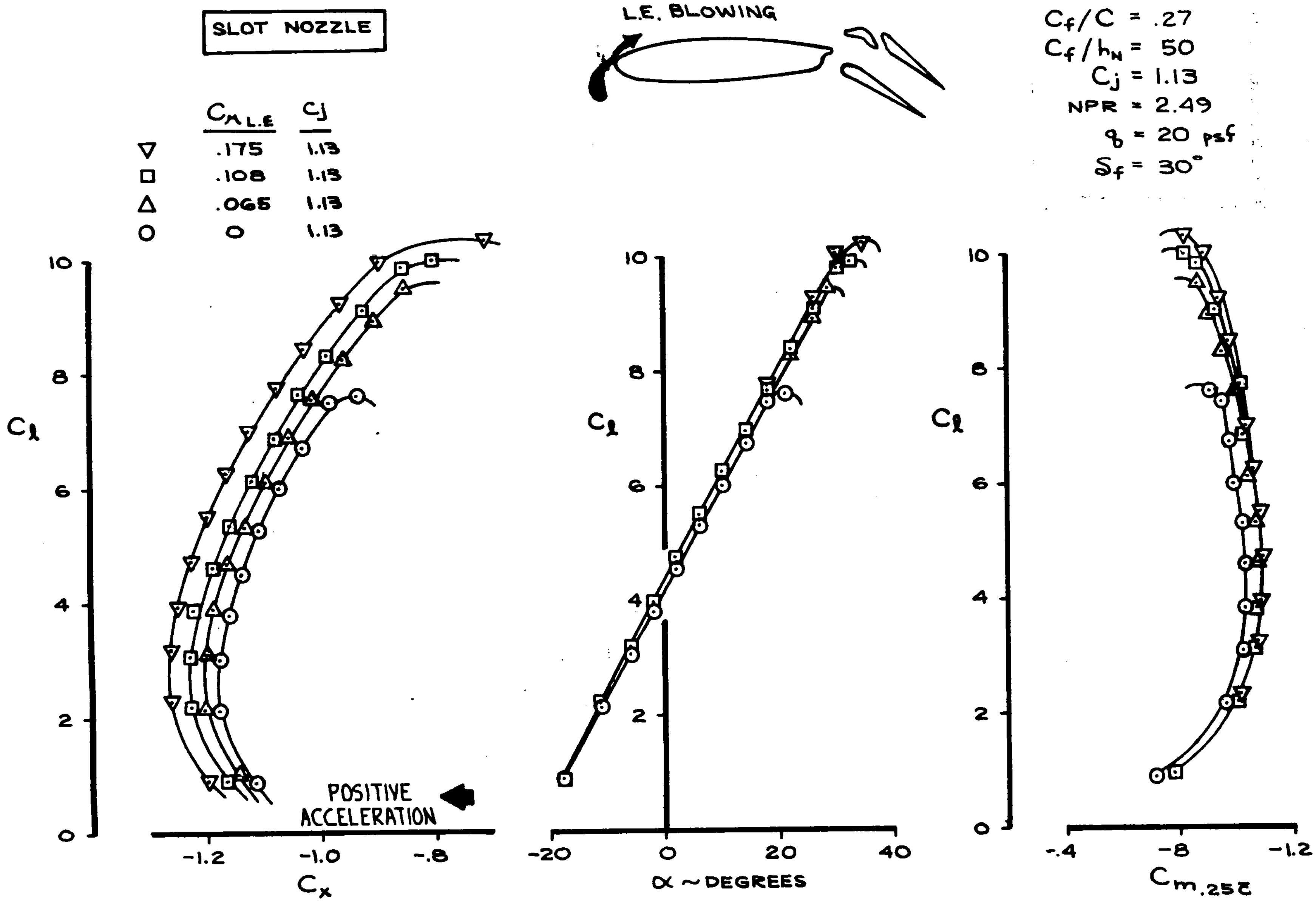

FIGURE 40.–INFLUENCE OF LEADING EDGE BLOWING FOR SCALED NASA SECTION AT $\delta_f = 30°$

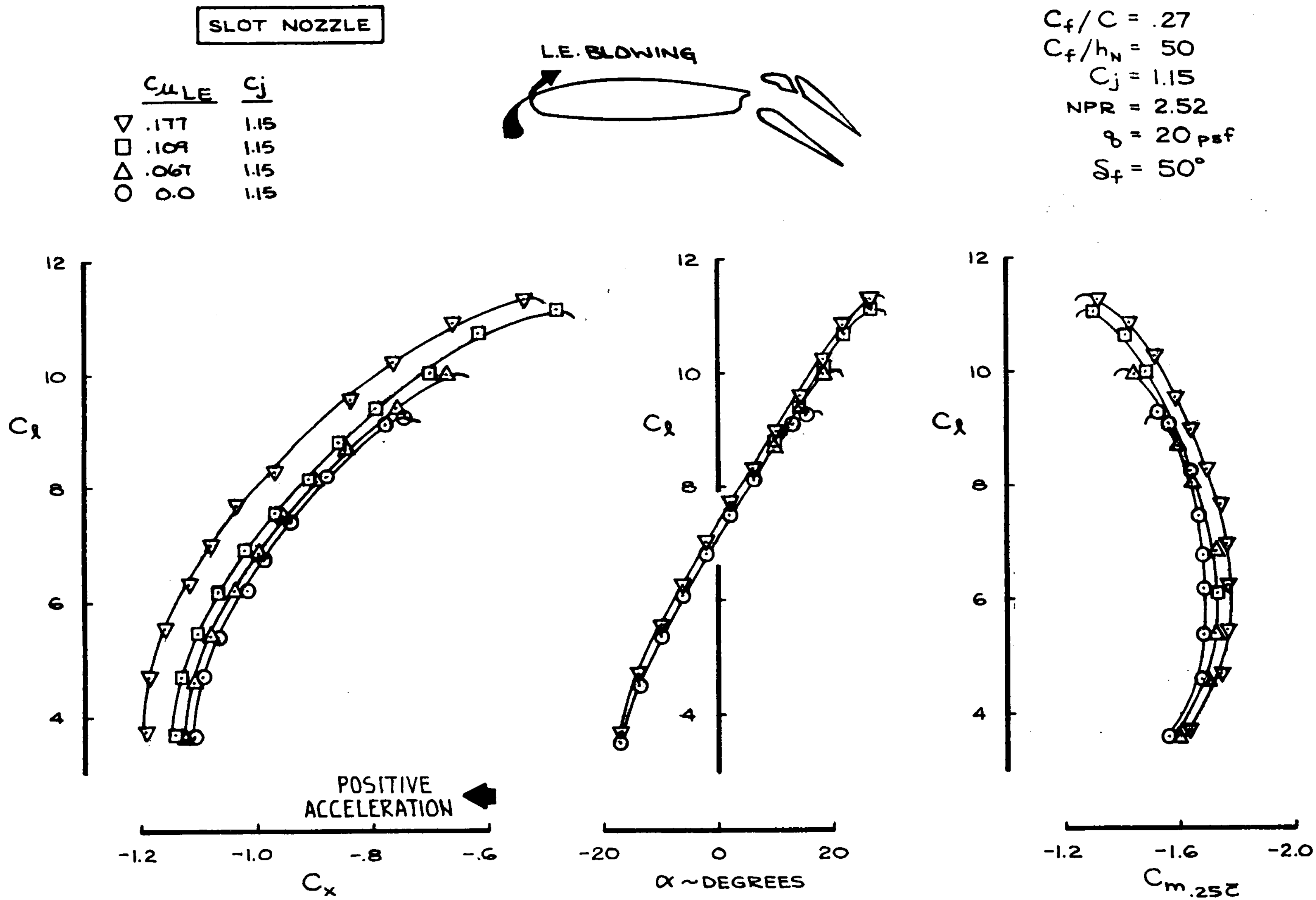

FIGURE 41.—INFLUENCE OF LEADING EDGE BLOWING FOR SCALED NASA SECTION AT $\delta_f = 50°$

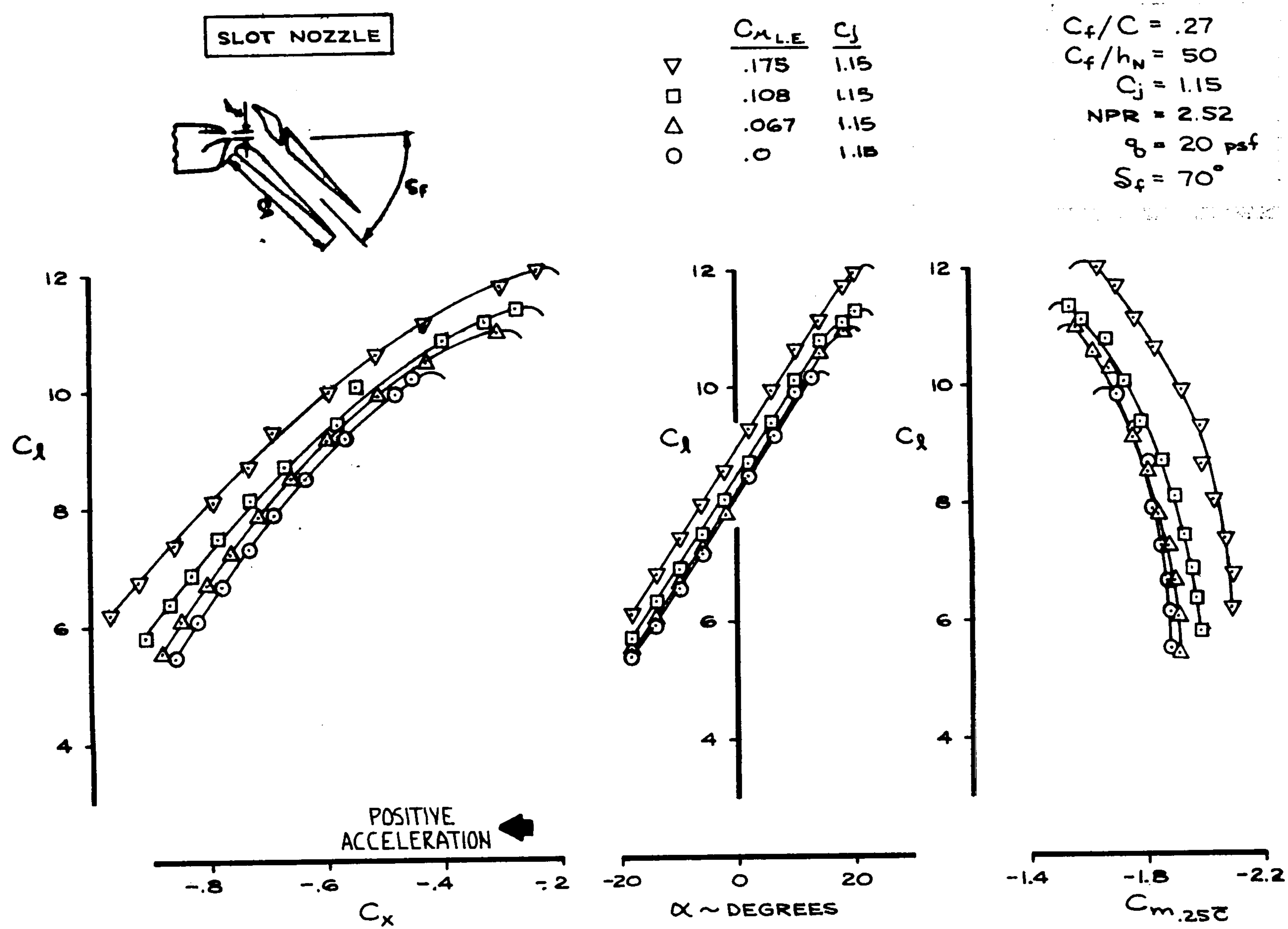

FIGURE 42.—INFLUENCE OF LEADING EDGE BLOWING FOR SCALED NASA SECTION AT $\delta_f = 70°$

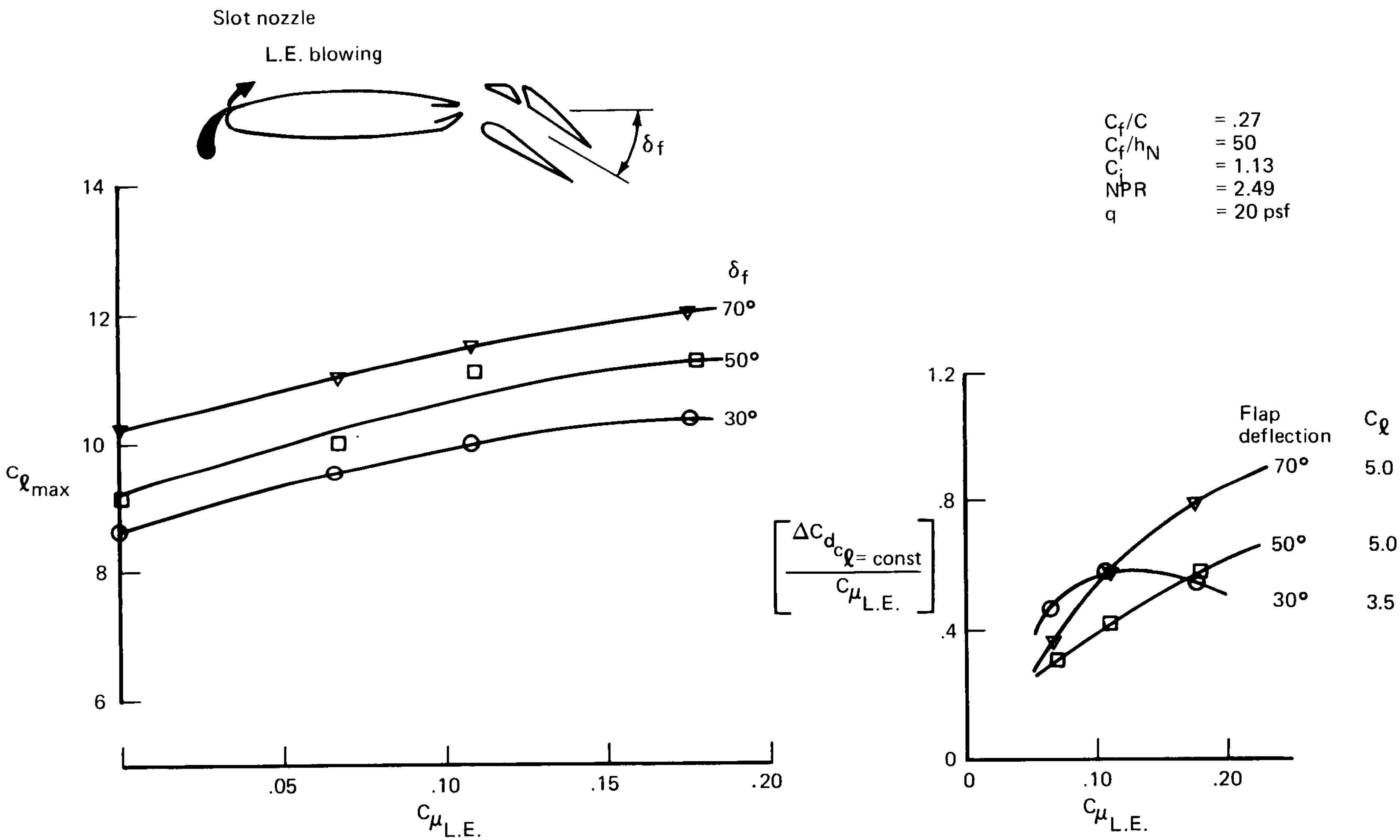

FIGURE 43.—MAXIMUM LIFT AND THRUST RECOVERY CAPABILITY OF LEADING EDGE BLOWING FOR SCALED NASA SECTION AT C_j = 1.13

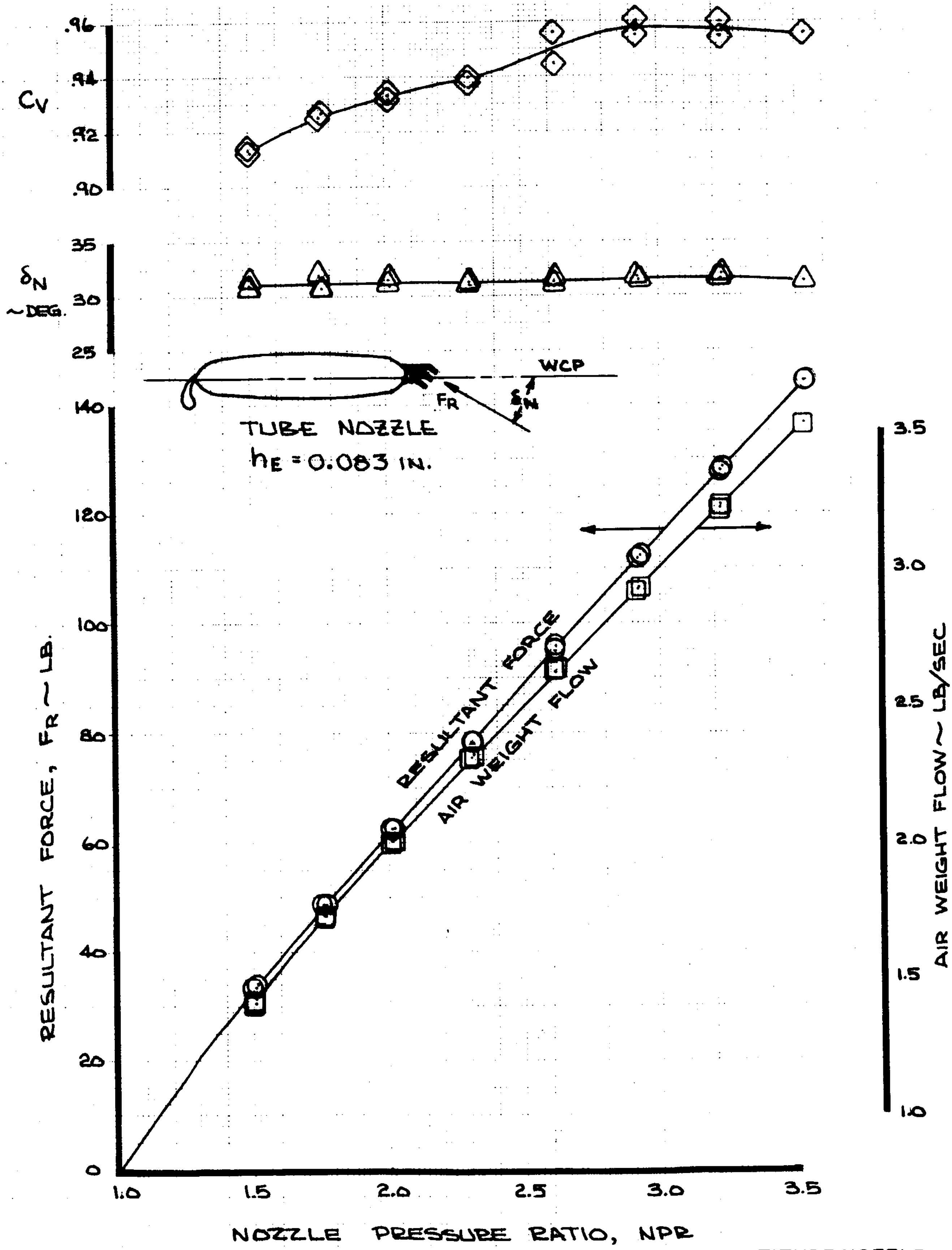

FIGURE 44.—NOZZLE CALIBRATION RESULTS FOR h_E = 0.083-IN. MULTITUBE NOZZLE

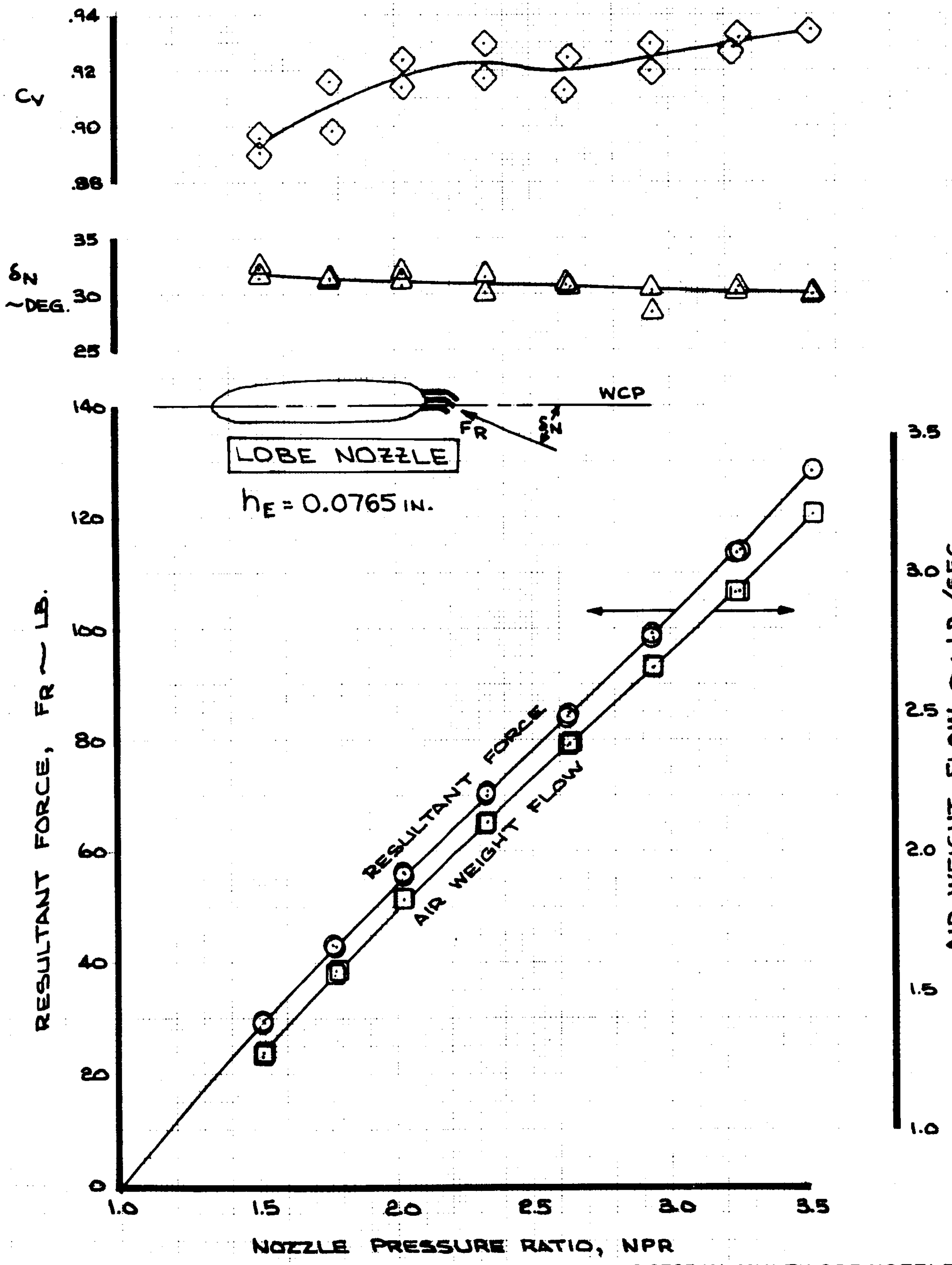

FIGURE 45.–NOZZLE CALIBRATION RESULTS FOR h_E = 0.0765-IN. MULTILOBE NOZZLE

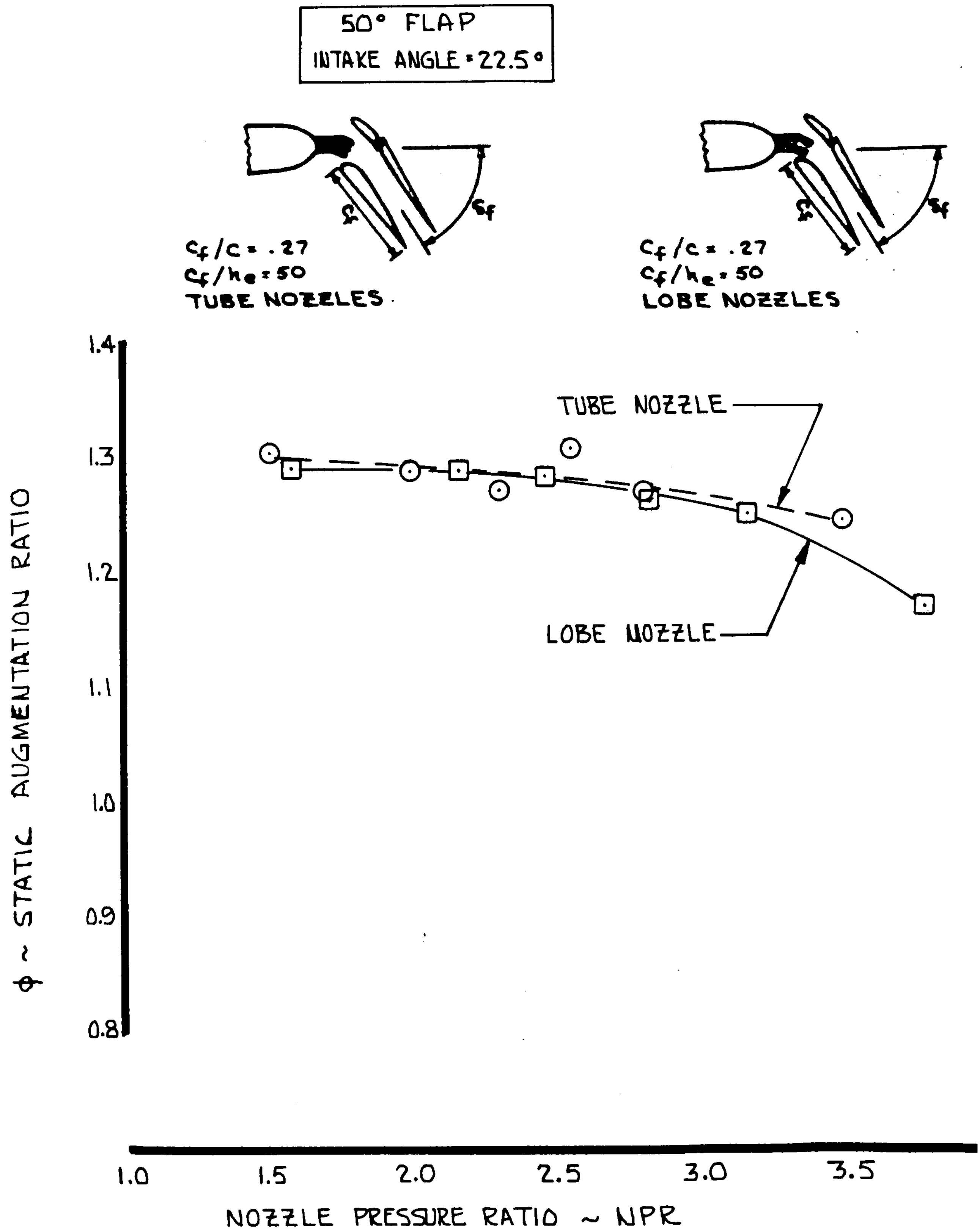

FIGURE 46.–STATIC THRUST AUGMENTATION RATIO COMPARISON FOR TUBE AND LOBE NOZZLE AUGMENTORS

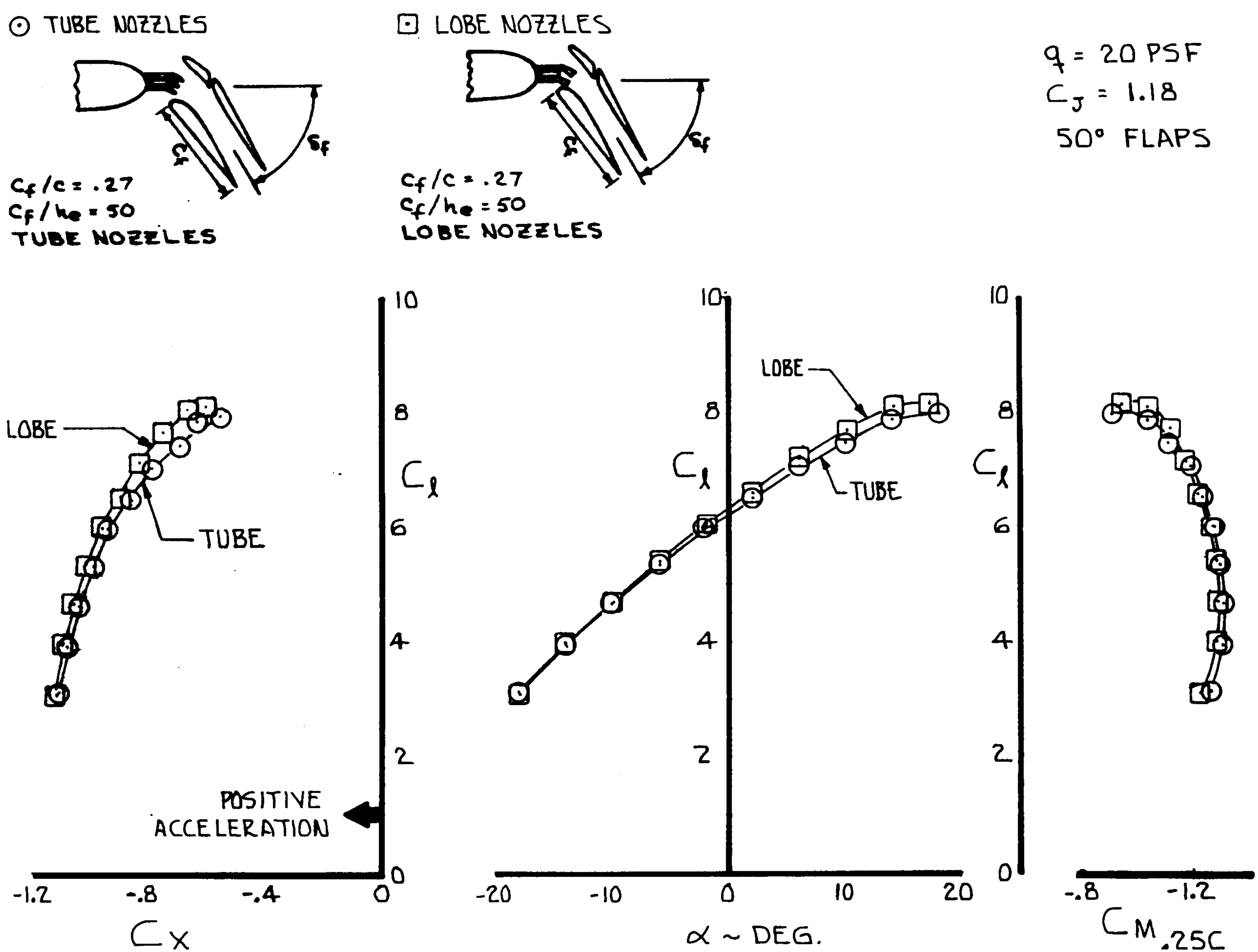

FIGURE 47.—COMPARISON OF AERODYNAMIC DATA FOR TUBE AND LOBE NOZZLE AUGMENTORS AT $\delta_f = 50°$ AND $C_j = 1.18$

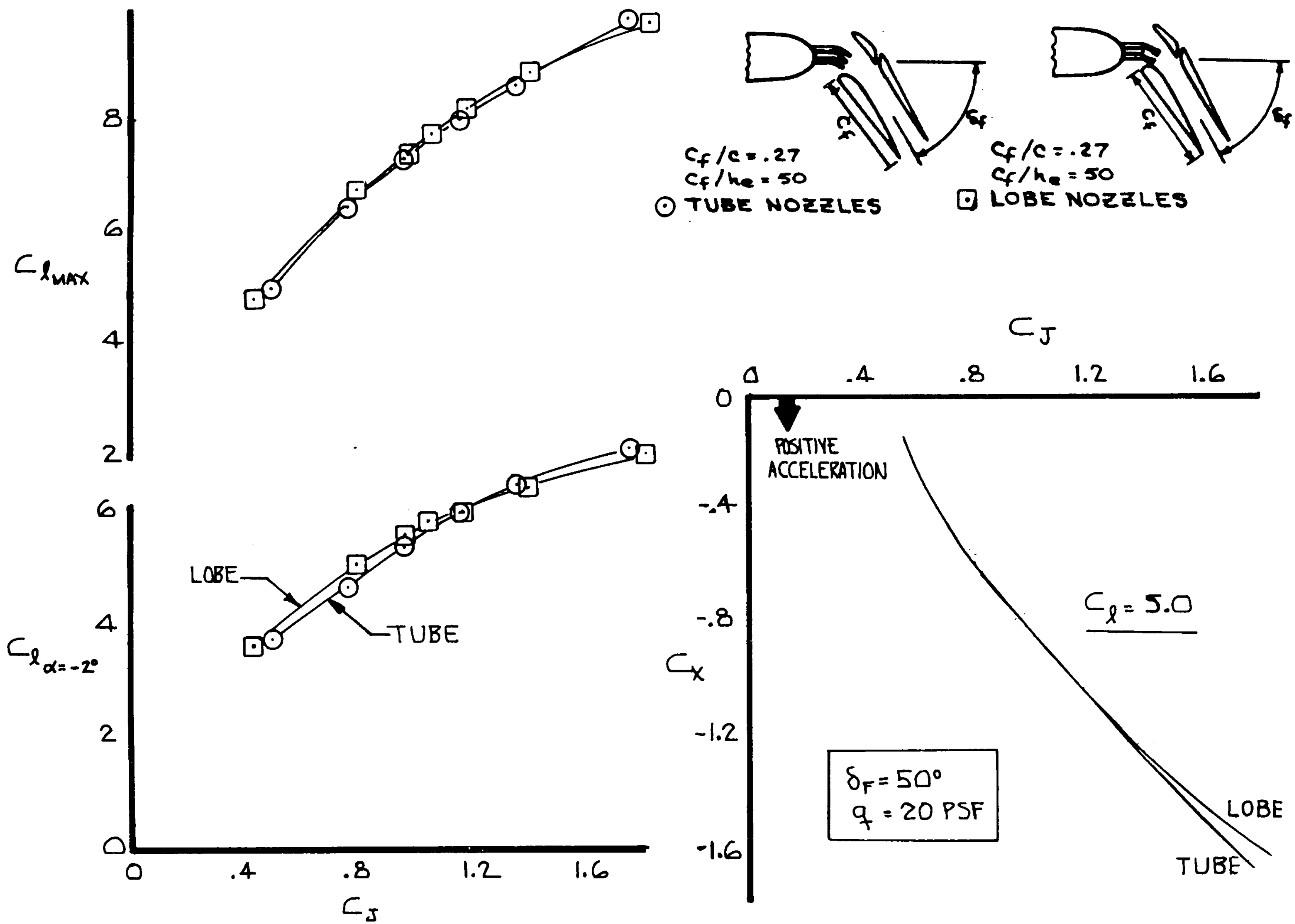

FIGURE 48.—COMPARISON OF LIFT AND DRAG VARIATION WITH C_j FOR TUBE AND LOBE NOZZLE AUGMENTORS AT $\delta_f = 50°$

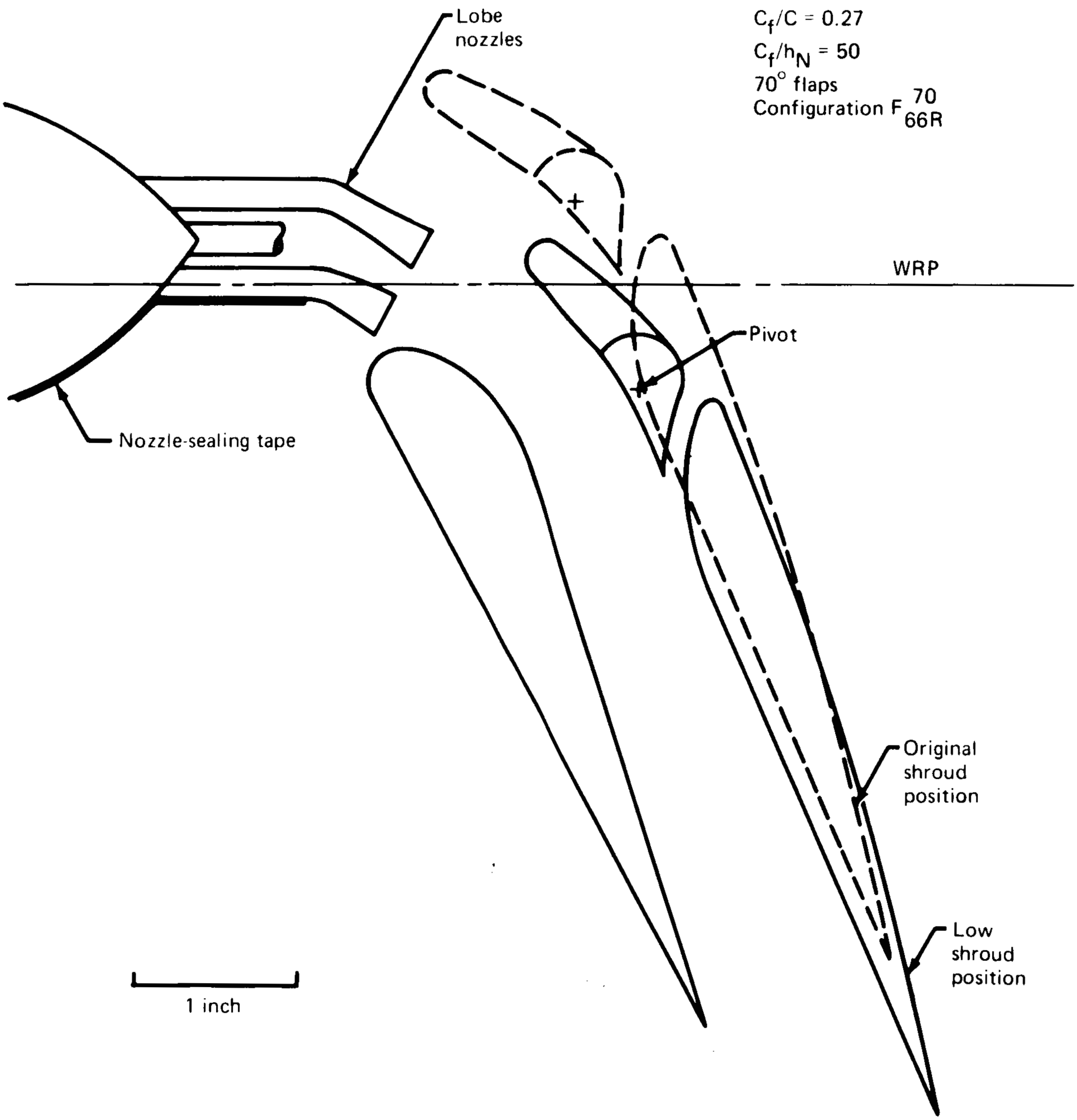

FIGURE 49.—NOZZLE TAPING AND SHROUD POSITIONS FOR LOBE NOZZLE AUGMENTOR CONFIGURATION AT $\delta_f = 70°$

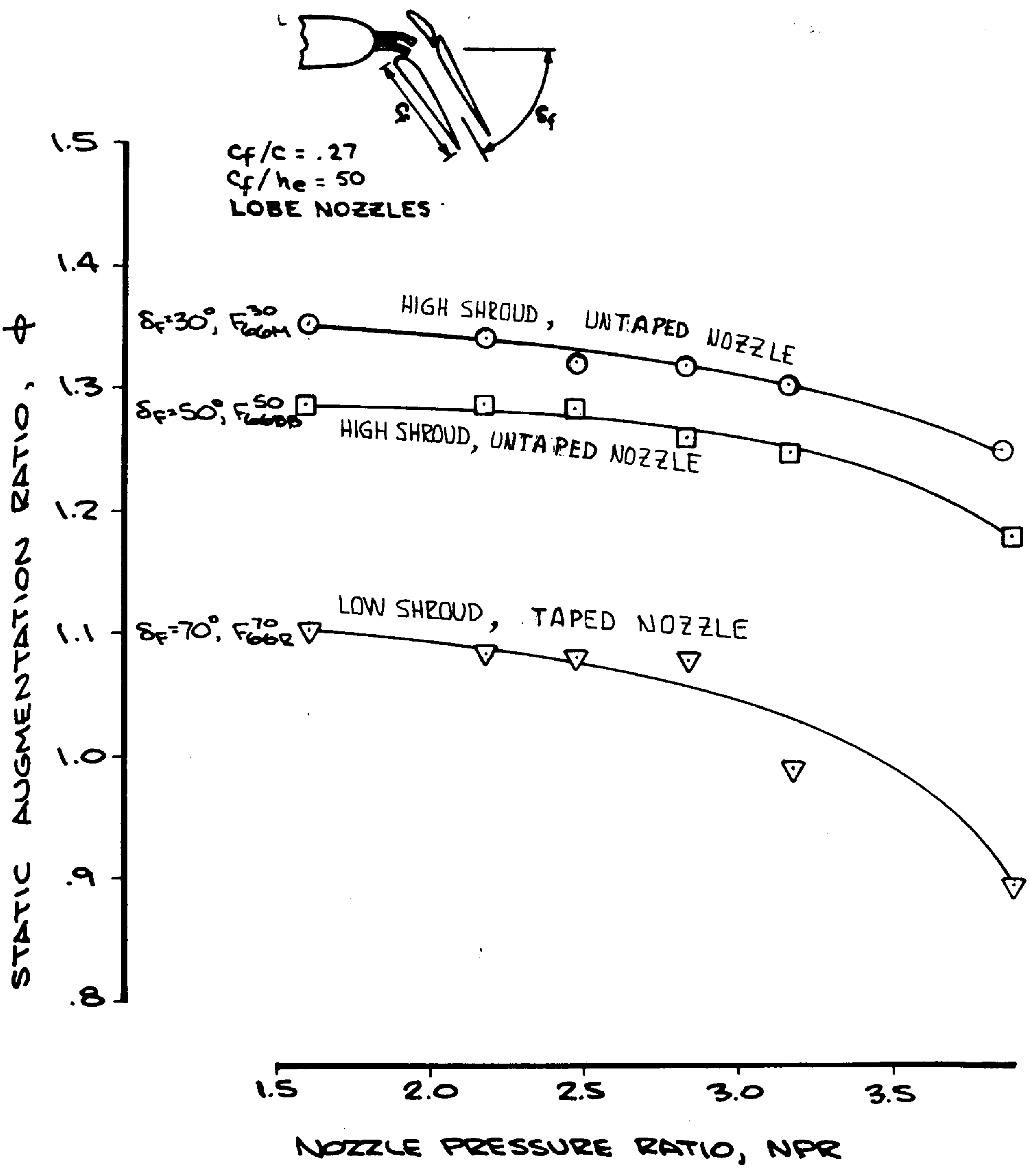

FIGURE 50.—STATIC THRUST AUGMENTATION RATIO FOR LOBE NOZZLE AUGMENTOR

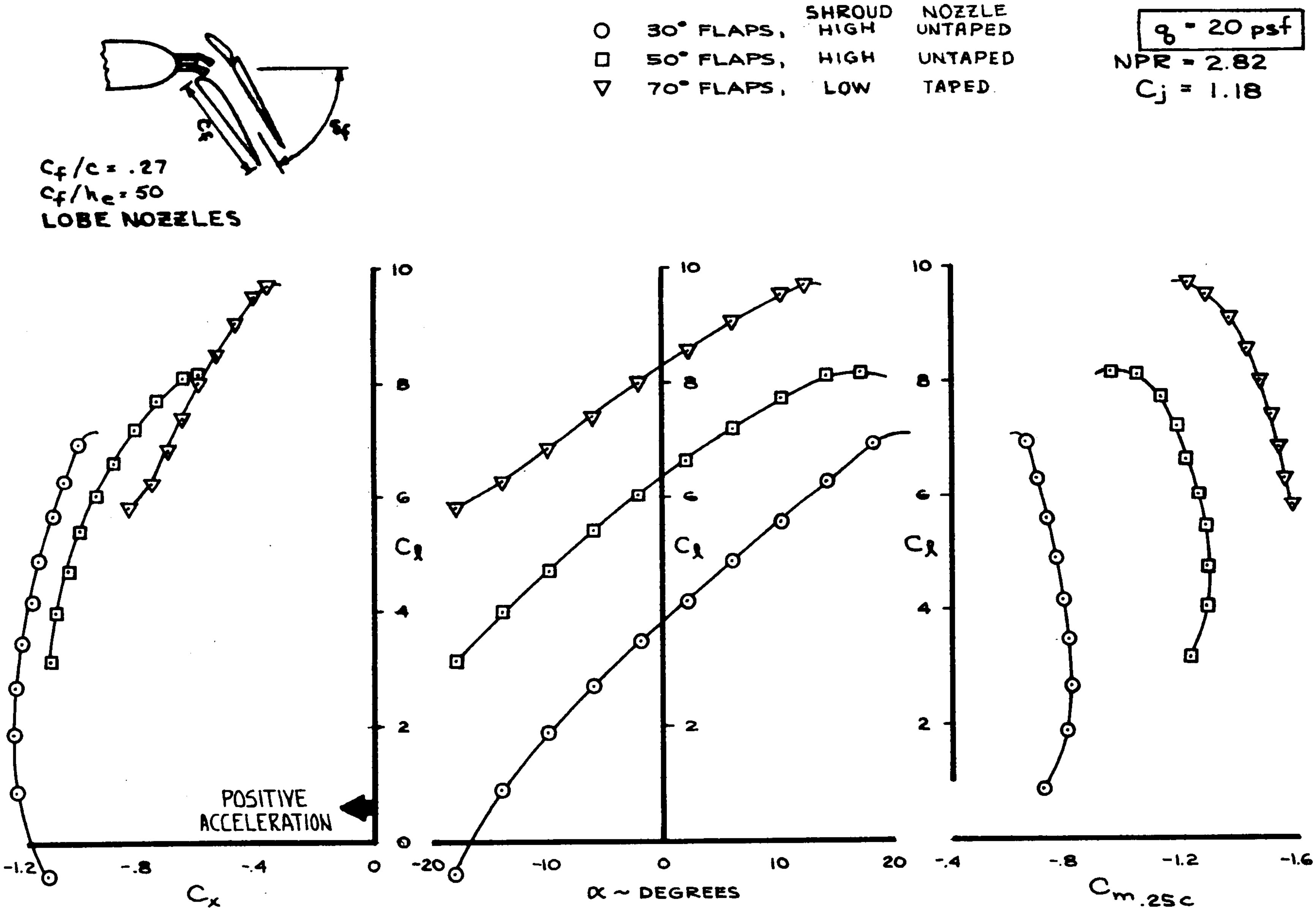

FIGURE 51.—LOBE NOZZLE AUGMENTOR FORWARD SPEED PERFORMANCE AT $C_j = 1.18$

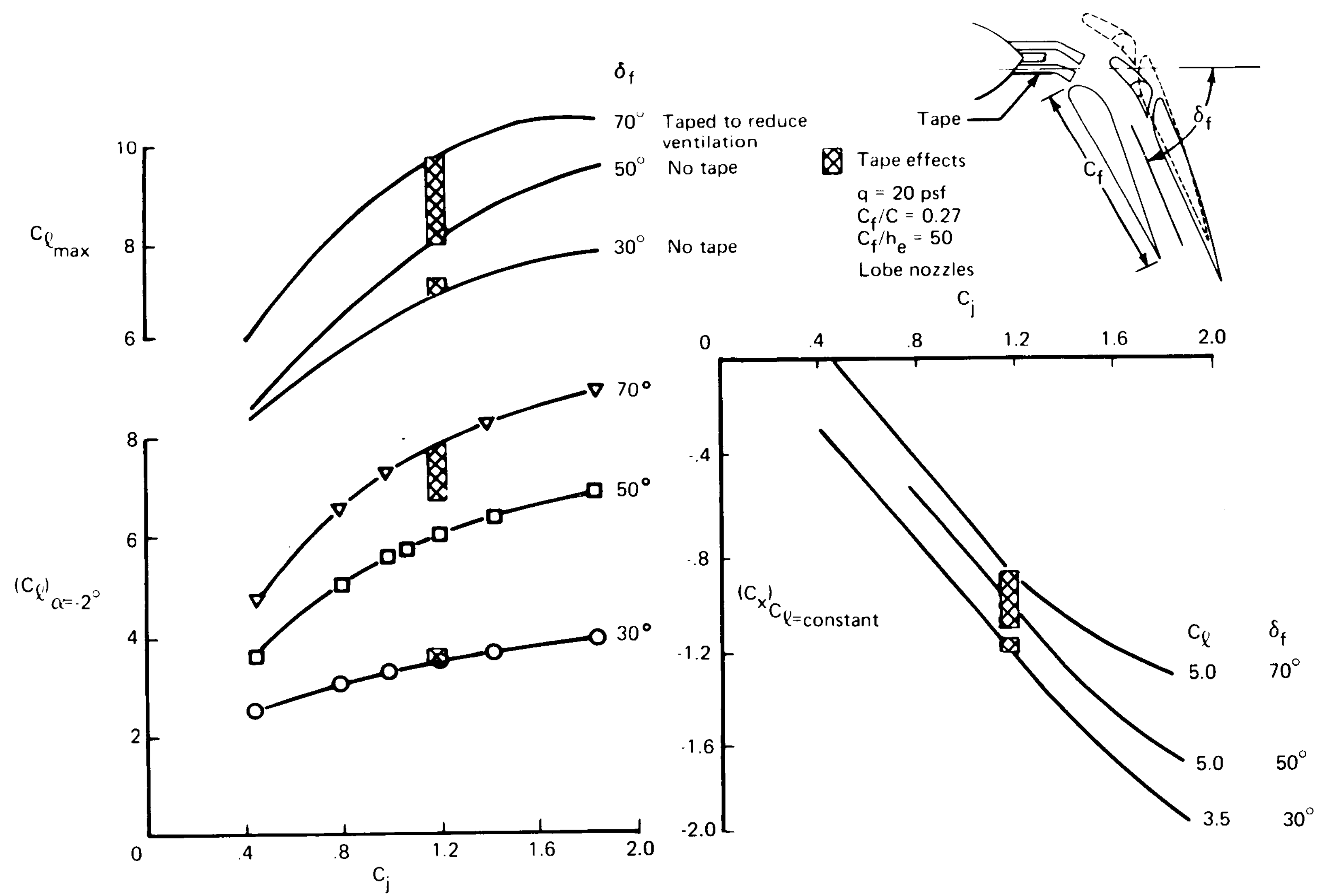

FIGURE 52.—VARIATION OF LIFT AND STREAMWISE FORCE WITH C_j FOR THE LOBE NOZZLE AUGMENTOR FLAP

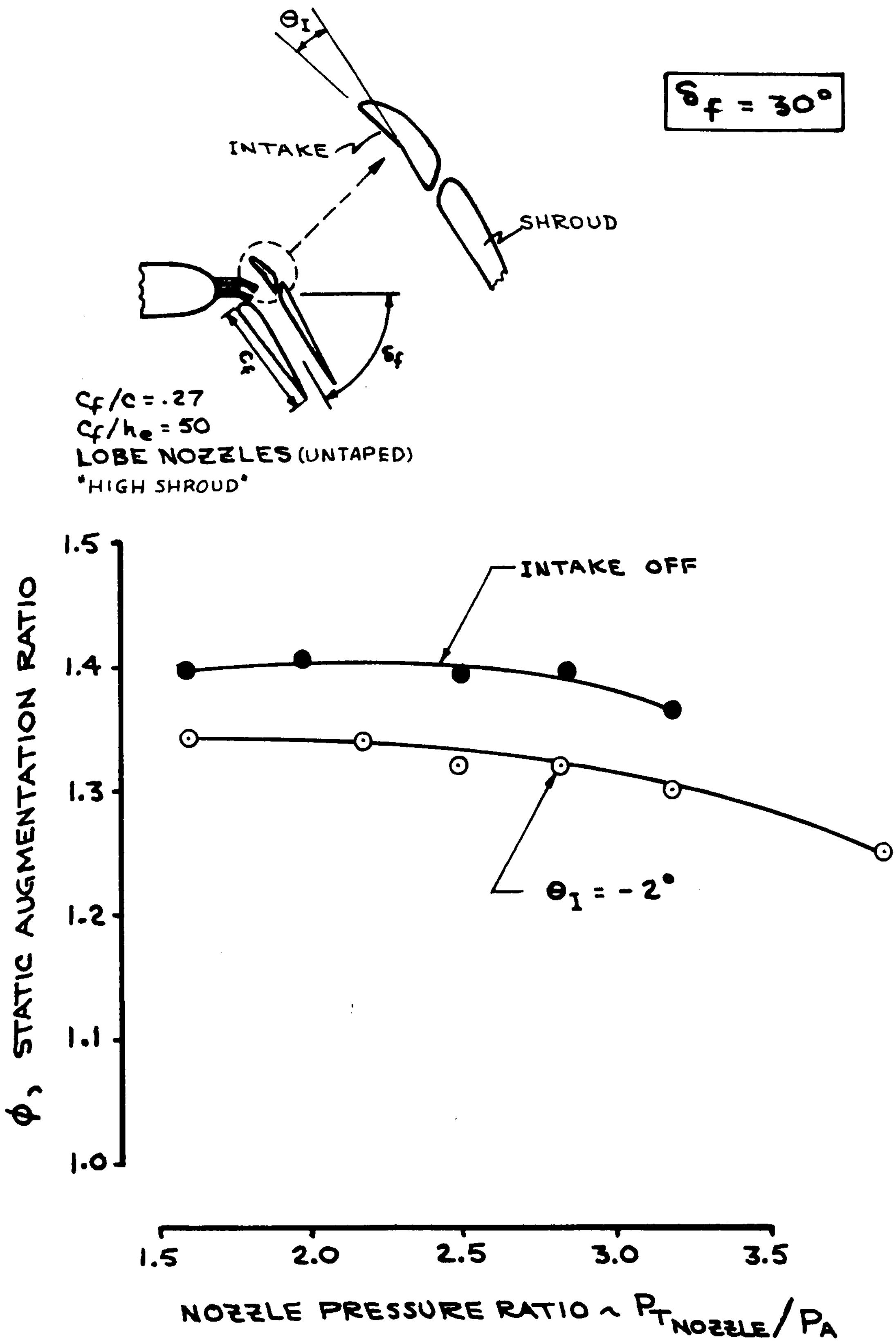

FIGURE 53.—EFFECT OF INTAKE ON STATIC THRUST AUGMENTATION RATIO FOR LOBE NOZZLE AUGMENTOR AT $\delta_f = 30°$

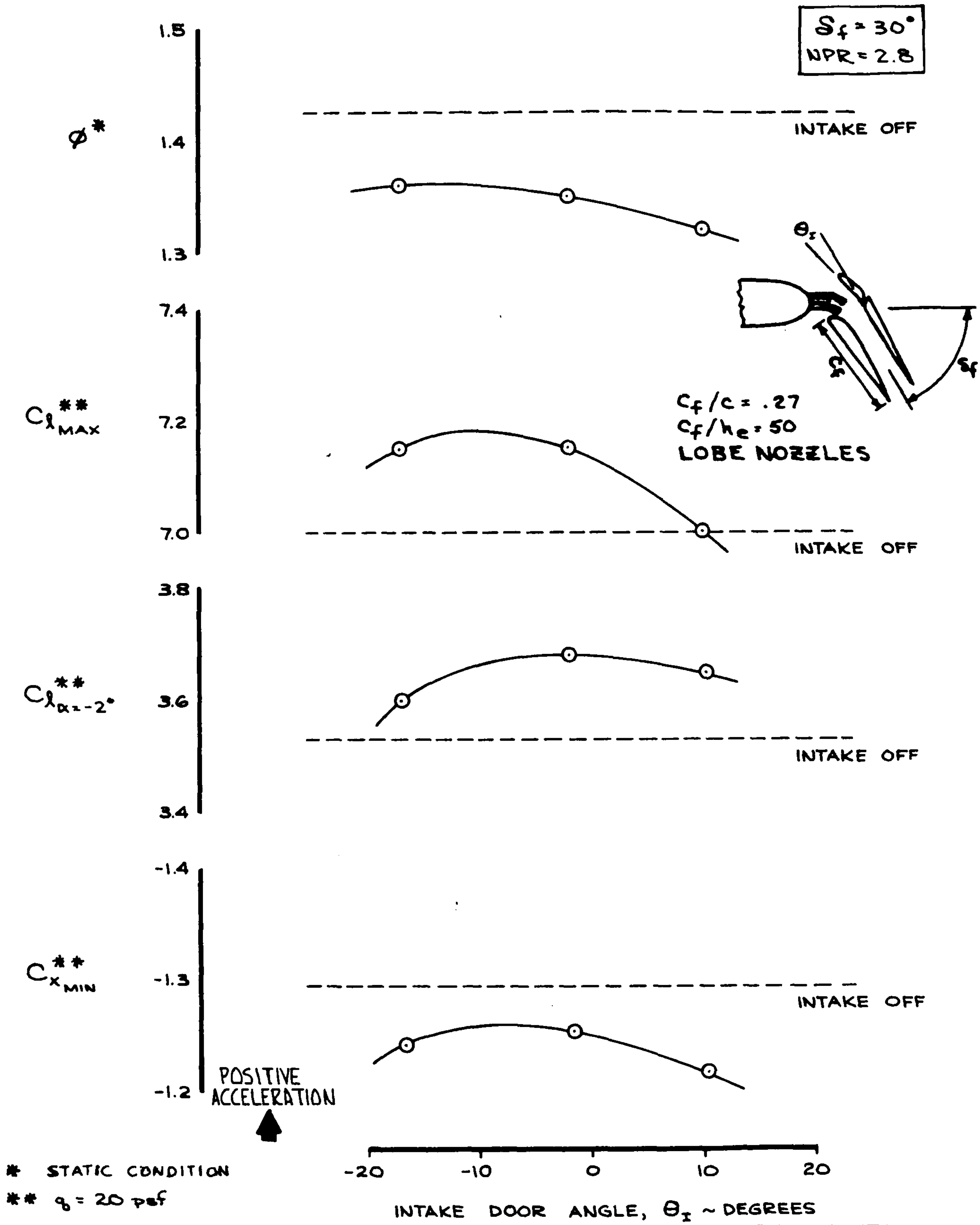

FIGURE 54.–EFFECT OF INTAKE DOOR ANGLE ON LOBE NOZZLE AUGMENTOR STATIC AND FORWARD SPEED CHARACTERISTICS AT $\delta_f = 30°$

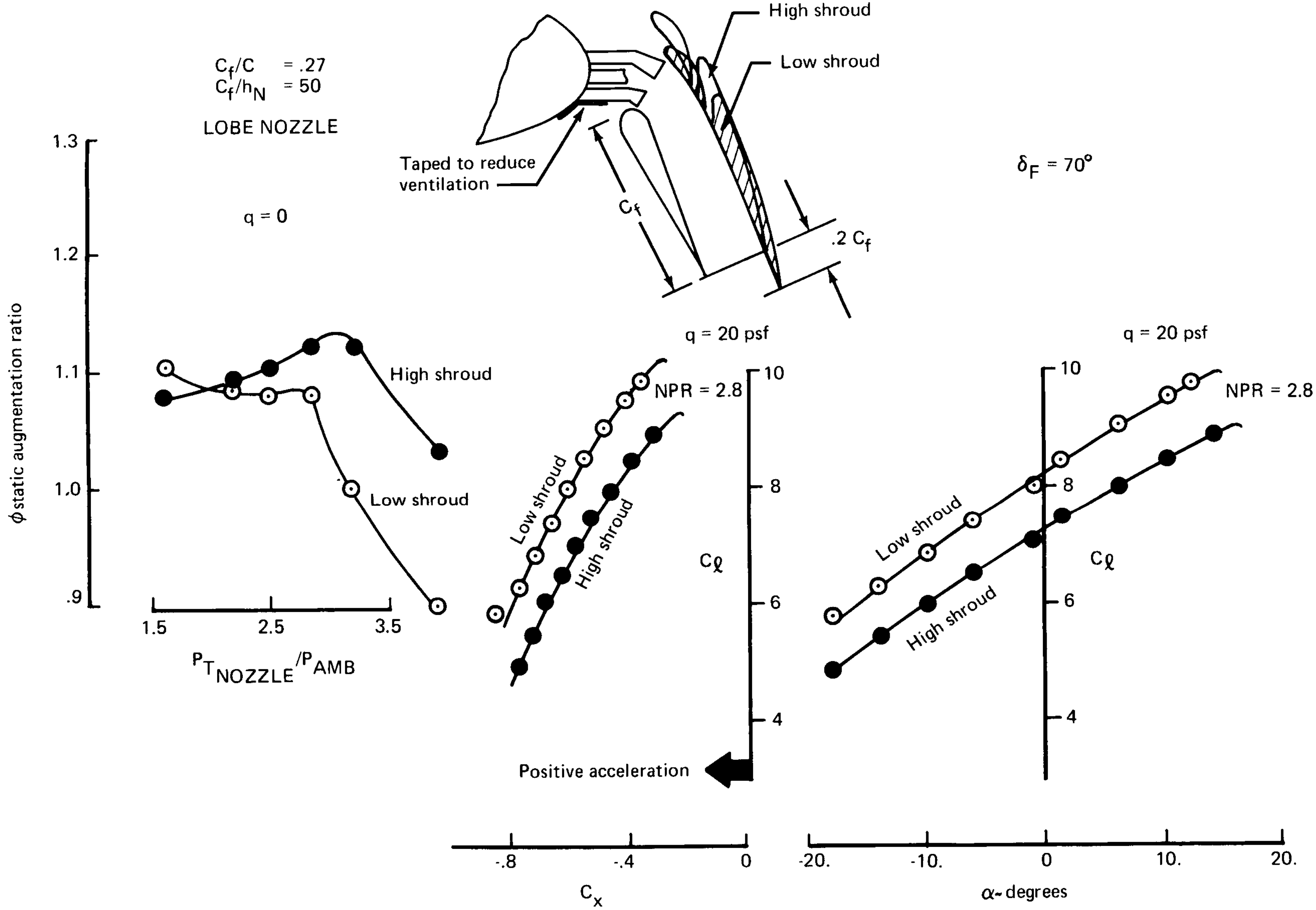

FIGURE 55.—EFFECT OF SHROUD POSITION ON LOBE NOZZLE AUGMENTOR STATIC AND FORWARD SPEED PERFORMANCE AT $\delta_f = 70°$

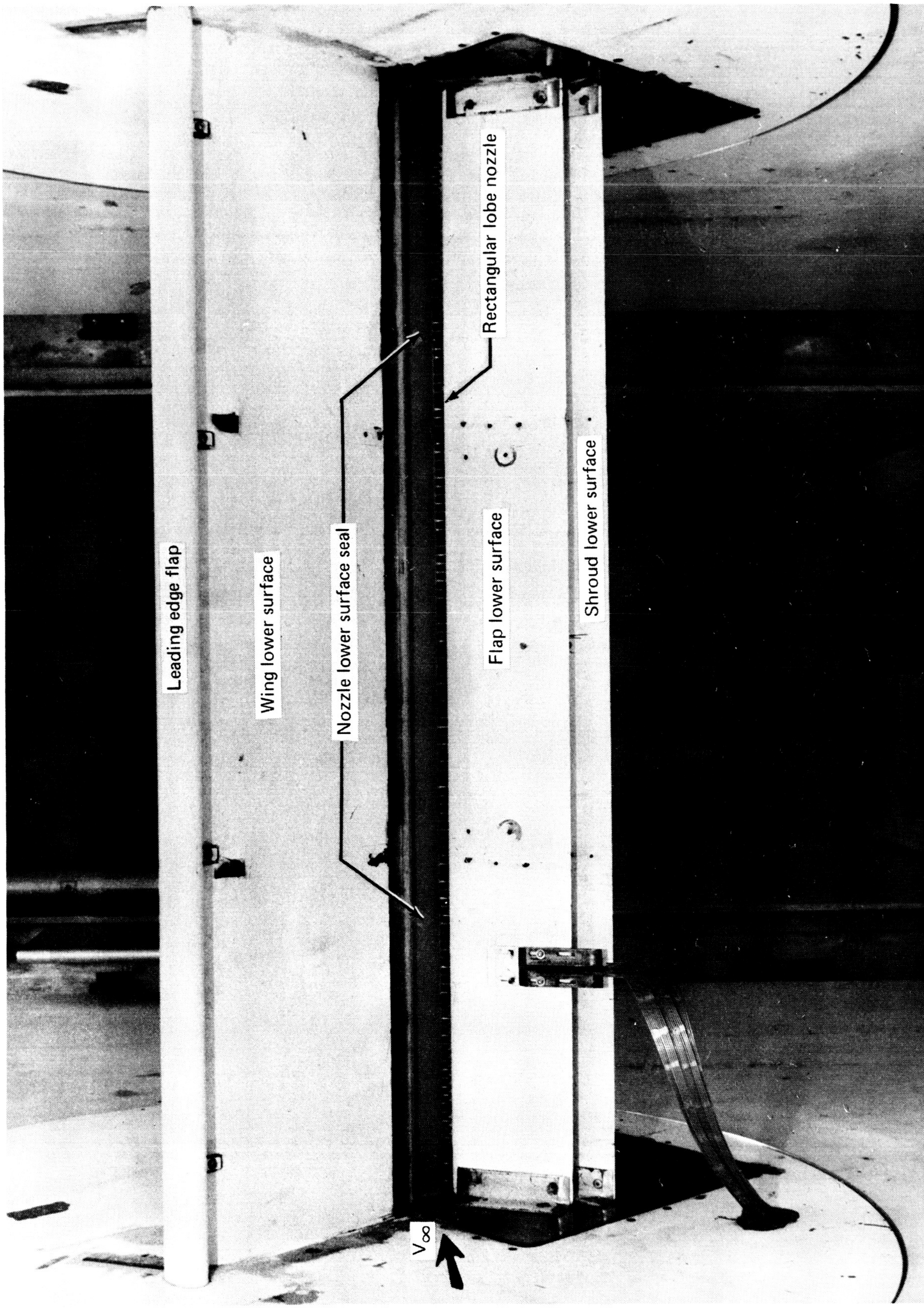

FIGURE 56.—LOWER SURFACE NOZZLE SEAL, RECTANGULAR LOBE NOZZLE

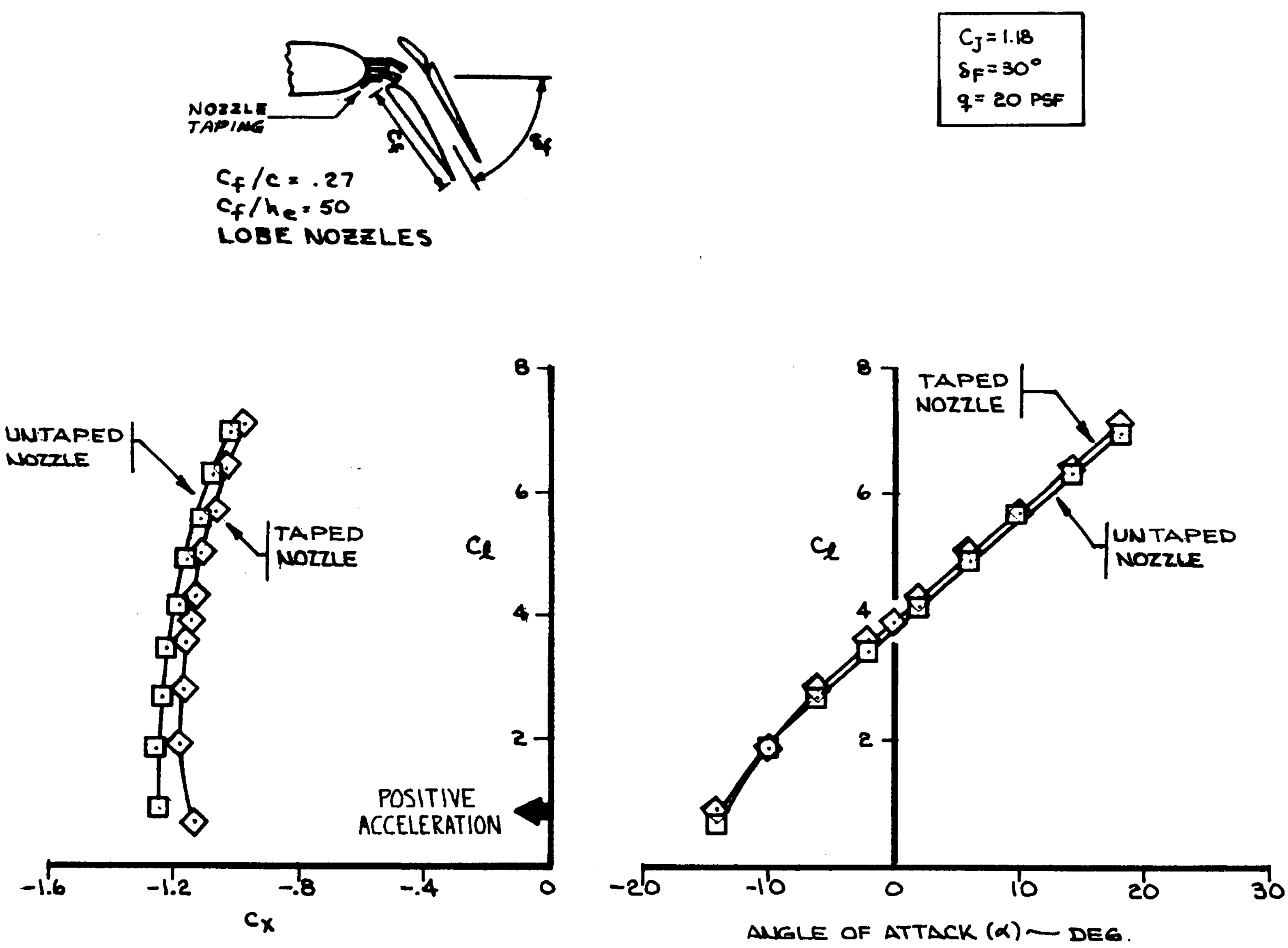

FIGURE 57.—CHANGE IN LIFT AND DRAG DUE TO NOZZLE TAPING AT $\delta_f = 30°$ FOR LOBE NOZZLE AUGMENTOR

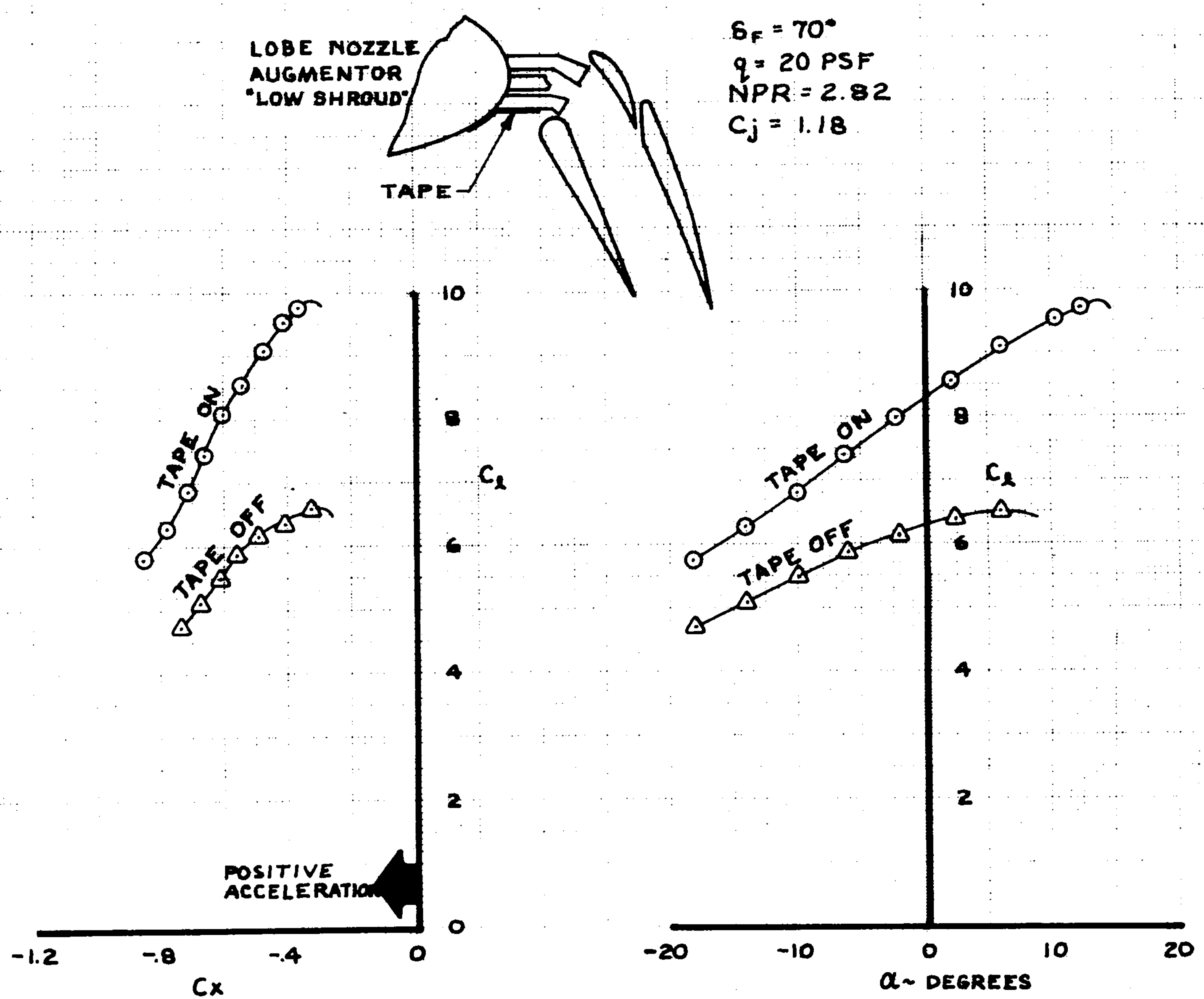

FIGURE 58.—EFFECT OF TAPE IN REDUCING NOZZLE VENTILATION ON FORCE COEFFICIENTS

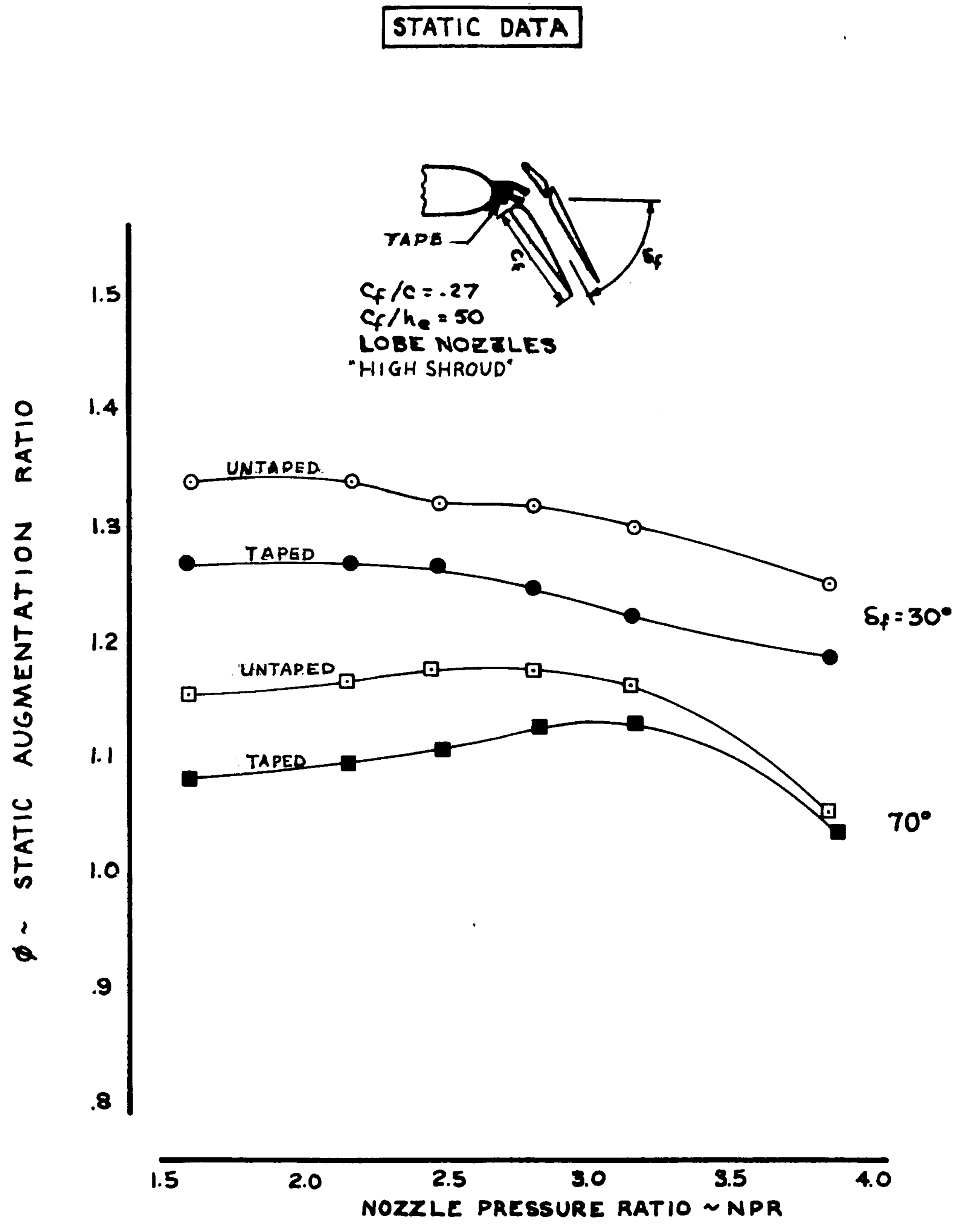

FIGURE 59.—EFFECT OF REDUCED VENTILATION ON STATIC AUGMENTATION RATIO

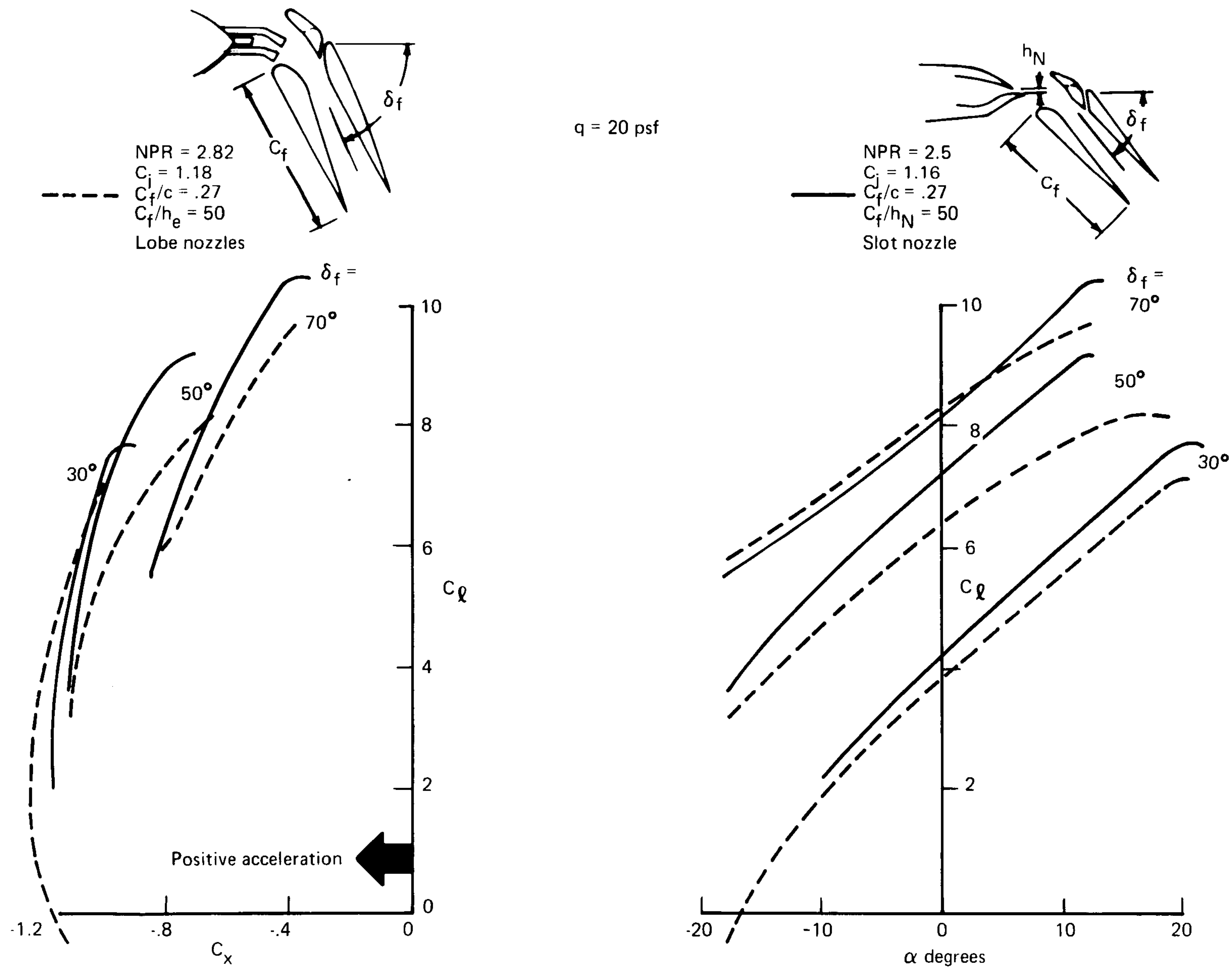

FIGURE 60.–COMPARISON OF AERODYNAMIC DATA FOR THE LOBE AND SLOT NOZZLE AUGMENTORS

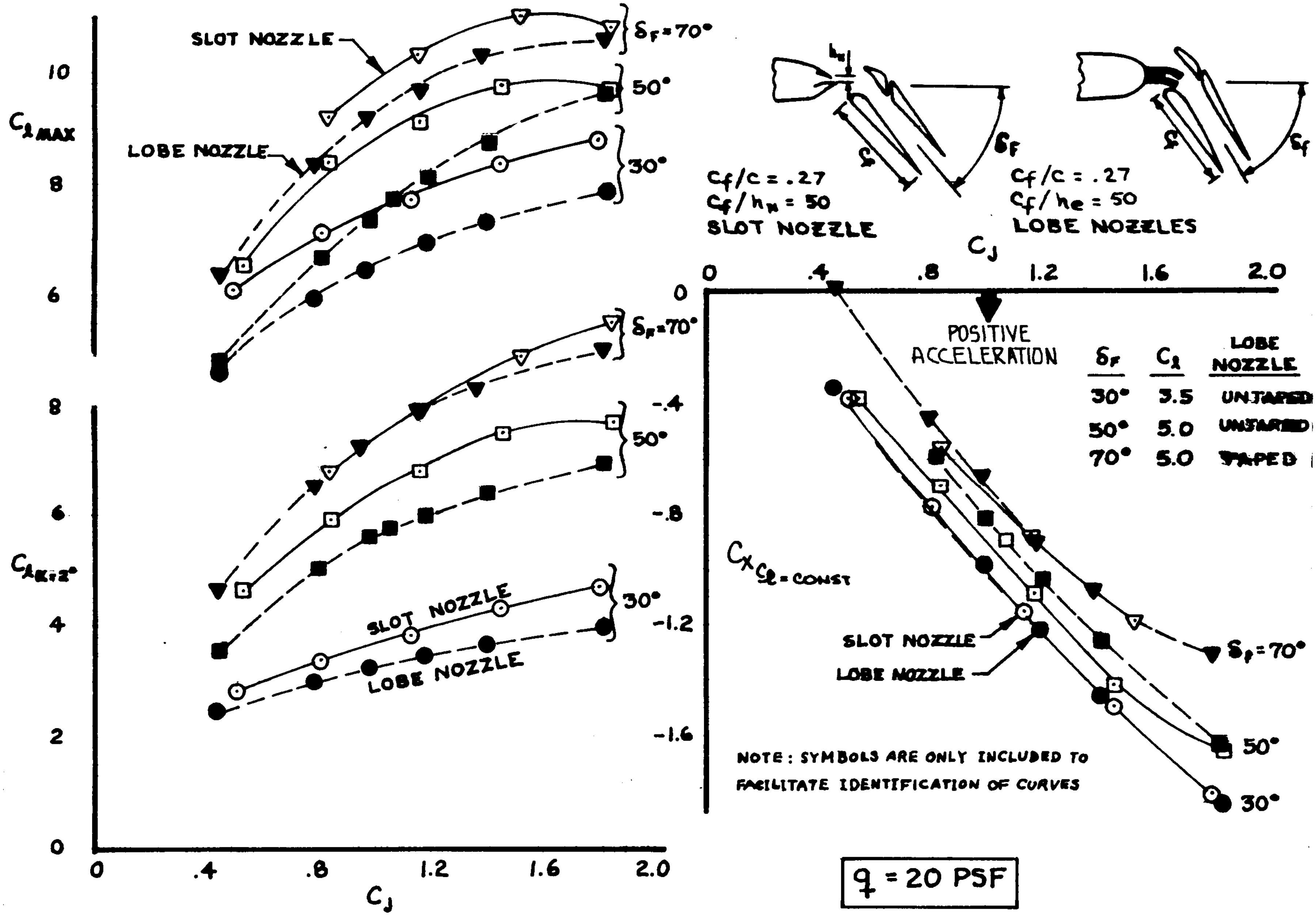

FIGURE 61.—COMPARISON OF LIFT AND DRAG AS A FUNCTION OF THRUST COEFFICIENT FOR SLOT VERSUS LOBE NOZZLE AUGMENTOR FLAPS

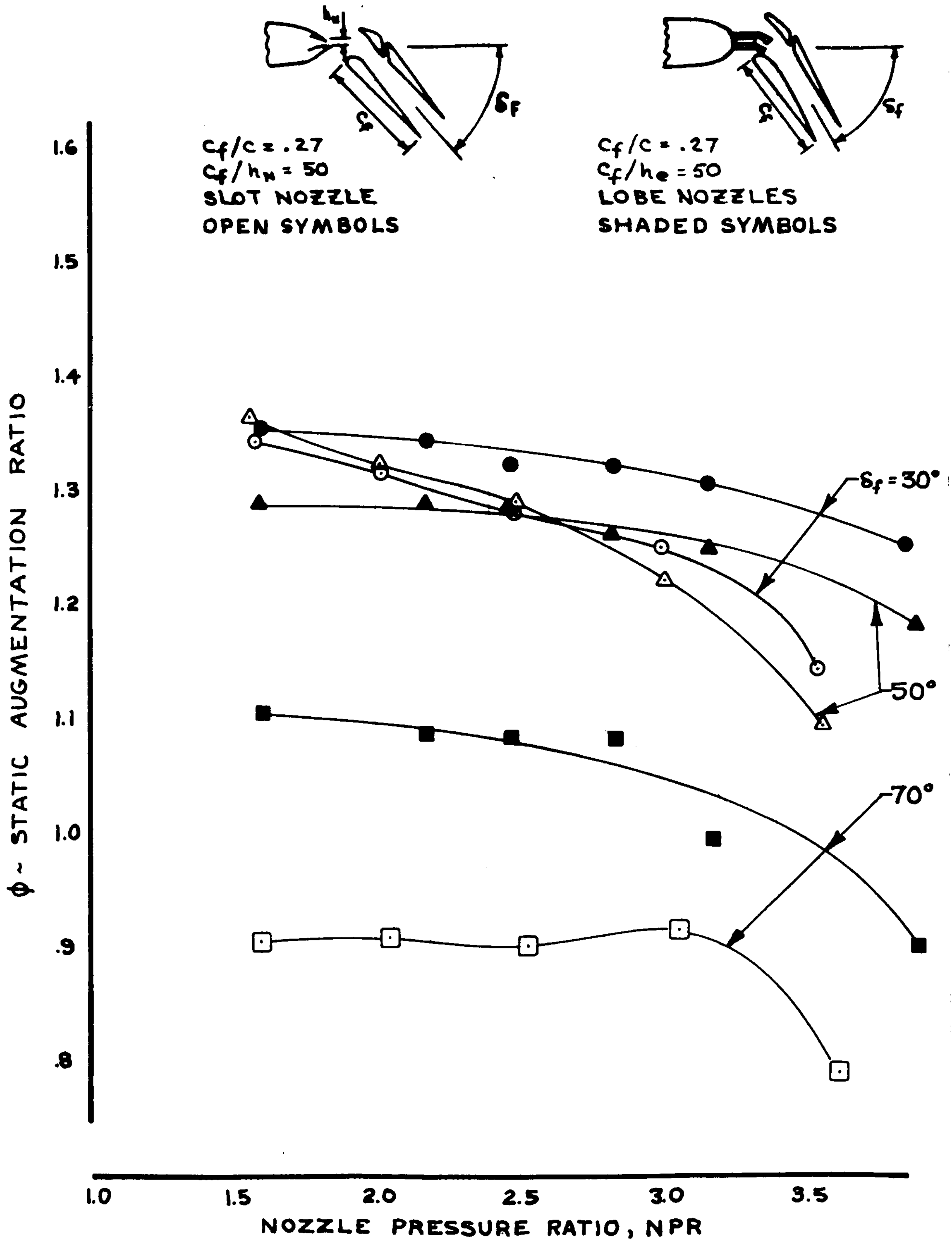

FIGURE 62.—COMPARISON OF STATIC THRUST AUGMENTATION RATIO FOR LOBE AND SLOT NOZZLE AUGMENTORS

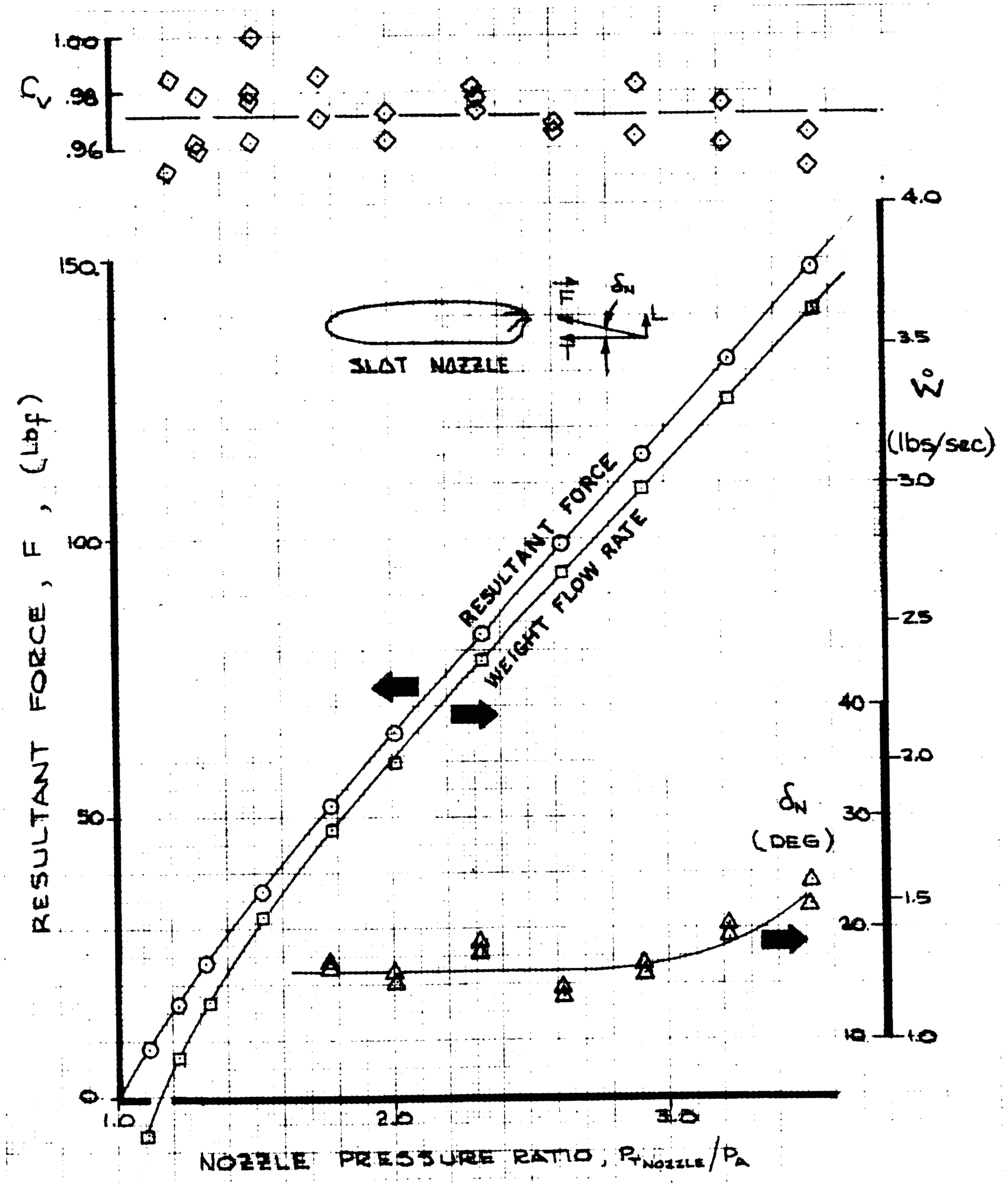

FIGURE 63.—NOZZLE CALIBRATION RESULTS FOR h_N = 0.086-IN. SLOT NOZZLE USED WITH δ_f = 30° AUGMENTOR AND JET FLAP

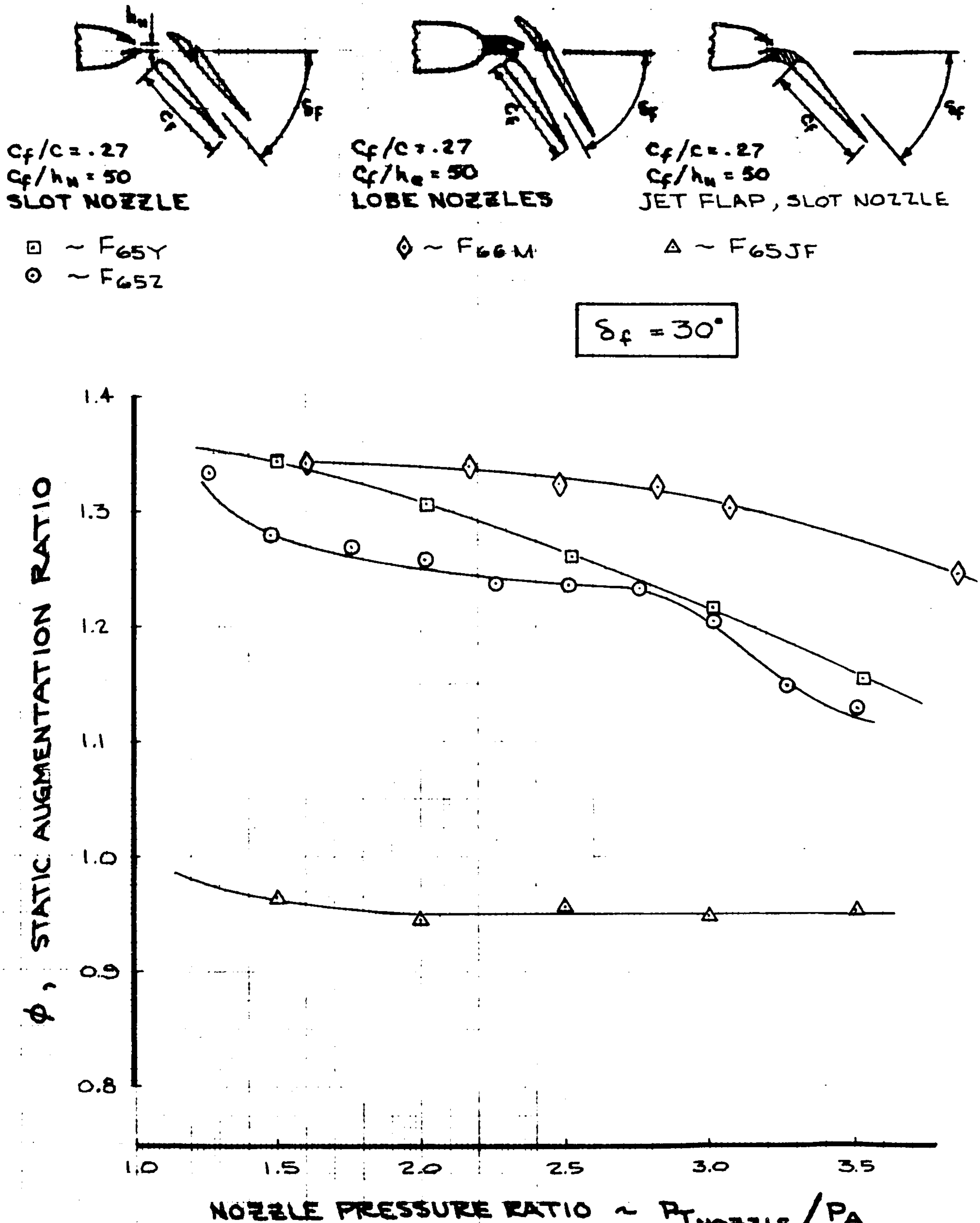

FIGURE 64.—COMPARISON OF STATIC THRUST AUGMENTATION—JET FLAP VERSUS AUGMENTOR FLAPS

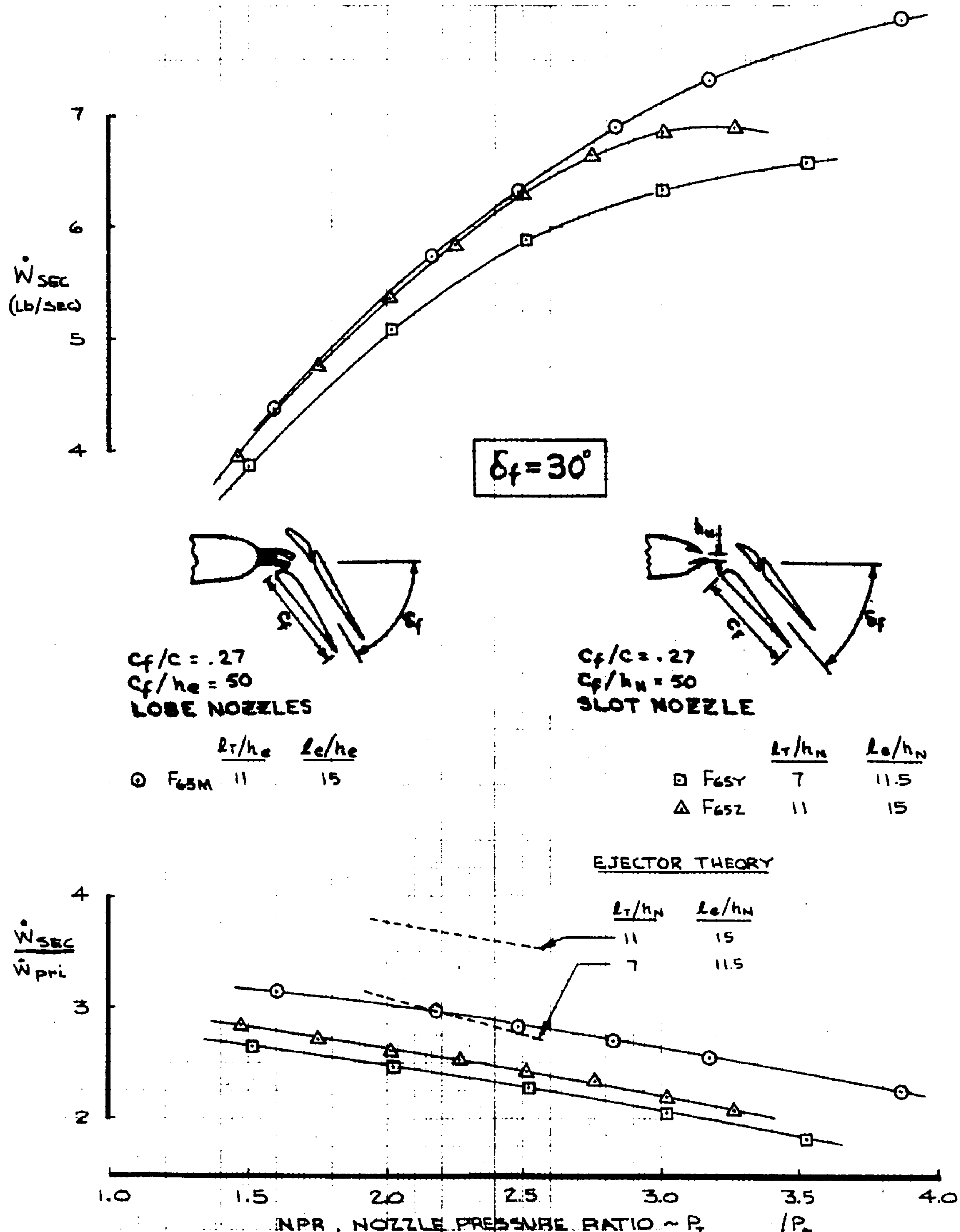

FIGURE 65.—ENTRAINMENT CHARACTERISTICS OF LOBE NOZZLE AND SLOT NOZZLE AUGMENTORS AT STATIC CONDITION

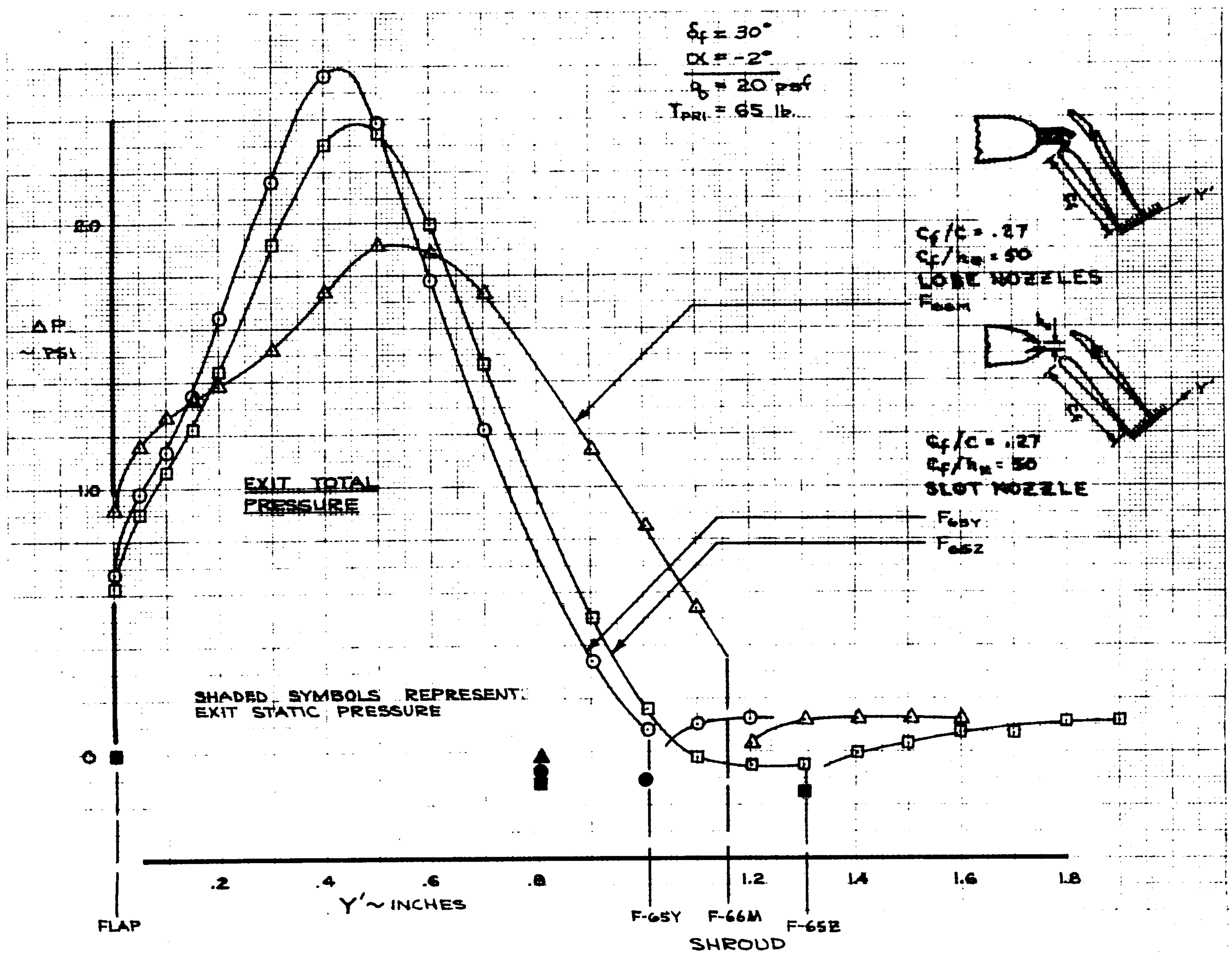

FIGURE 66.—COMPARISON OF AUGMENTOR EXIT TOTAL PRESSURE PROFILE

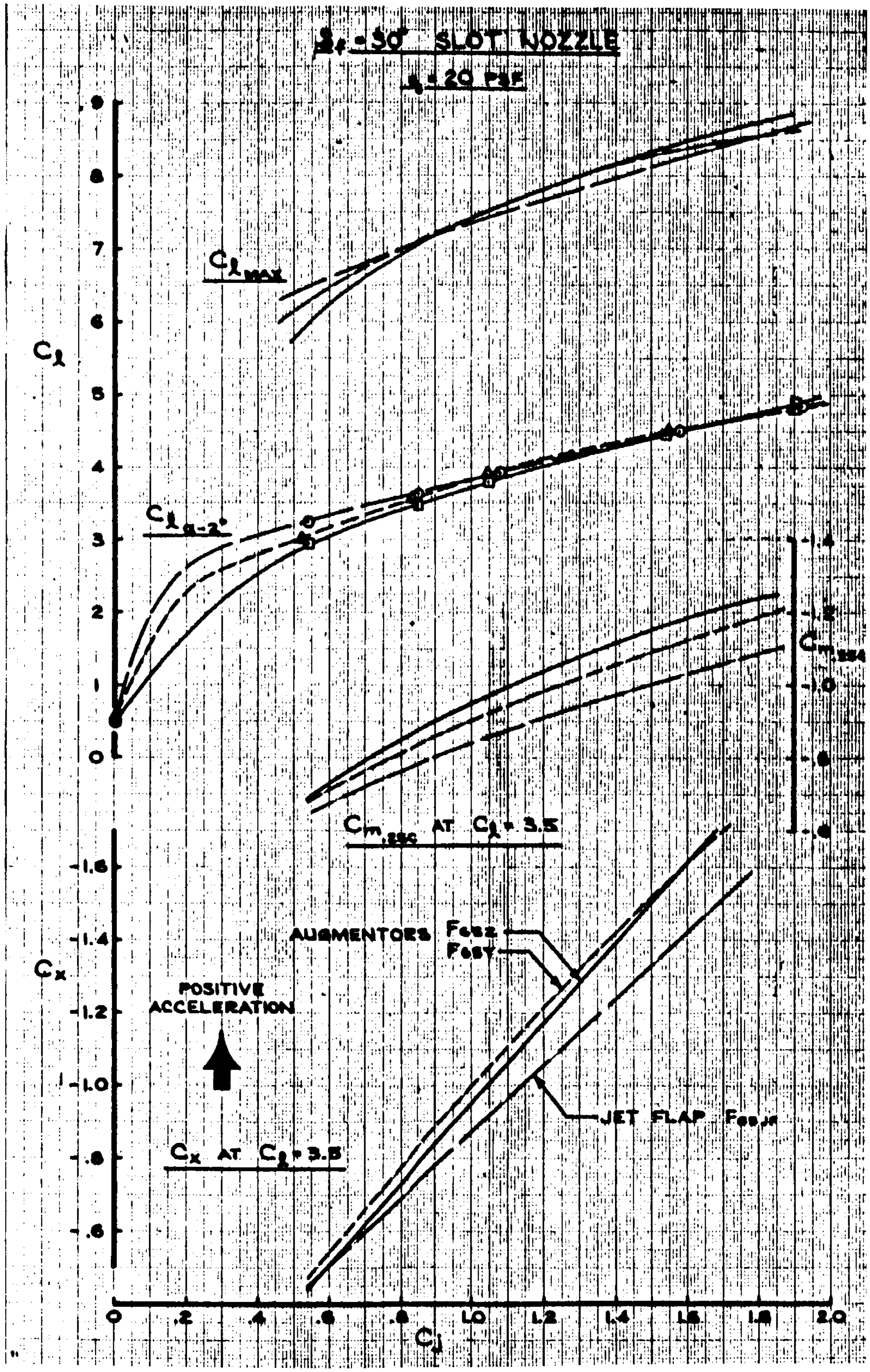

FIGURE 67.—COMPARISON OF PERFORMANCE OF JET FLAP AND AUGMENTORS AT $q = 20$ PSF

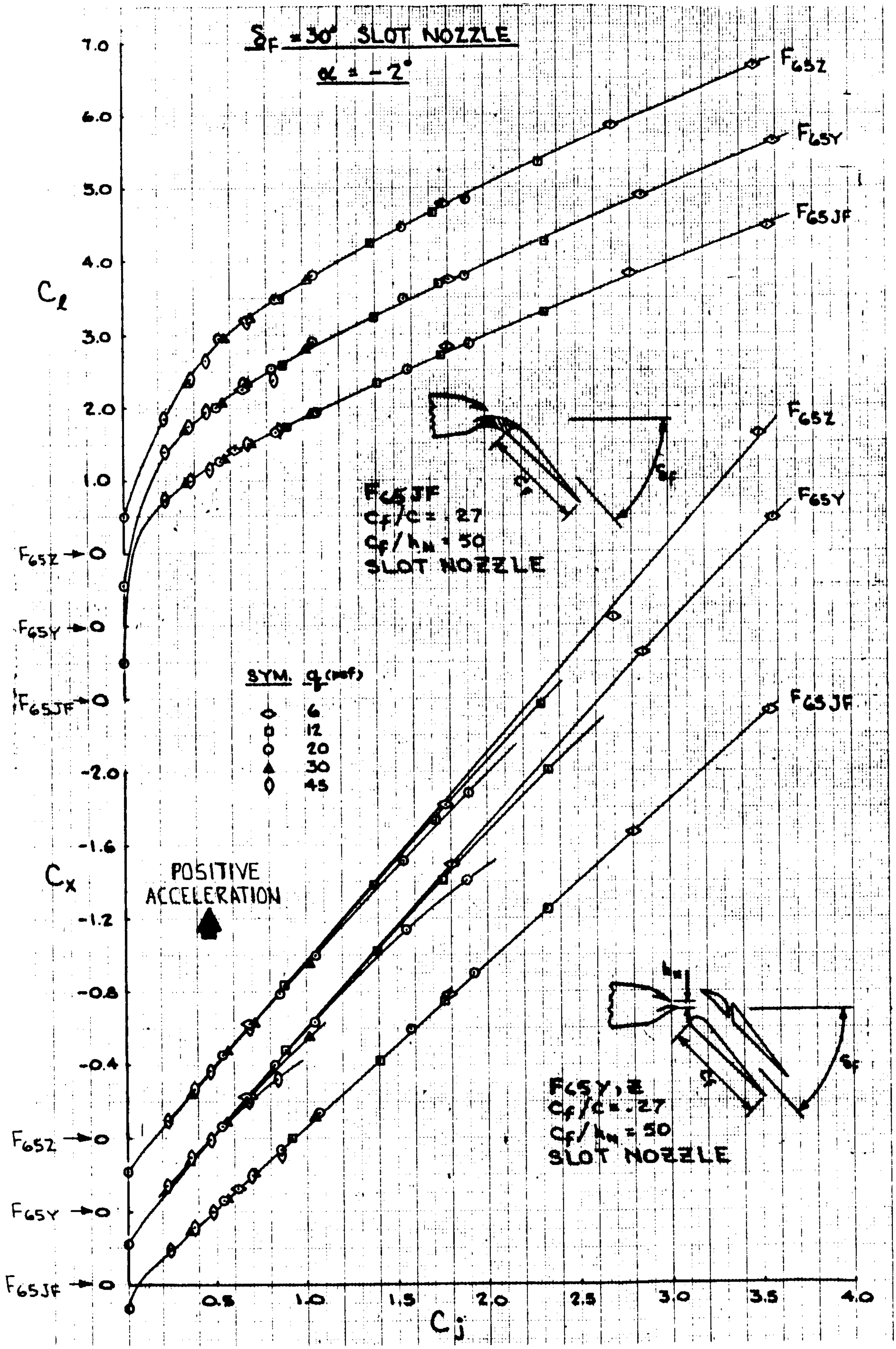

FIGURE 68.—JET FLAP AND AUGMENTOR FLAP EFFECTIVENESS

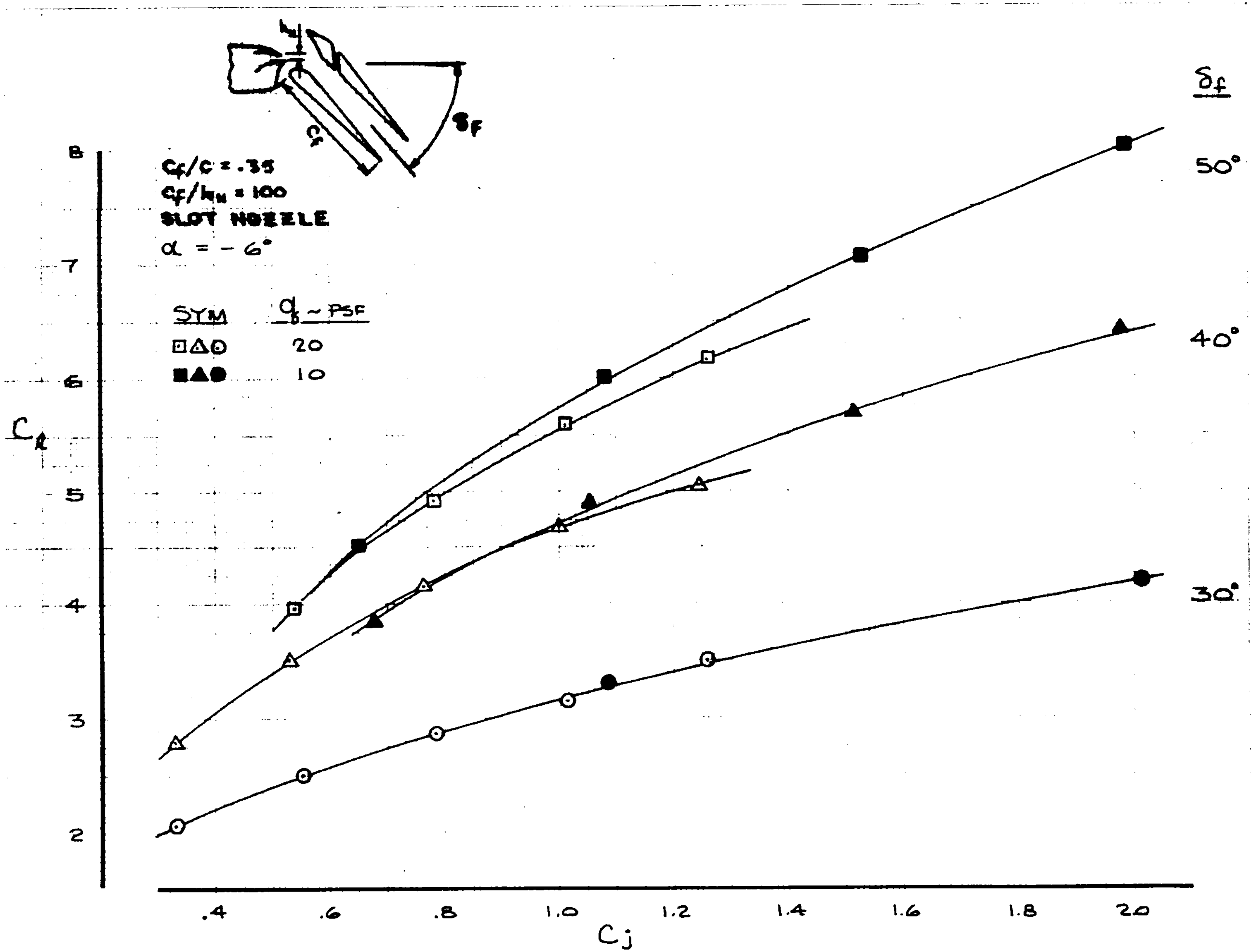

FIGURE 69.—EFFECT OF AIRSPEED ON LIFT OF THE NASA AUGMENTOR WING SECTION

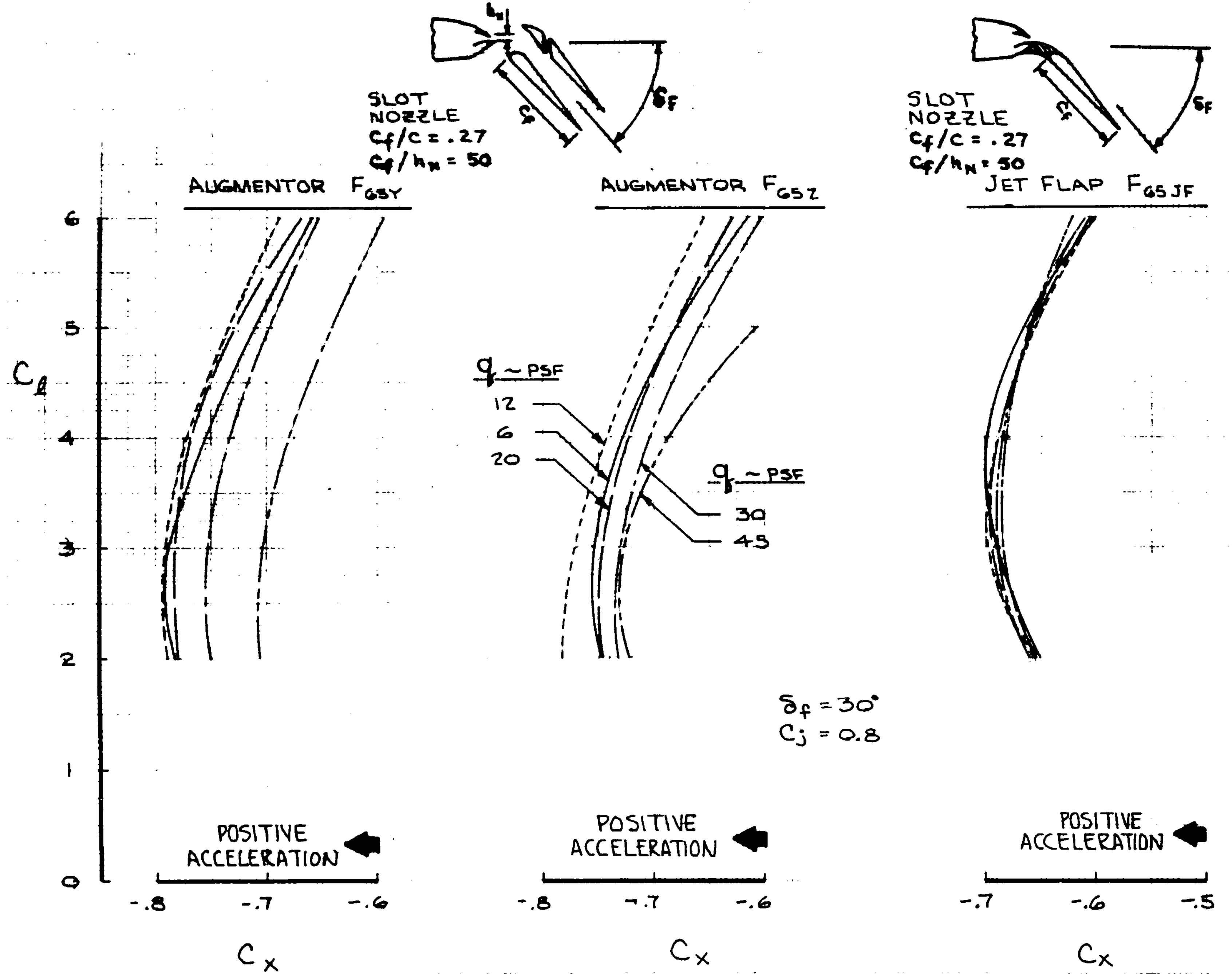

FIGURE 70.—AIRSPEED EFFECT ON INTERPOLATED DRAG POLAR AT $C_j = 0.8$

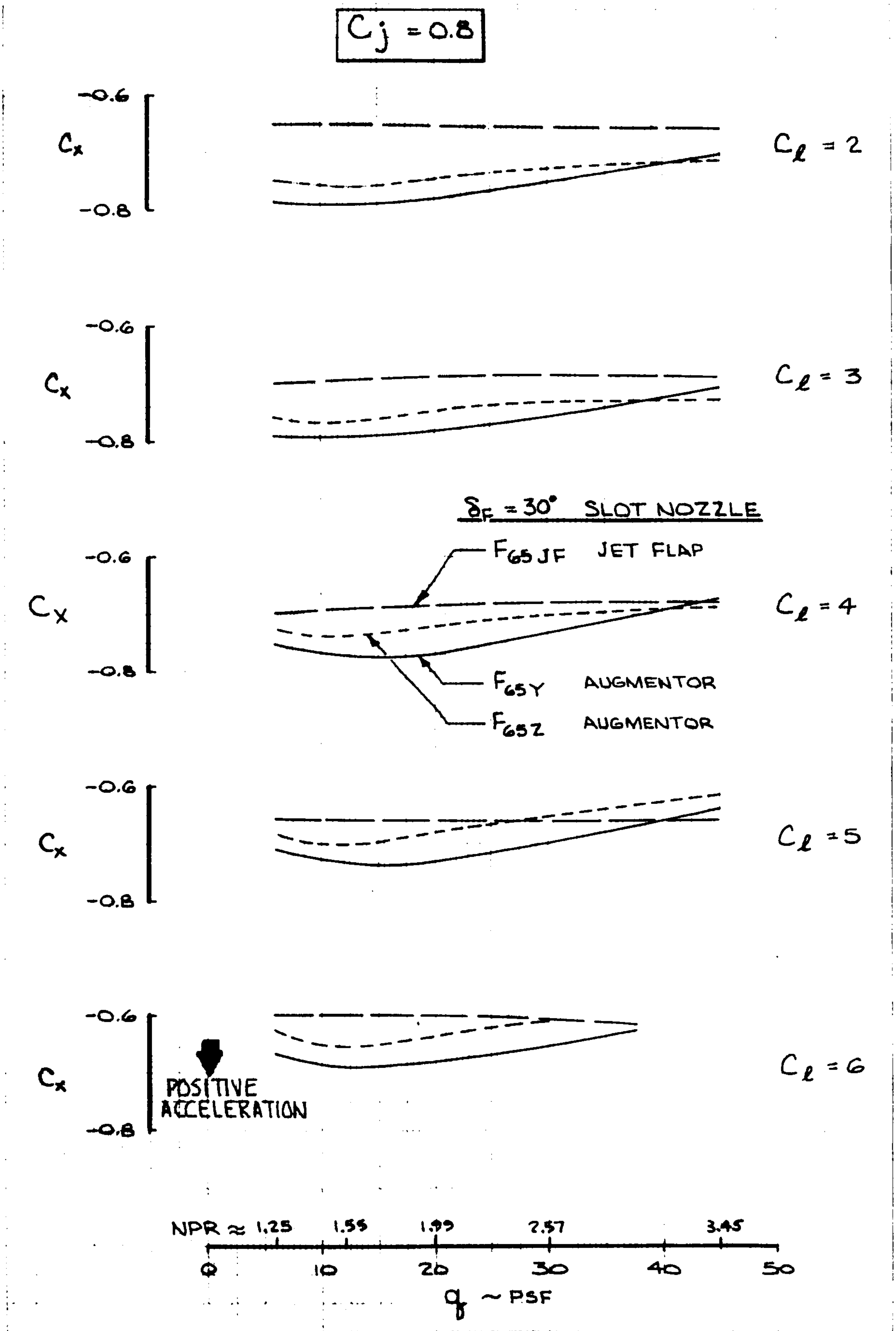

FIGURE 71.—VARIATION OF STREAMWISE FORCE WITH q AT $C_j = 0.8$

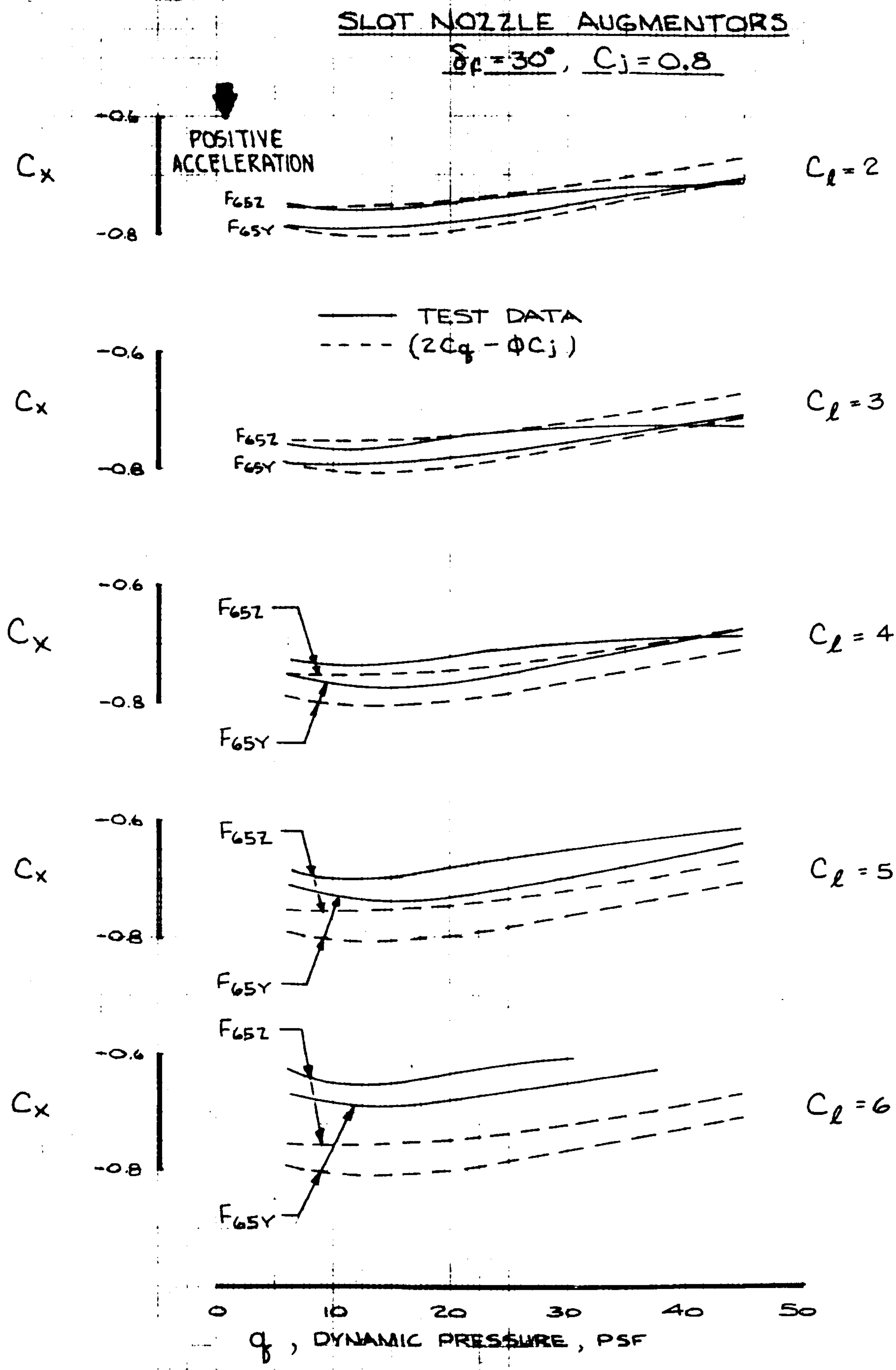

FIGURE 72.—COMPARISON OF RAM DRAG PLUS STATIC GROSS THRUST WITH MEASURED STREAMWISE FORCE

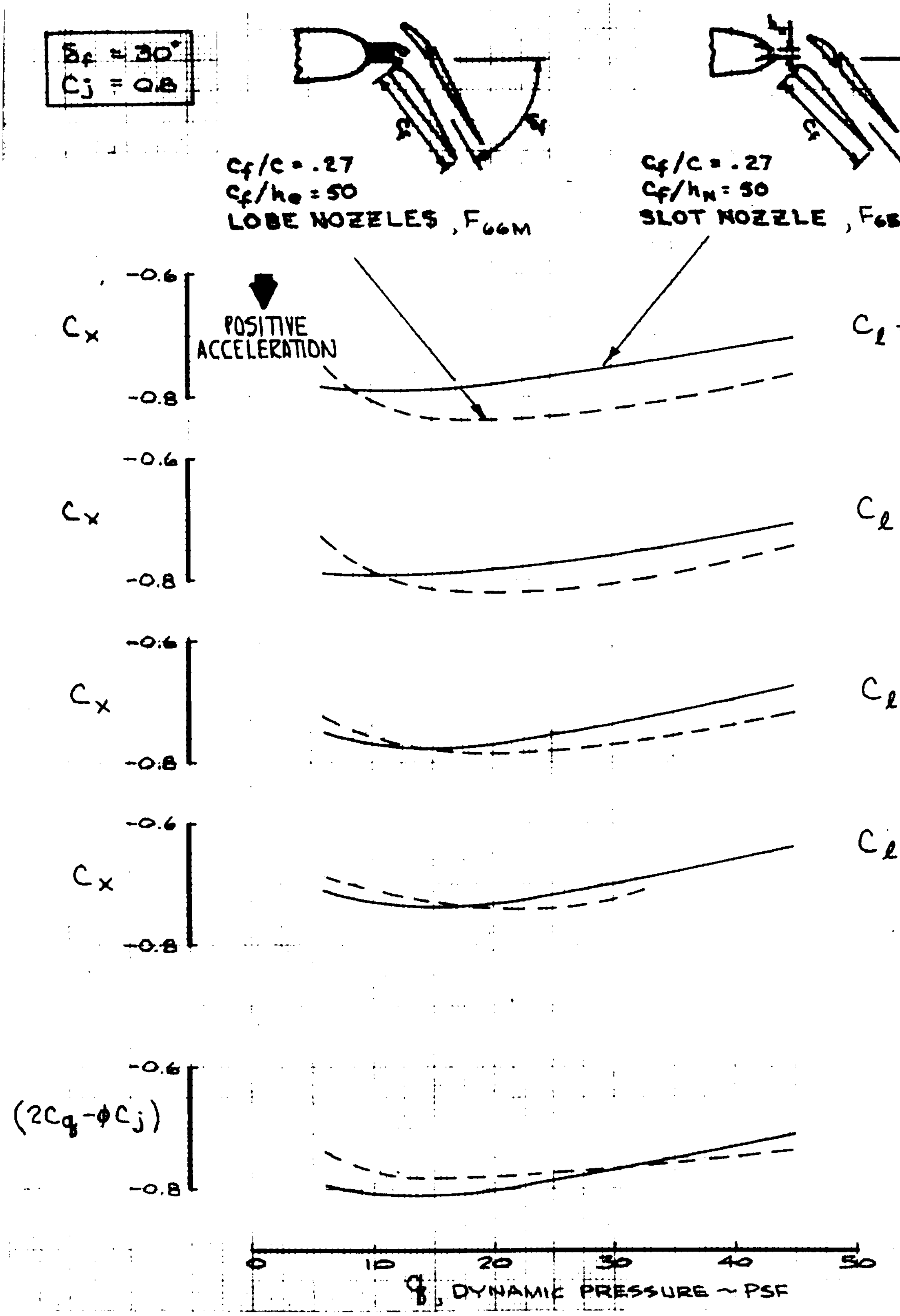

FIGURE 73.—VARIATION OF STREAMWISE FORCE COEFFICIENT WITH AIRSPEED—COMPARING SLOT NOZZLE AND LOBE NOZZLE AUGMENTOR FLAPS

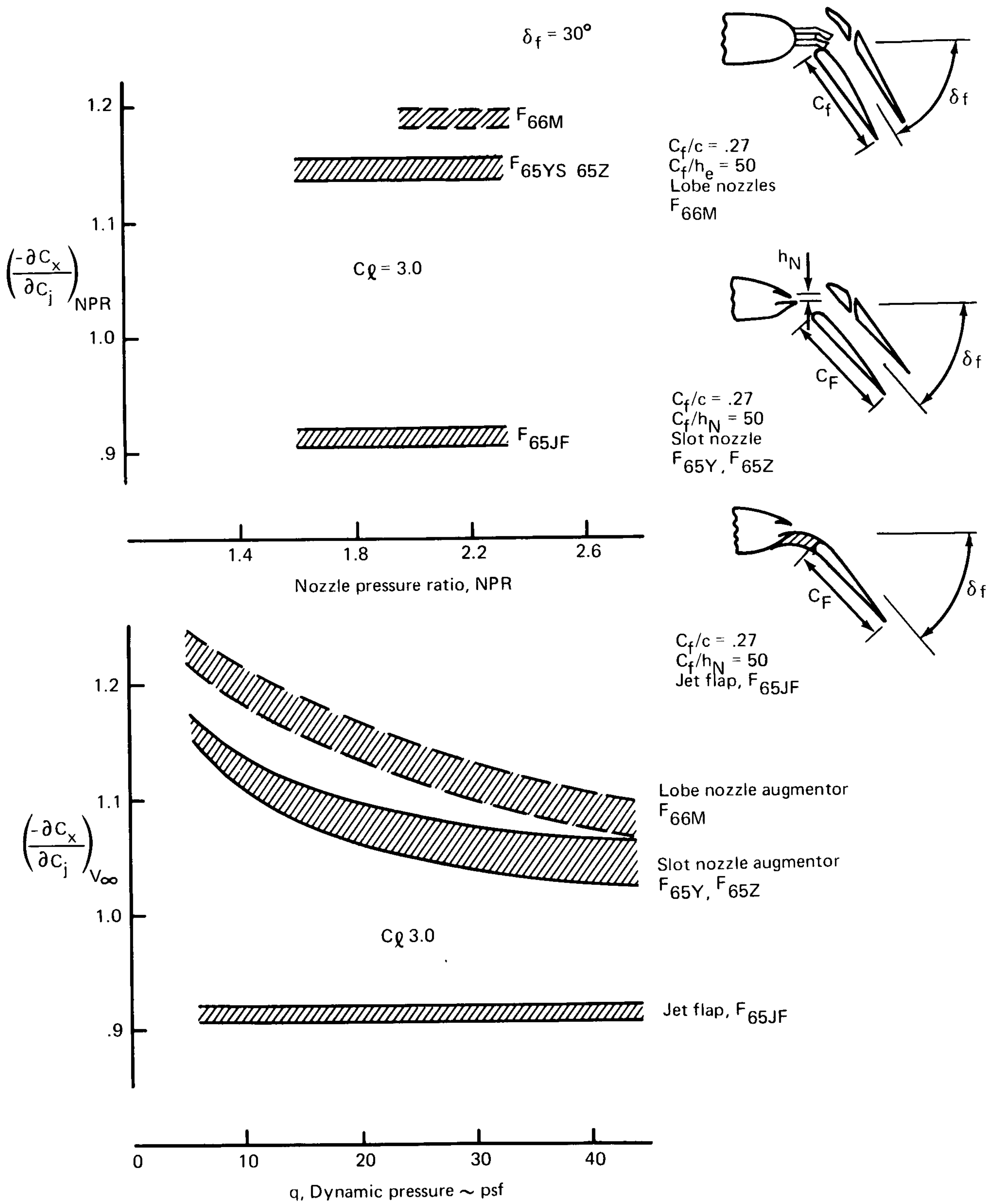

FIGURE 74.– COMPARISON OF THRUST EFFECTIVENESS FOR AUGMENTORS AND FOR JET FLAP

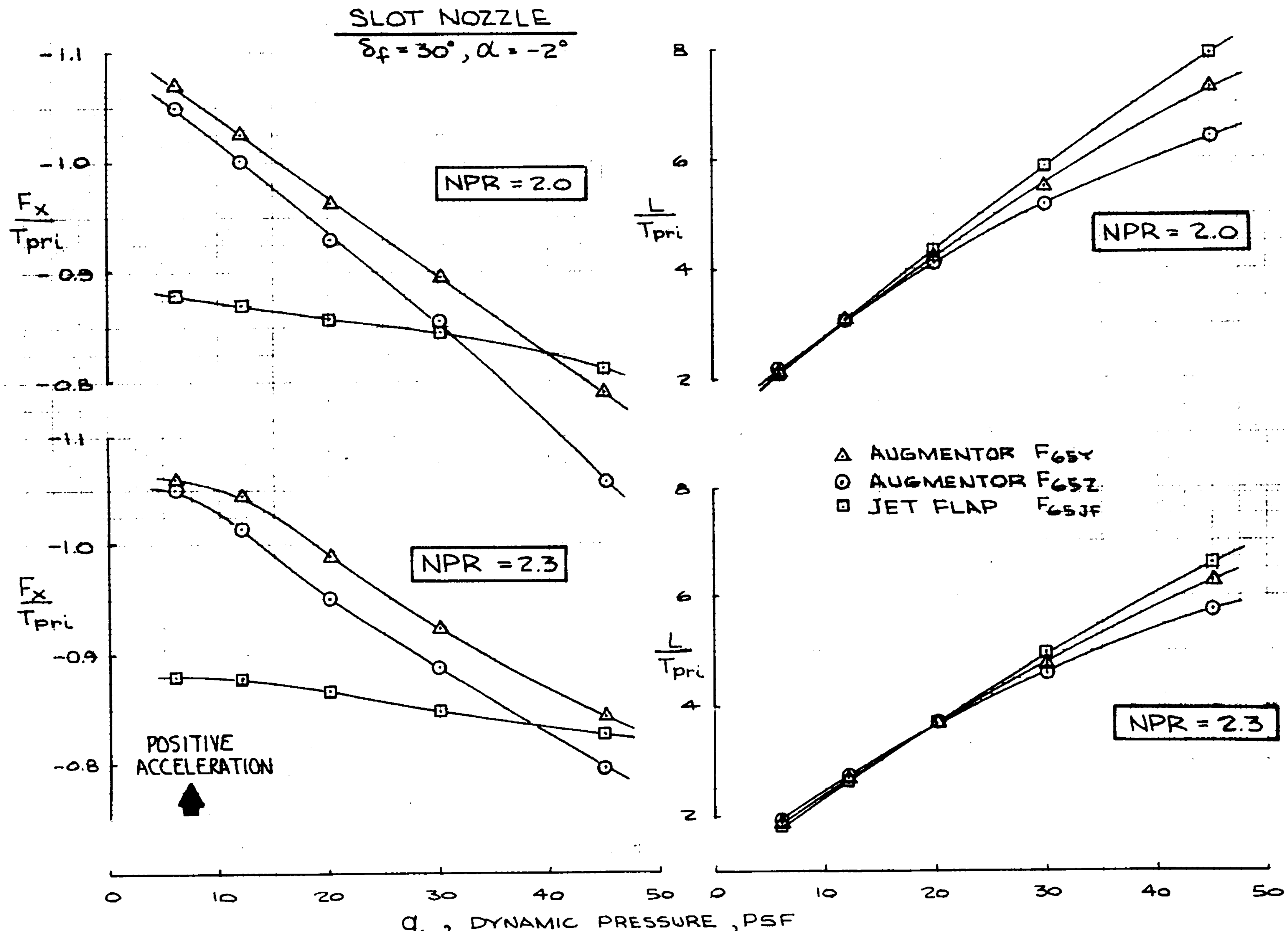

FIGURE 75.—AIRSPEED EFFECTS AT CONSTANT α AND NPR

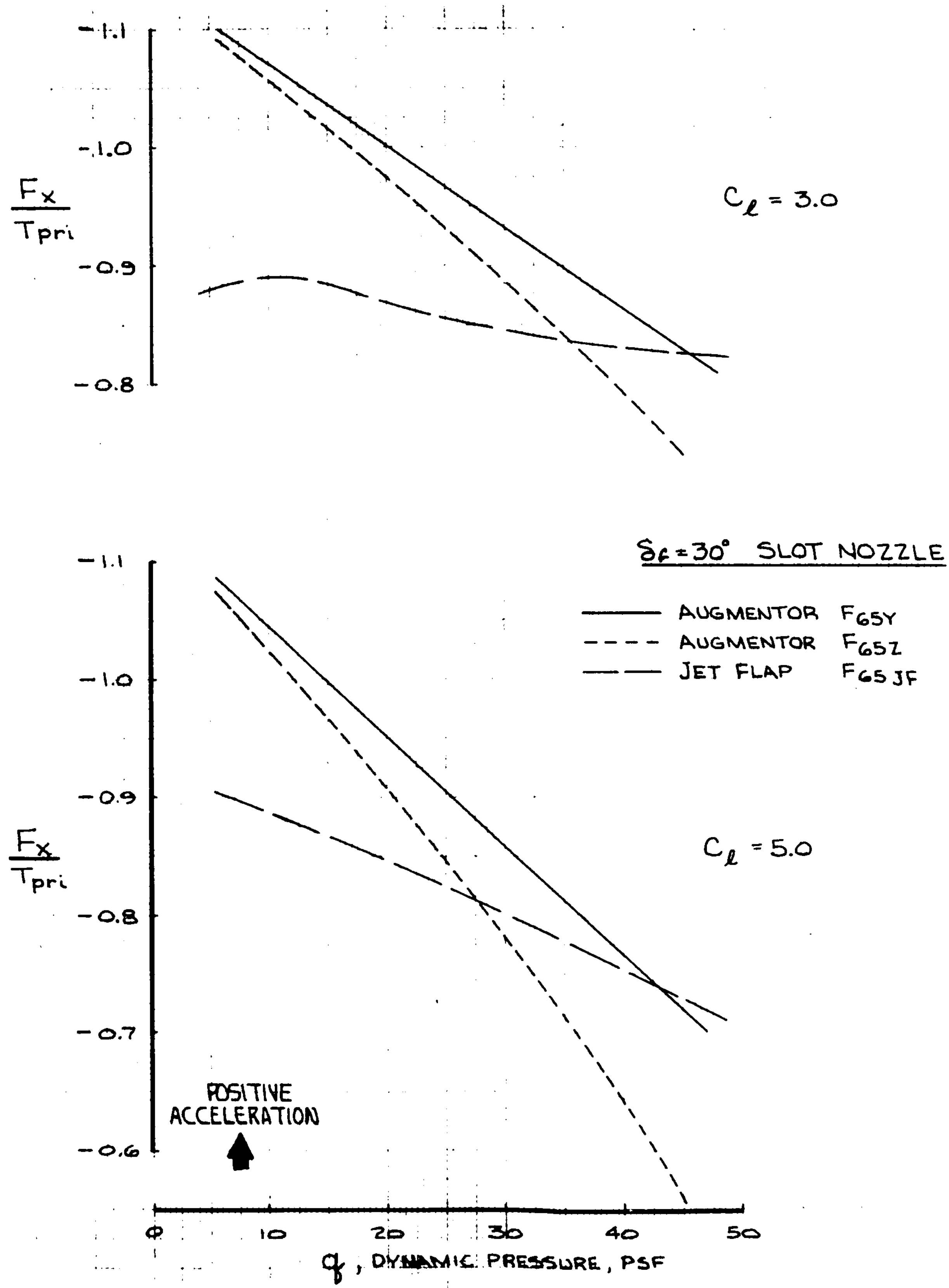

FIGURE 76.—AIRSPEED EFFECTS AT CONSTANT C_ℓ AND NPR = 2.3

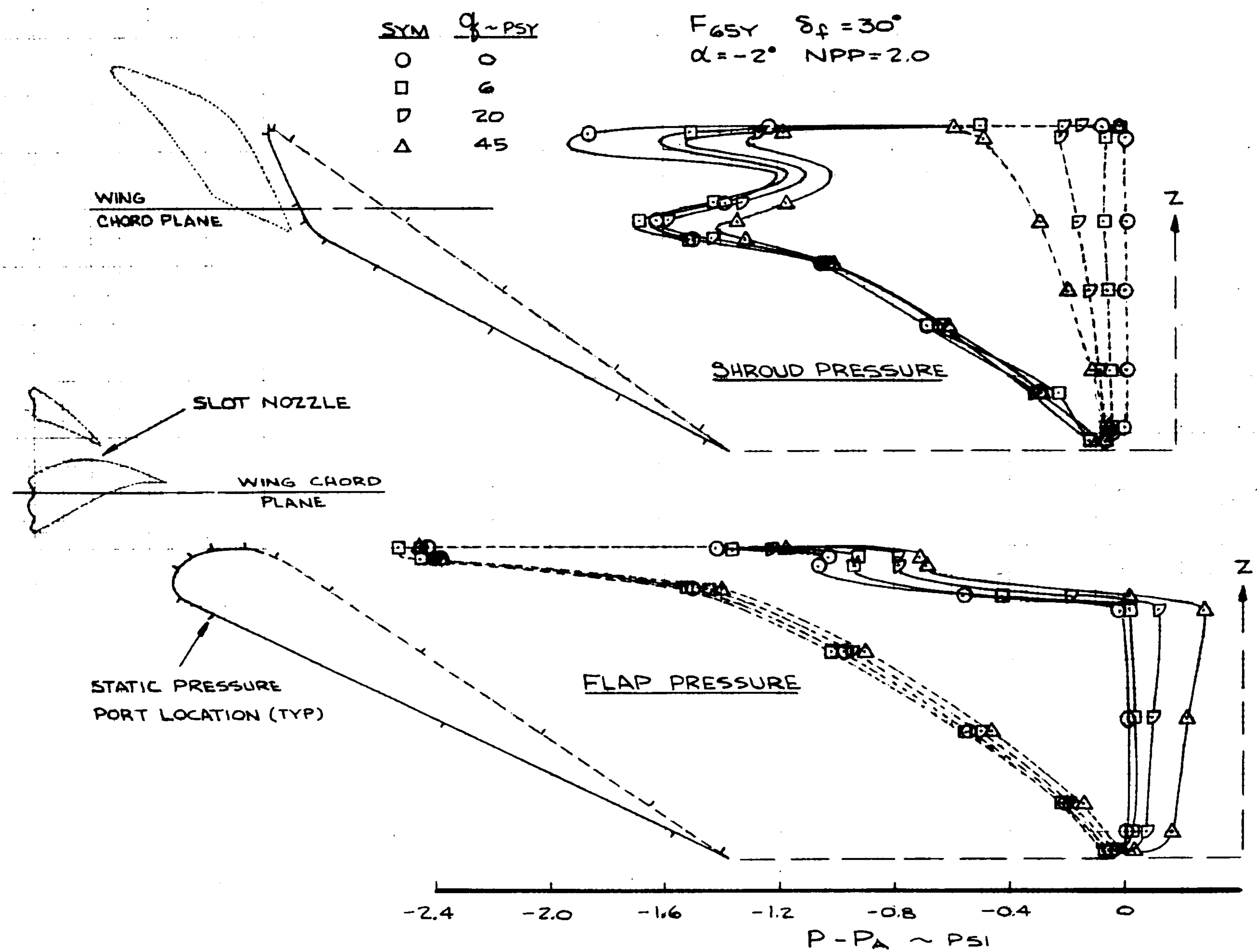

FIGURE 77.–EFFECT OF AIRSPEED ON AUGMENTOR FLAP (F-65Y) PRESSURE DISTRIBUTION

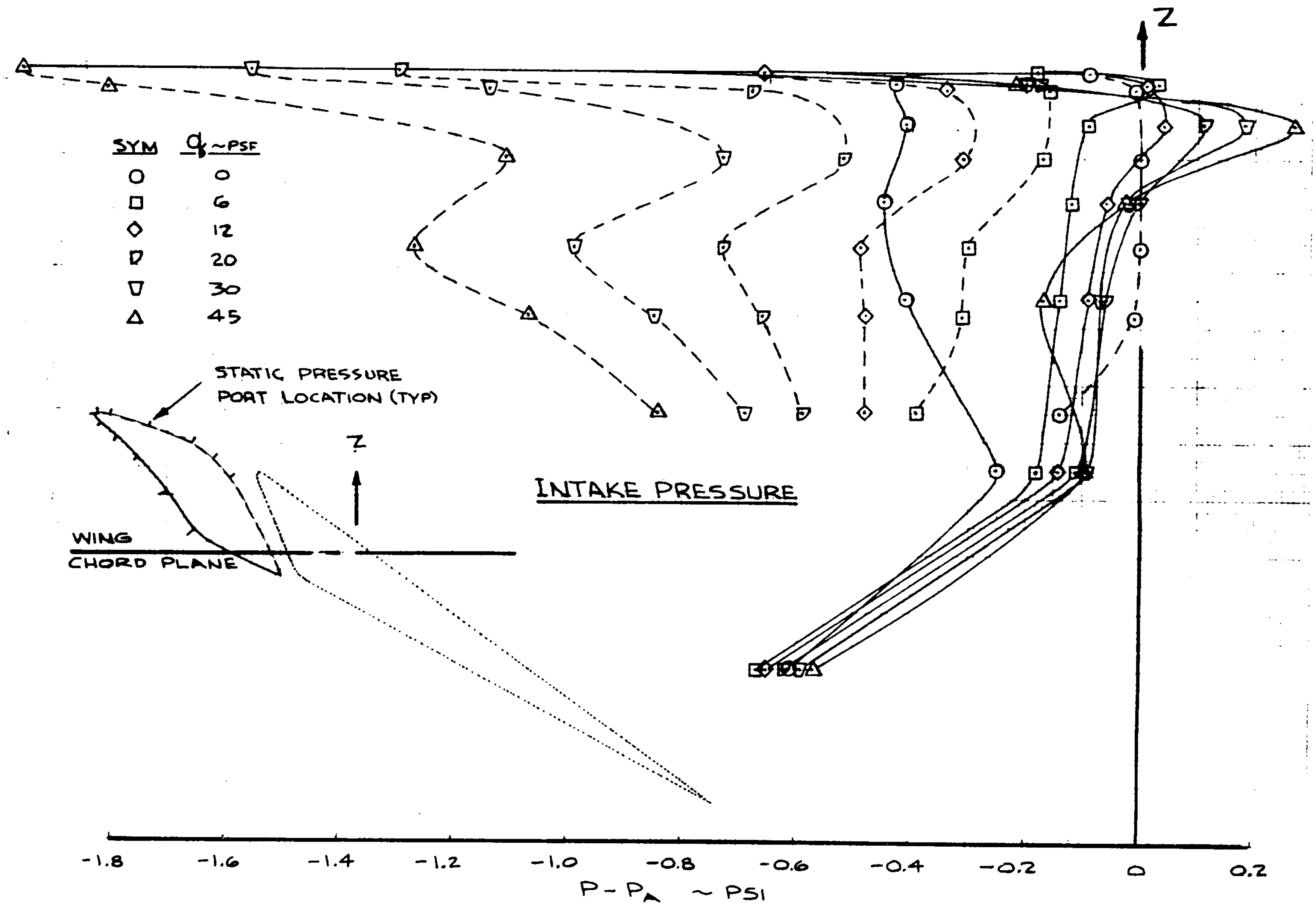

FIGURE 77.—Concluded

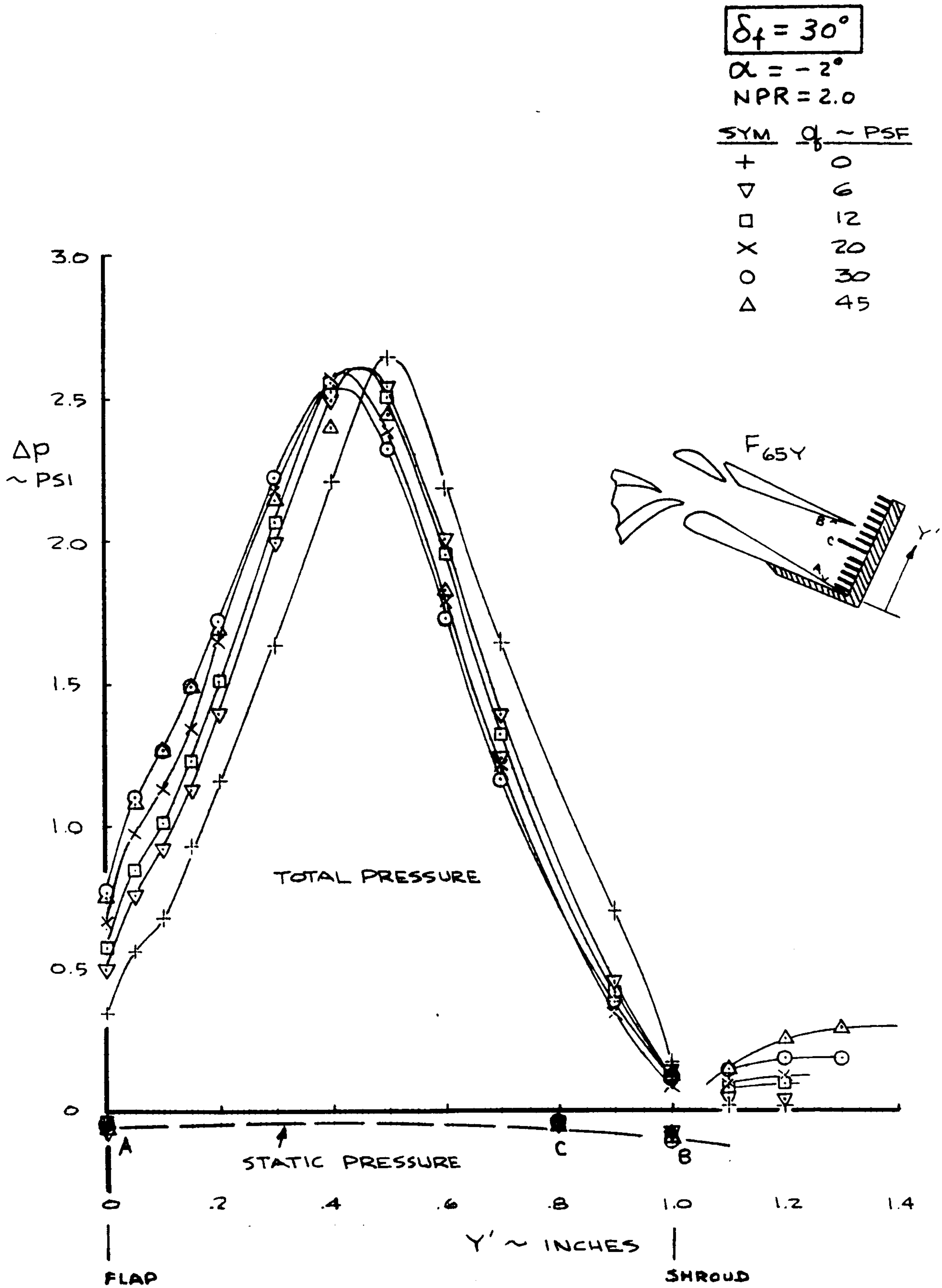

FIGURE 78.—EFFECT OF AIRSPEED ON SLOT NOZZLE AUGMENTOR EXIT TOTAL PRESSURE PROFILE

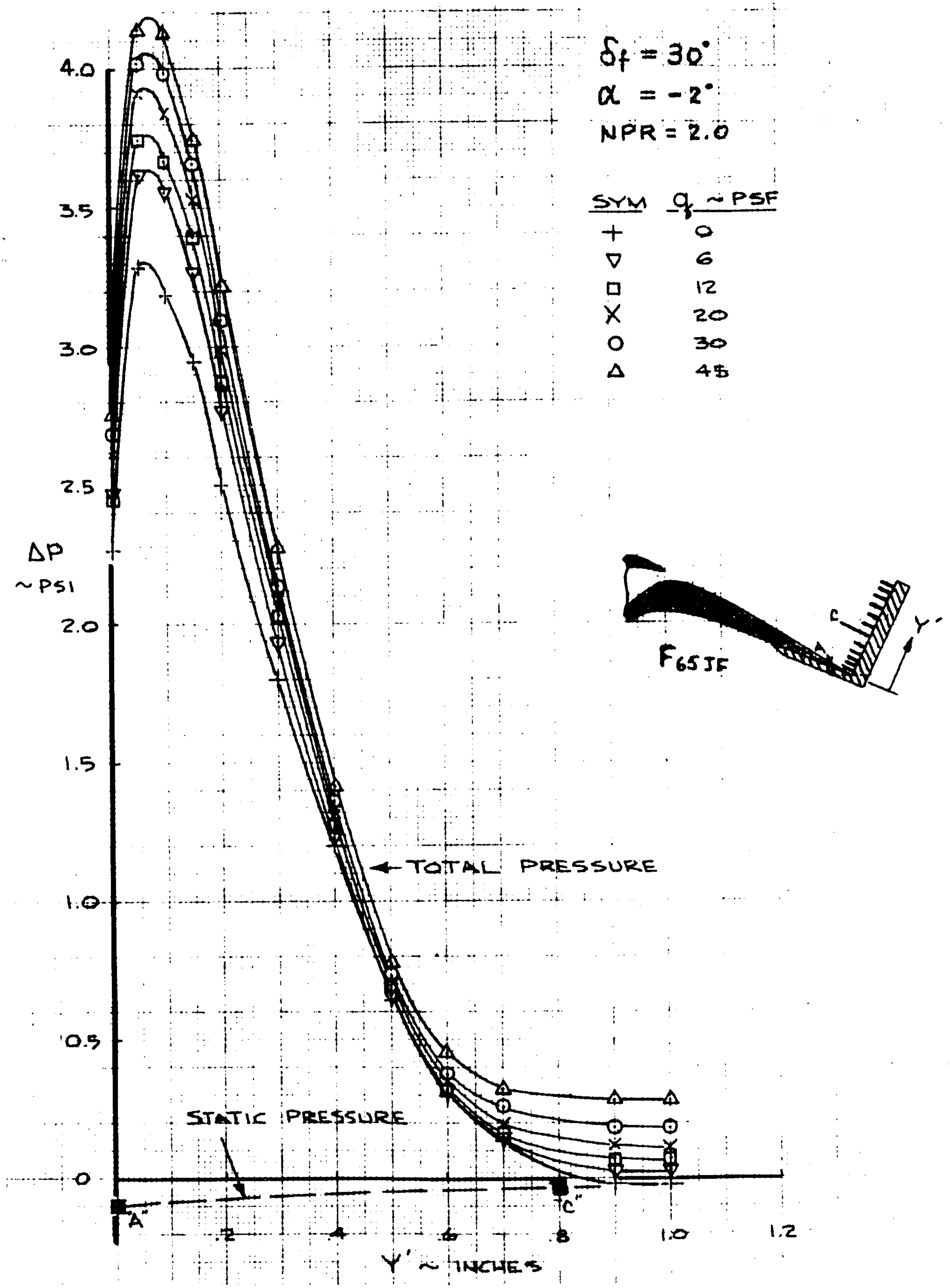

FIGURE 79.—EFFECT OF AIRSPEED ON JET FLAP TRAILING EDGE TOTAL PRESSURE PROFILE

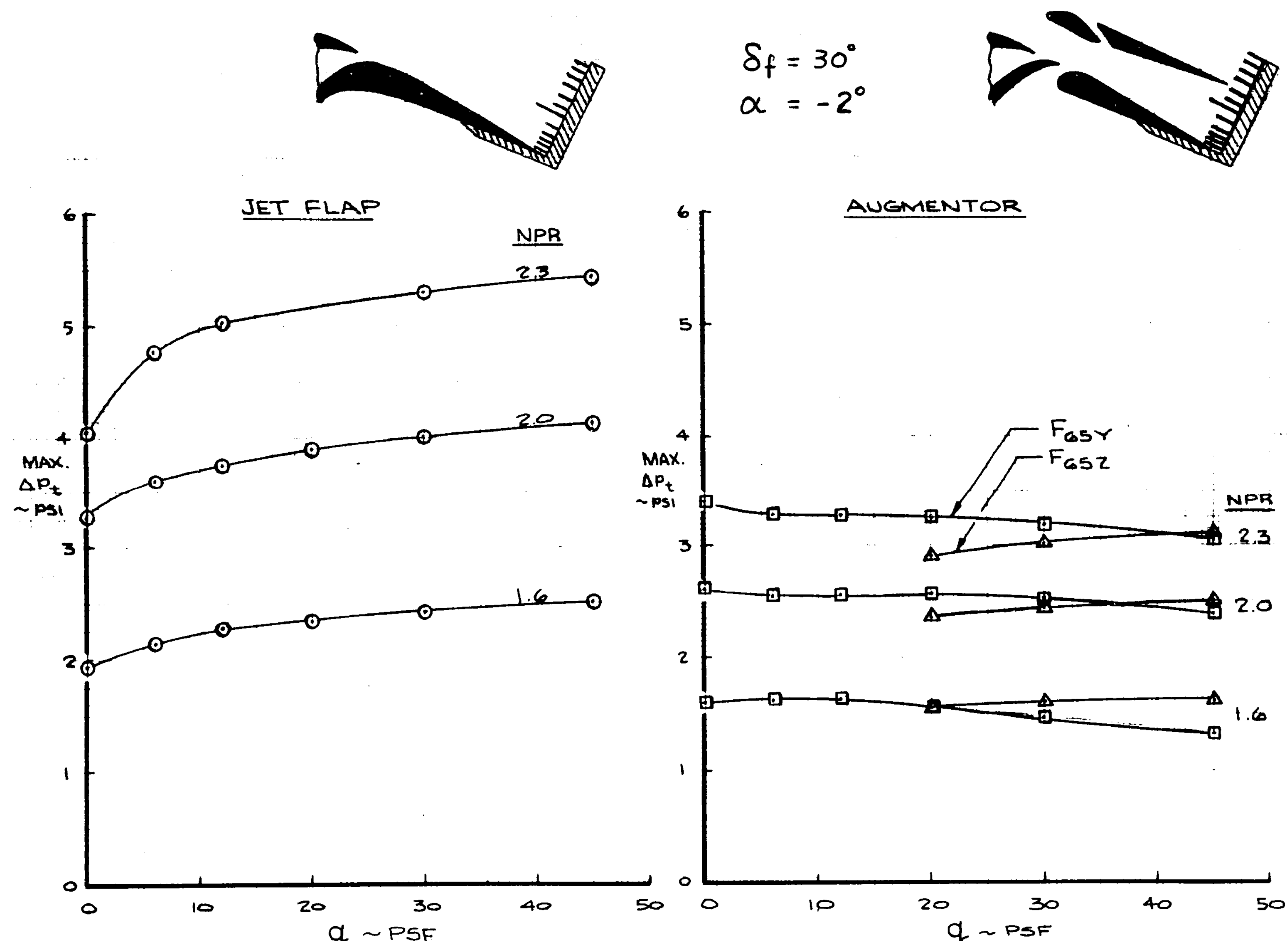

FIGURE 80.—EFFECT OF AIRSPEED ON MAXIMUM TOTAL PRESSURE MEASURED AT THE FLAP TRAILING EDGE

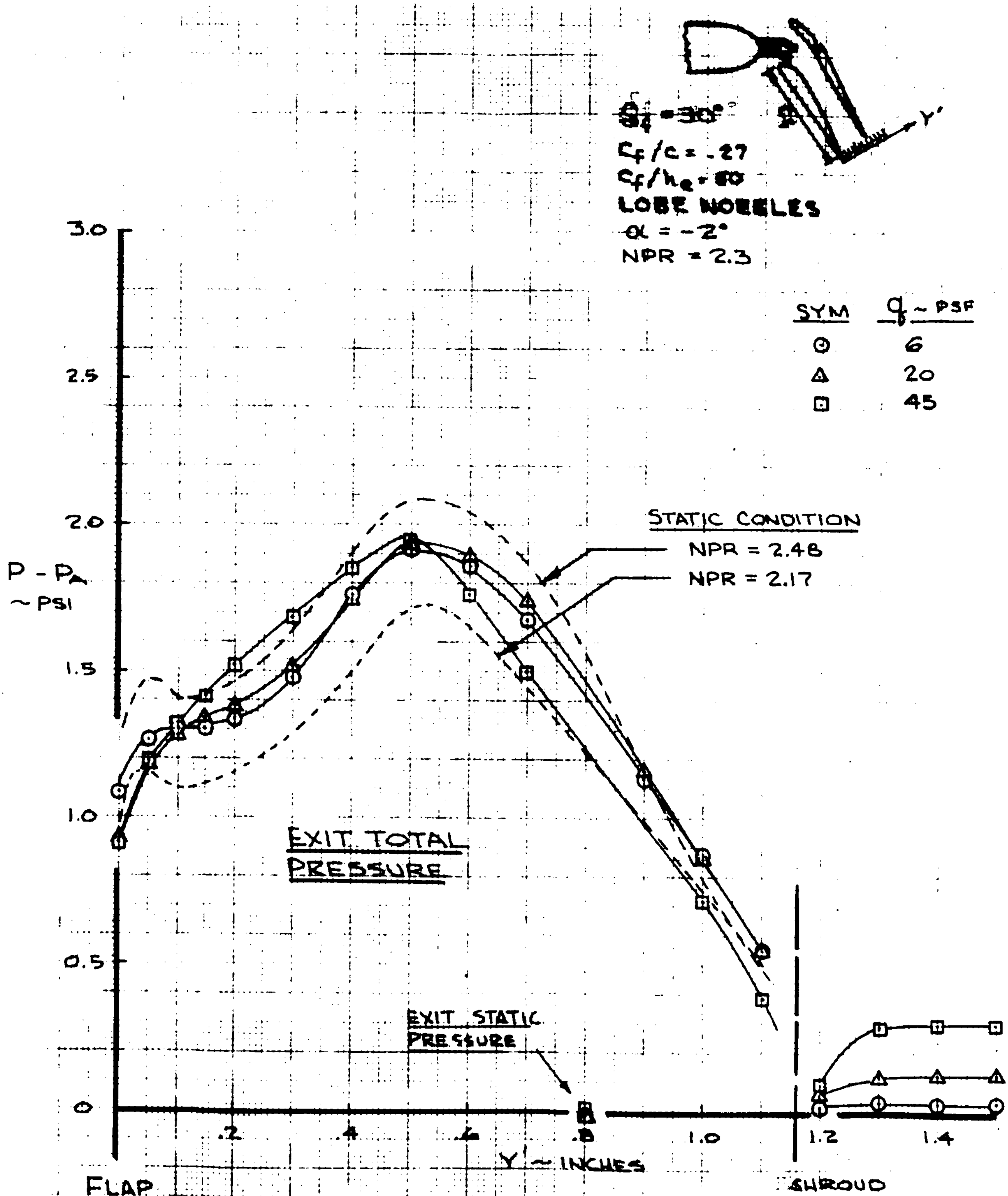

FIGURE 81.—EFFECT OF AIRSPEED ON LOBE NOZZLE AUGMENTOR EXIT TOTAL PRESSURE PROFILE

 c 3